Advanced Textbooks in Control and Signal Processing

Series Editors

Professor Michael J. Grimble, Professor of Industrial Systems and Director
Professor Michael A. Johnson, Professor Emeritus of Control Systems and Deputy Director
Industrial Control Centre, Department of Electronic and Electrical Engineering,
University of Strathclyde, Graham Hills Building, 50 George Street, Glasgow G1 1QE, UK

Other titles published in this series:

Genetic Algorithms
K.F. Man, K.S. Tang and S. Kwong

Neural Networks for Modelling and Control of Dynamic Systems
M. Nørgaard, O. Ravn, L.K. Hansen and N.K. Poulsen

Modelling and Control of Robot Manipulators (2nd Edition)
L. Sciavicco and B. Siciliano

Fault Detection and Diagnosis in Industrial Systems
L.H. Chiang, E.L. Russell and R.D. Braatz

Soft Computing
L. Fortuna, G. Rizzotto, M. Lavorgna, G. Nunnari, M.G. Xibilia and R. Caponetto

Statistical Signal Processing
T. Chonavel

Discrete-time Stochastic Processes (2nd Edition)
T. Söderström

Parallel Computing for Real-time Signal Processing and Control
M.O. Tokhi, M.A. Hossain and M.H. Shaheed

Multivariable Control Systems
P. Albertos and A. Sala

Control Systems with Input and Output Constraints
A.H. Glattfelder and W. Schaufelberger

Analysis and Control of Non-linear Process Systems
K. Hangos, J. Bokor and G. Szederkényi

Model Predictive Control (2nd Edition)
E.F. Camacho and C. Bordons

Principles of Adaptive Filters and Self-learning Systems
A. Zaknich

Digital Self-tuning Controllers
V. Bobál, J. Böhm, J. Fessl and J. Macháček

Control of Robot Manipulators in Joint Space
R. Kelly, V. Santibáñez and A. Loría

Active Noise and Vibration Control
M.O. Tokhi
Publication due November 2005

D.-W. Gu, P. Hr. Petkov and M. M. Konstantinov

Robust Control Design with MATLAB®

With 288 Figures

Springer

Da-Wei Gu, PhD, DIC, CEng
Engineering Department, University of Leicester, University Road, Leicester,
LE1 7RH, UK

Petko Hristov Petkov, PhD
Department of Automatics, Technical University of Sofia, 1756 Sofia, Bulgaria

Mihail Mihaylov Konstantinov, PhD
University of Architecture, Civil Engineering and Geodesy,
1 Hristo Smirnenski Blvd., 1046 Sofia, Bulgaria

British Library Cataloguing in Publication Data
Gu, D.-W.
Robust control design with MATLAB. - (Advanced textbooks in
control and signal processing)
1. MATLAB (Computer file) 2. Robust control 3. Control theory
I. Title II. Petkov, P. Hr (Petko Hr.), 1948-
III. Konstantinov, M. M. (Mihail M.), 1948-
629.8'312
ISBN-10: 1852339837

Library of Congress Control Number: 2005925110

Apart from any fair dealing for the purposes of research or private study, or criticism or review, as permitted under the Copyright, Designs and Patents Act 1988, this publication may only be reproduced, stored or transmitted, in any form or by any means, with the prior permission in writing of the publishers, or in the case of reprographic reproduction in accordance with the terms of licences issued by the Copyright Licensing Agency. Enquiries concerning reproduction outside those terms should be sent to the publishers.

Advanced Textbooks in Control and Signal Processing series ISSN 1439-2232
ISBN-10: 1-85233-983-7
ISBN-13: 978-1-85233-983-8
Springer Science+Business Media
springeronline.com

© Springer-Verlag London Limited 2005

MATLAB® and Simulink® are the registered trademarks of The MathWorks, Inc., 3 Apple Hill Drive, Natick, MA 01760-2098, U.S.A. http://www.mathworks.com

The software disk accompanying this book and all material contained on it is supplied without any warranty of any kind. The publisher accepts no liability for personal injury incurred through use or misuse of the disk.

The use of registered names, trademarks, etc. in this publication does not imply, even in the absence of a specific statement, that such names are exempt from the relevant laws and regulations and therefore free for general use.

The publisher makes no representation, express or implied, with regard to the accuracy of the information contained in this book and cannot accept any legal responsibility or liability for any errors or omissions that may be made.

Typesetting: Camera ready by authors
Production: LE-TEX Jelonek, Schmidt & Vöckler GbR, Leipzig, Germany
Printed in Germany
69/3141-543210 Printed on acid-free paper SPIN 11309833

To our families

Series Editors' Foreword

The topics of control engineering and signal processing continue to flourish and develop. In common with general scientific investigation, new ideas, concepts and interpretations emerge quite spontaneously and these are then discussed, used, discarded or subsumed into the prevailing subject paradigm. Sometimes these innovative concepts coalesce into a new sub-discipline within the broad subject tapestry of control and signal processing. This preliminary battle between old and new usually takes place at conferences, through the Internet and in the journals of the discipline. After a little more maturity has been acquired by the new concepts then archival publication as a scientific or engineering monograph may occur.

A new concept in control and signal processing is known to have arrived when sufficient material has evolved for the topic to be taught as a specialised tutorial workshop or as a course to undergraduate, graduate or industrial engineers. *Advanced Textbooks in Control and Signal Processing* are designed as a vehicle for the systematic presentation of course material for both popular and innovative topics in the discipline. It is hoped that prospective authors will welcome the opportunity to publish a structured and systematic presentation of some of the newer emerging control and signal processing technologies in the textbook series.

It is always interesting to look back at how a particular field of control systems theory developed. The impetus for change and realization that a new era in a subject is dawning always seems to be associated with short, sharp papers that make the academic community think again about the prevalent theoretical paradigm. In the case of the evolution of robust control theory, the conference papers of Zames (circa. 1980) on robustness and the very short paper of Doyle on the robustness of linear quadratic Gaussian control systems seem to stand as landmarks intimating that control theory was going to change direction again. And the change did come; all through the 1980s came a steady stream of papers re-writing control theory, introducing system uncertainty, H_∞ robust control and μ-synthesis as part of a new control paradigm.

Change, however did not come easily to the industrial applications community because the new theories and methods were highly mathematical. In the early stages even the classical feedback diagram which so often opened control engineering courses was replaced by a less intuitively obvious diagram. Also it

was difficult to see the benefits to be gained from the new development. Throughout the 1990s the robust control theory and methods consolidated and the first major textbooks and software toolboxes began to appear. Experience with some widely disseminated benchmark problems such as control design for distillation columns, the control design for hard-disk drives, and the inverted-pendulum control problem helped the industrial community see how to apply the new method and the control benefits that accrued.

This advanced course textbook on robust control system design using MATLAB® by Da-Wei Gu, Petko Petkov and Mihail Konstantinov has arrived at a very opportune time. More than twenty years of academic activity in the robust control field forms the bedrock on which this course book and its set of insightful applications examples are developed. Part I of the volume presents the theory – a systematic presentation of: systems notation, uncertainty modelling, robust design specification, the H_∞ design method, H_∞ loop shaping, μ-analysis and synthesis and finally the algorithms for providing the low-order controllers that will be implemented. This is a valuable and concise presentation of all the necessary theoretical concepts prior to their application which is covered in Part II.

Inspired by the adage "practice makes perfect", Part II of the volume comprises six fully worked-out extended examples. To learn how to apply the complex method of H_∞ design and μ-synthesis there can be no surer route than to work through a set of carefully scripted examples. In this volume, the examples range from the academic mass-damper-spring system through to the industrially relevant control of a distillation column and a flexible manipulator system. The benchmark example of the ubiquitous hard-disk drive control system is also among the examples described. The MATLAB® tools of the Robust Control Toolbox, the Control System Toolbox and Simulink® are used in these application examples. The CD-ROM contains all the necessary files and instructions together with a pdf containing colour reproductions of many of the figures in the book.

In summary, after academic development of twenty years or so, the robust control paradigm is now fully fledged and forms a vital component of advanced control engineering courses. This new volume in our series of advanced control and signal processing course textbooks on applying the methods of H_∞ and μ-synthesis control design will be welcomed by postgraduate students, lecturers and industrial control engineers alike.

M.J. Grimble and M.A. Johnson
Glasgow, Scotland, U.K.
February 2005

Preface

Robustness has been an important issue in control-systems design ever since 1769 when James Watt developed his flyball governor. A successfully designed control system should be always able to maintain stability and performance level in spite of uncertainties in system dynamics and/or in the working environment to a certain degree. Design requirements such as gain margin and phase margin in using classical frequency-domain techniques are solely for the purpose of robustness. The robustness issue was not that prominently considered during the period of 1960s and 1970s when system models could be much more accurately described and design methods were mainly mathematical optimisations in the time domain. Due to its importance, however, the research on robust design has been going on all the time. A breakthrough came in the late 1970s and early 1980s with the pioneering work by Zames [170] and Zames and Francis [171] on the theory, now known as the $\mathcal{H}_\infty$ optimal control theory. The $\mathcal{H}_\infty$ optimisation approach and the μ-synthesis/analysis method are well developed and elegant. They provide systematic design procedures of robust controllers for linear systems, though the extension into nonlinear cases is being actively researched.

Many books have since been published on $\mathcal{H}_\infty$ and related theories and methods [26, 38, 65, 137, 142, 145, 174, 175]. The algorithms to implement the design methods are readily available in software packages such as MATLAB® and Slicot [119]. However, from our experience in teaching and research projects, we have felt that a reasonable percentage of people, students as well as practising engineers, still have difficulties in applying the $\mathcal{H}_\infty$ and related theory and in using MATLAB® routines. The mathematics behind the theory is quite involved. It is not straightforward to formulate a practical design problem, which is usually nonlinear, into the $\mathcal{H}_\infty$ or μ design framework and then apply MATLAB® routines. This hinders the application of such a powerful theory. It also motivated us to prepare this book.

This book is for people who want to learn how to deal with robust control-system design problems but may not want to research the relevant theoretic developments. Methods and solution formulae are introduced in the first part

of the book, but kept to a minimum. The majority of the book is devoted to several practical design case studies (Part II). These design examples, ranging from teaching laboratory experiments such as a mass-damper-spring system to complex systems such as a supersonic rocket autopilot and a flexible-link manipulator, are discussed with detailed presentations. The design exercises are all conducted using the new *Robust Control Toolbox v3.0* and are in a hands-on, tutorial manner. Studying these examples with the attached MATLAB® and Simulink® programs (170 plus M- and MDL-files) used in all designs will help the readers learn how to deal with nonlinearities involved in the system, how to parameterise dynamic uncertainties and how to use MATLAB® routines in the analysis and design, *etc.*. It is also hoped that by going through these exercises the readers will understand the essence of robust control system design and develop their own skills to design real, industrial, robust control systems.

The readership of this book is postgraduates and control engineers, though senior undergraduates may use it for their final-year projects. The material included in the book has been adopted in recent years for MSc and PhD engineering students at Leicester University and at the Technical University of Sofia. The design examples are independent of each other. They have been used extensively in the laboratory projects on the course *Robust and Optimal Control Systems* taught in a masters programme in the Technical University of Sofia.

The authors are indebted to several people and institutions who helped them in the preparation of the book. We are particularly grateful to The MathWorks, Inc. for their continuous support, to Professor Sigurd Skogestad of Norwegian University of Science and Technology who kindly provided the nonlinear model of the Distillation Column and to Associate Professor Georgi Lehov from Technical University of Russe, Bulgaria, who developed the uncertainty model of the Flexible-Link Manipulator.

Using the CD ROM

The attached CD ROM contains six folders with M- and MDL-files intended for design, analysis and simulation of the six design examples, plus a pdf file with colour hypertext version of the book. In order to use the M- and MDL-files the reader should have at his (her) disposition of MATLAB® v7.0.2 with Robust Control Toolbox v 3.0, Control System Toolbox v6.1 and Simulink® v6.1. Further information on the use of the files can be found in the file Readme.m on the disc.

Contents

Part I Basic Methods and Theory

1 Introduction 3
1.1 Control-system Representations 4
1.2 System Stabilities 6
1.3 Coprime Factorisation and Stabilising Controllers 7
1.4 Signals and System Norms 9
1.4.1 Vector Norms and Signal Norms 9
1.4.2 System Norms 10

2 Modelling of Uncertain Systems 13
2.1 Unstructured Uncertainties 13
2.2 Parametric Uncertainty 17
2.3 Linear Fractional Transformations 20
2.4 Structured Uncertainties 23

3 Robust Design Specifications 25
3.1 Small-gain Theorem and Robust Stabilisation 25
3.2 Performance Consideration 28
3.3 Structured Singular Values 29

4 $\mathcal{H}_\infty$ Design 35
4.1 Mixed Sensitivity $\mathcal{H}_\infty$ Optimisation 35
4.2 2-Degree-Of-Freedom $\mathcal{H}_\infty$ Design 38
4.3 $\mathcal{H}_\infty$ Suboptimal Solutions 39
4.3.1 Solution Formulae for Normalised Systems 39
4.3.2 Solution to S-over-KS Design 43
4.3.3 The Case of $D_{22} \neq 0$ 44
4.3.4 Normalisation Transformations 45
4.3.5 Direct Formulae for $\mathcal{H}_\infty$ Suboptimal Central Controller 47
4.4 Formulae for Discrete-time Cases 50

5 $\mathcal{H}_\infty$ Loop-shaping Design Procedures 55
5.1 Robust Stabilisation Against Normalised Coprime Factor Perturbations 56
5.2 Loop-shaping Design Procedures 58
5.3 Formulae for the Discrete-time Case 61
5.3.1 Normalised Coprime Factorisation of Discrete-time Plant 61
5.3.2 Robust Controller Formulae 62
5.3.3 The Strictly Proper Case 63
5.3.4 On the Three DARE Solutions 65
5.4 A Mixed Optimisation Design Method with LSDP 67

6 μ-Analysis and Synthesis 71
6.1 Consideration of Robust Performance 71
6.2 μ-Synthesis: D-K Iteration Method 74
6.3 μ-Synthesis: μ-K Iteration Method 77

7 Lower-order Controllers 79
7.1 Absolute-error Approximation Methods 80
7.1.1 Balanced Truncation Method 81
7.1.2 Singular Perturbation Approximation 82
7.1.3 Hankel-norm Approximation 83
7.1.4 *Remarks* 85
7.2 Reduction via Fractional Factors 86
7.3 Relative-error Approximation Methods 90
7.4 Frequency-weighted Approximation Methods 92

Part II Design Examples

8 Robust Control of a Mass-Damper-Spring System 101
8.1 System Model 101
8.2 Frequency Analysis of Uncertain System 107
8.3 Design Requirements of Closed-loop System 108
8.4 System Interconnections 112
8.5 Suboptimal $\mathcal{H}_\infty$ Controller Design 115
8.6 Analysis of Closed-loop System with K_{hin} 117
8.7 $\mathcal{H}_\infty$ Loop-shaping Design 125
8.8 Assessment of $\mathcal{H}_\infty$ Loop-shaping Design 128
8.9 μ-Synthesis and D-K Iterations 131
8.10 Robust Stability and Performance of K_{mu} 141
8.11 Comparison of $\mathcal{H}_\infty$, $\mathcal{H}_\infty$ LSDP and μ-controllers 150
8.12 Order Reduction of μ-controller 158
8.13 Conclusions 162

9 A Triple Inverted Pendulum Control-system Design 163
9.1 System Description 164
9.2 Modelling of Uncertainties 167
9.3 Design Specifications 180
9.4 System Interconnections 182
9.5 $\mathcal{H}_\infty$ Design 186
9.6 μ-Synthesis 191
9.7 Nonlinear System Simulation 199
9.8 Conclusions 202

10 Robust Control of a Hard Disk Drive 203
10.1 Hard Disk Drive Servo System 203
10.2 Derivation of Uncertainty Model 209
10.3 Closed-loop System-design Specifications 215
10.4 System Interconnections 218
10.5 Controller Design in Continuous-time 219
10.5.1 μ-Design 221
10.5.2 $\mathcal{H}_\infty$ Design 228
10.5.3 $\mathcal{H}_\infty$ Loop-shaping Design 228
10.6 Comparison of Designed Controllers 229
10.7 Controller-order Reduction 237
10.8 Design of Discrete-time Controller 239
10.9 Nonlinear System Simulation 244
10.10 Conclusions 247

11 Robust Control of a Distillation Column 249
11.1 Introduction 249
11.2 Dynamic Model of the Distillation Column 250
11.3 Uncertainty Modelling 254
11.4 Closed-loop System-performance Specifications 256
11.5 Open-loop and Closed-loop System Interconnections 261
11.6 Controller Design 261
11.6.1 Loop-shaping Design 262
11.6.2 μ-Synthesis 271
11.7 Nonlinear System Simulation 283
11.8 Conclusions 286

12 Robust Control of a Rocket 289
12.1 Rocket Dynamics 289
12.2 Uncertainty Modelling 301
12.3 Performance Requirements 306
12.4 $\mathcal{H}_\infty$ Design 310
12.5 μ-Synthesis 315
12.6 Discrete-time μ-Synthesis 324
12.7 Simulation of the Nonlinear System 328

12.8 Conclusions . . . 332

13 Robust Control of a Flexible-Link Manipulator . . . 335
13.1 Dynamic Model of the Flexible Manipulator . . . 336
13.2 A Linear Model of the Uncertain System . . . 339
13.3 System-performance Specifications . . . 355
13.4 System Interconnections . . . 359
13.5 Controller Design and Analysis . . . 361
13.6 Nonlinear System Simulations . . . 372
13.7 Conclusions . . . 375

References . . . 377

Index . . . 387

Part I

Basic Methods and Theory

1

Introduction

Robustness is of crucial importance in control-system design because real engineering systems are vulnerable to external disturbance and measurement noise and there are always differences between mathematical models used for design and the actual system. Typically, a control engineer is required to design a controller that will stabilise a plant, if it is not stable originally, and satisfy certain performance levels in the presence of disturbance signals, noise interference, unmodelled plant dynamics and plant-parameter variations. These design objectives are best realised *via* the feedback control mechanism, although it introduces in the issues of high cost (the use of sensors), system complexity (implementation and safety) and more concerns on stability (thus internal stability and stabilising controllers).

Though always being appreciated, the need and importance of robustness in control-systems design has been particularly brought into the limelight during the last two decades. In classical single-input single-output control, robustness is achieved by ensuring good gain and phase margins. Designing for good stability margins usually also results in good, well-damped time responses, *i.e.* good performance. When multivariable design techniques were first developed in the 1960s, the emphasis was placed on achieving good performance, and not on robustness. These multivariable techniques were based on linear quadratic performance criteria and Gaussian disturbances, and proved to be successful in many aerospace applications where accurate mathematical models can be obtained, and descriptions for external disturbances/noise based on white noise are considered appropriate. However, application of such methods, commonly referred to as the linear quadratic Gaussian (LQG) methods, to other industrial problems made apparent the poor robustness properties exhibited by LQG controllers. This led to a substantial research effort to develop a theory that could explicitly address the robustness issue in feedback design. The pioneering work in the development of the forthcoming theory, now known as the $\mathcal{H}_\infty$ optimal control theory, was conducted in the early 1980s by Zames [170] and Zames and Francis [171]. In the $\mathcal{H}_\infty$ approach, the designer from the outset specifies a model of system uncertainty, such as additive perturbation

and/or output disturbance (details in Chapter 2), that is most suited to the problem at hand. A constrained optimisation is then performed to maximise the robust stability of the closed-loop system to the type of uncertainty chosen, the constraint being the internal stability of the feedback system. In most cases, it would be sufficient to seek a feasible controller such that the closed-loop system achieves certain robust stability. Performance objectives can also be included in the optimisation cost function. Elegant solution formulae have been developed, which are based on the solutions of certain algebraic Riccati equations, and are readily available in software packages such as Slicot [119] and MATLAB®.

Despite the mature theory ([26, 38, 175]) and availability of software packages, commercial or licensed freeware, many people have experienced difficulties in solving industrial control-systems design problems with these $\mathcal{H}_\infty$ and related methods, due to the complex mathematics of the advanced approaches and numerous presentations of formulae as well as adequate translations of industrial design into relevant configurations. This book aims at bridging the gap between the theory and applications. By sharing the experiences in industrial case studies with minimum exposure to the theory and formulae, the authors hope readers will obtain an insight into robust industrial control-system designs using major $\mathcal{H}_\infty$ optimisation and related methods.

In this chapter, the basic concepts and representations of systems and signals will be discussed.

1.1 Control-system Representations

A control system or plant or process is an interconnection of components to perform certain tasks and to yield a desired response, *i.e.* to generate desired signal (the output), when it is driven by manipulating signal (the input). A control system is a causal, dynamic system, *i.e.* the output depends not only the present input but also the input at the previous time.

In general, there are two categories of control systems, the open-loop systems and closed-loop systems. An open-loop system uses a controller or control actuator to obtain the design response. In an open-loop system, the output has no effect on the input. In contrast to an open-loop system, a closed-loop control system uses sensors to measure the actual output to adjust the input in order to achieve desired output. The measure of the output is called the feedback signal, and a closed-loop system is also called a feedback system. It will be shown in this book that only feedback configurations are able to achieve the robustness of a control system.

Due to the increasing complexity of physical systems under control and rising demands on system properties, most industrial control systems are no longer single-input and single-output (SISO) but multi-input and multi-output (MIMO) systems with a high interrelationship (coupling) between these chan-

8.11 Comparison of $\mathcal{H}_\infty$, $\mathcal{H}_\infty$ LSDP and μ-controllers

The comparison of the designed systems with $\mathcal{H}_\infty$, $\mathcal{H}_\infty$ loop-shaping and μ-controllers begins with the frequency responses of these three controllers. These responses are produced by using the file `kf_mds.m` below and are shown in Figure 8.41.

File `kf_mds.m`

```
omega = logspace(-2,3,100);
%
% H_infinity controller
K_hing = frsp(K_hin,omega);
%
% Loop Shaping controller
K_lshg = frsp(K_lsh,omega);
%
% mu-controller
K_mug = frsp(K_mu,omega);
%
figure(1)
vplot('bode',K_hing,'r-',K_lshg,'m--',K_mug,'c-.')
subplot(2,1,1)
title('BODE PLOTS OF ALL CONTROLLERS')
subplot(2,1,2)
```

It can be seen from Figure 8.41 that the $\mathcal{H}_\infty$ loop-shaping controller and μ-controller are characterised by larger gains compared with the $\mathcal{H}_\infty$ controller, in the frequency range above 5 rad/s. All the phase responses are close to each other up to about 3 rad/s and after that frequency the $\mathcal{H}_\infty$ controller continues to introduce a larger phase delay.

The comparison of frequency responses of the nominal closed-loop systems is conducted by the commands included in the file `clf_mds.m`, and the results are shown in Figure 8.42.

File `clf_mds.m`

```
sim_mds
omega = logspace(-2,2,100);
%
% H_infinity controller
clp_hin = starp(sim_ic,K_hin);
ref_hin = sel(clp_hin,4,4);
ref_hing = frsp(ref_hin,omega);
```

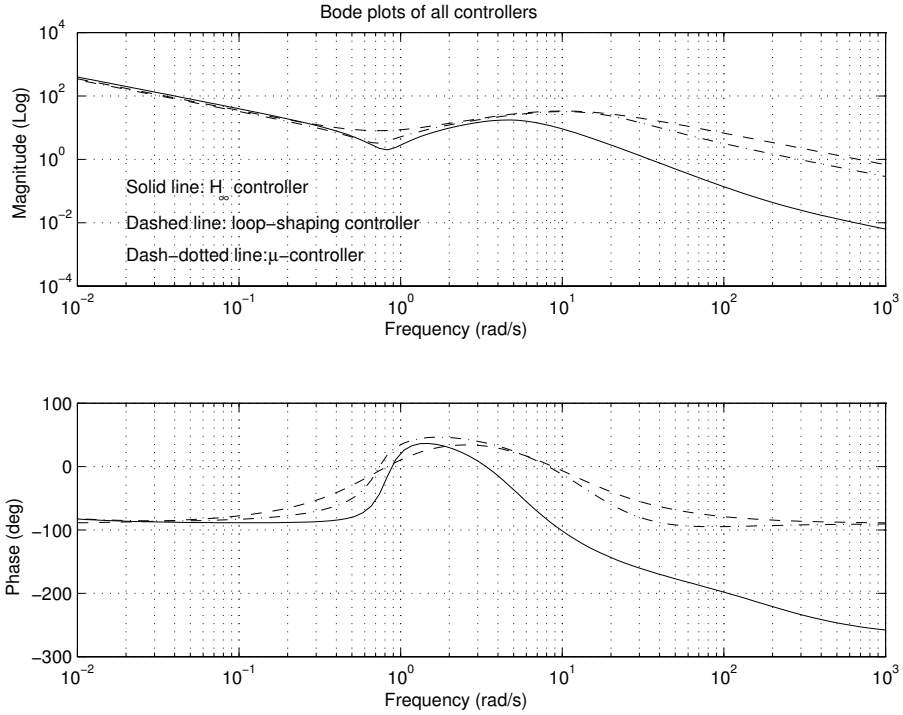

Fig. 8.41. Frequency responses of controllers

```
%
% Loop Shaping controller
clp_lsh = starp(sim_ic,K_lsh);
ref_lsh = sel(clp_lsh,4,4);
ref_lshg = frsp(ref_lsh,omega);
%
% mu-controller
clp_mu = starp(sim_ic,K_mu);
ref_mu = sel(clp_mu,4,4);
ref_mug = frsp(ref_mu,omega);
figure(1)
vplot('bode',ref_hing,'r-',ref_lshg,'m--',ref_mug,'c-.')
subplot(2,1,1)
title('BODE PLOTS OF CLOSED-LOOP SYSTEMS')
subplot(2,1,2)
```

Figure 8.42 shows that the systems with the $\mathcal{H}_\infty$ loop-shaping and μ-controllers are characterised by larger bandwidth that leads to faster dynamics of the corresponding closed-loop systems.

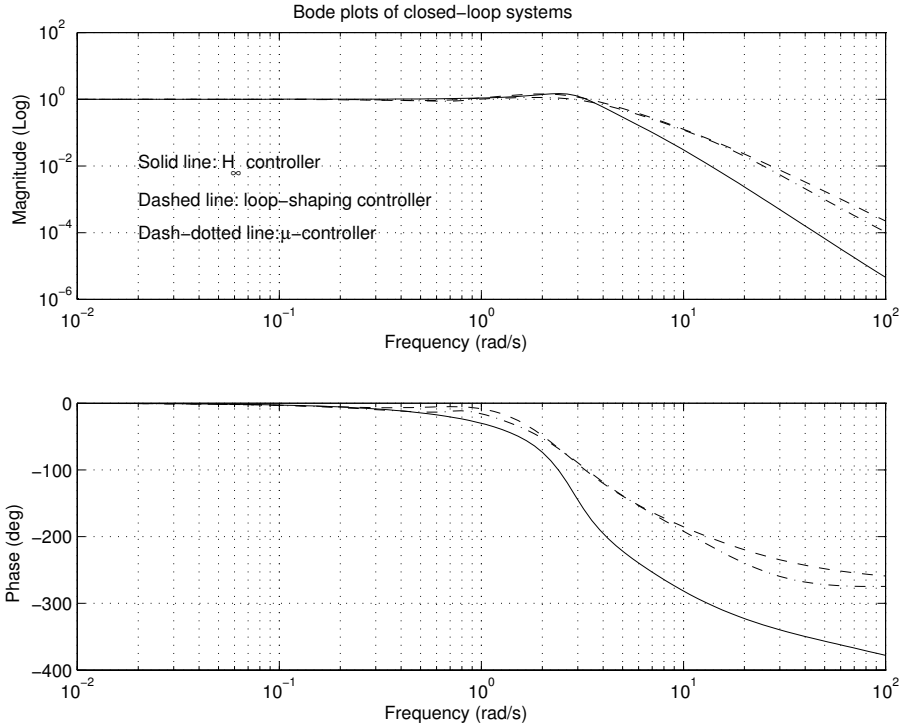

Fig. 8.42. Frequency responses of closed-loop systems

The comparison of the robust stability is conducted by the file `rbs_mds.m`.

File `rbs_mds.m`

```
omega = logspace(-1,2,100);
% Real perturbations
blkrs_R = [-1 1;-1 1;-1 1];
blkrs = [blkrsR; abs(blkrsR)];
pdim = 3;
%
% Hinf controller
clp_h = starp(sys_ic,K_hin);
clp_hg = frsp(clp_h,omega);
rob_stab = sel(clp_hg,[1:3],[1:3]);
fixl = [eye(pdim); 0.1*eye(pdim)]; % 1% Complex
fixr = fixl';
clp_mix = mmult(fixl,rob_stab,fixr);
```

```
rbnds_h = mu(clp_mix,blkrs);
%
% Loop Shaping controller
clp_lsh = starp(sys_ic,K_lsh);
clp_lshg = frsp(clp_lsh,omega);
rob_stab = sel(clp_lshg,[1:3],[1:3]);
fixl = [eye(pdim); 0.1*eye(pdim)]; % 1% Complex
fixr = fixl';
clp_mix = mmult(fixl,rob_stab,fixr);
rbnds_lsh = mu(clp_mix,blkrs);
%
% mu-controller
clp_mu = starp(sys_ic,K_mu);
clp_mug = frsp(clp_mu,omega);
rob_stab = sel(clp_mug,[1:3],[1:3]);
fixl = [eye(pdim); 0.1*eye(pdim)]; % 1% Complex
fixr = fixl';
clp_mix = mmult(fixl,rob_stab,fixr);
rbnds_mu = mu(clp_mix,blkrs);
%
figure(1)
vplot('liv,lm',sel(rbnds_h,1,1),'r-', ...
            sel(rbnds_lsh,1,1),'m--', ...
            sel(rbnds_mu,1,1),'c-.')
title('ROBUST STABILITY FOR ALL CONTROLLERS')
xlabel('Frequency (rad/s)')
ylabel('Upper bound of \mu')
```

The frequency responses of μ for three controllers are shown in Figure 8.43. The system with the $\mathcal{H}_\infty$ loop-shaping controller is characterized with best robust stability since in this case the destabilising perturbations have the largest norm (note that the norm of these perturbations is inversely proportional to the maximum value of μ).

The nominal performance of the closed-loop systems is obtained by the file `prf_mds.m`. The frequency responses of the weighted sensitivity functions of the nominal systems are shown in Figure 8.44. Again, the systems with the $\mathcal{H}_\infty$ loop-shaping and μ-controllers achieve better performance.

File `prf_mds.m`

```
omega = logspace(-2,2,100);
%
% H_infinity controller
clp_hin = starp(sys_ic,K_hin);
```

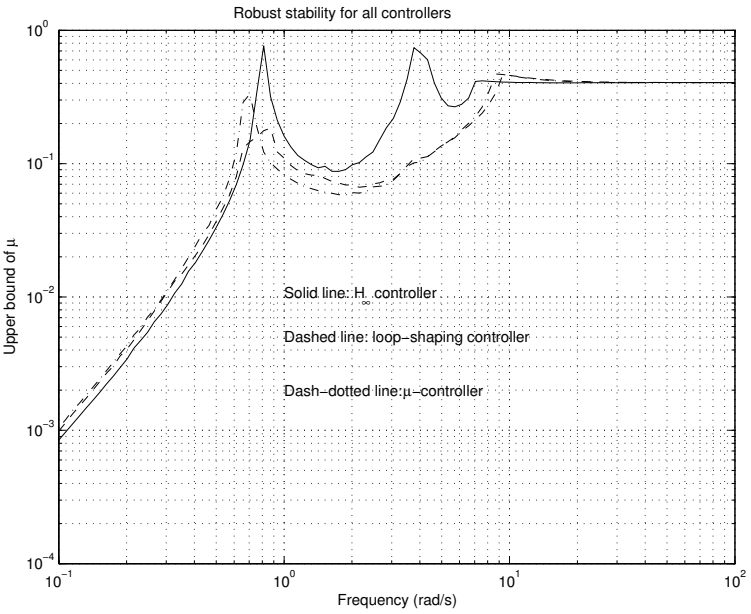

Fig. 8.43. Comparison of robust stability for 3 controllers

```
prf_hin = sel(clp_hin,4,4);
prf_hing = frsp(prf_hin,omega);
%
% Loop Shaping controller
clp_lsh = starp(sys_ic,K_lsh);
prf_lsh = sel(clp_lsh,4,4);
prf_lshg = frsp(prf_lsh,omega);
%
% mu-controller
clp_mu = starp(sys_ic,K_mu);
prf_mu = sel(clp_mu,4,4);
prf_mug = frsp(prf_mu,omega);
figure(1)
vplot('liv,m',vnorm(prf_hing),'r-',vnorm(prf_lshg), ...
      'm--',vnorm(prf_mug),'c-.')
title('NOMINAL PERFORMANCE: ALL CONTROLLERS')
xlabel('Frequency (rad/sec)')
```

The comparison of the robust performance is obtained by the file `rbp_mds.m`.

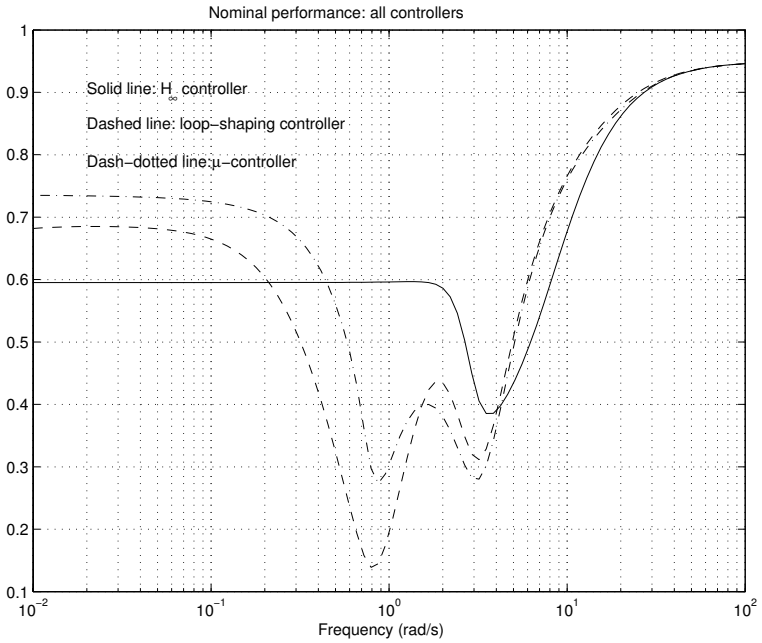

Fig. 8.44. Comparison of nominal performance for 3 controllers

File `rbp_mds.m`

```
blkrsR = [-1 1;-1 1;-1 1];
blkrp = [blkrsR;[1 2]];
omega = logspace(-2,2,100);
%
% H_infinity controller
clp_hin = starp(sys_ic,K_hin);
rbp_hin = frsp(clp_hin,omega);
bnd_hin = mu(rbp_hin,blkrp);
%
% Loop Shaping controller
clp_lsh = starp(sys_ic,K_lsh);
rbp_lsh = frsp(clp_lsh,omega);
bnd_lsh = mu(rbp_lsh,blkrp);
%
% mu-controller
clp_mu = starp(sys_ic,K_mu);
rbp_mu = frsp(clp_mu,omega);
bnd_mu = mu(rbp_mu,blkrp);
figure(1)
```

```
vplot('liv,m',bnd_hin,'r-',bnd_lsh,'m--',bnd_mu,'c-.')
title('ROBUST PERFORMANCE: ALL CONTROLLERS')
xlabel('Frequency (rad/sec)')
ylabel('\mu')
text(2.D+0,1.7D+0,'-   H_\infty controller')
text(2.D+0,1.6D+0,'--  Loop shaping controller')
text(2.D+0,1.5D+0,'-.  \mu-controller')
```

The μ values over the frequency range for all three designed systems are plotted in Figure 8.45. This confirms again that the system with the $\mathcal{H}_\infty$ controller does not achieve the robust performance criterion.

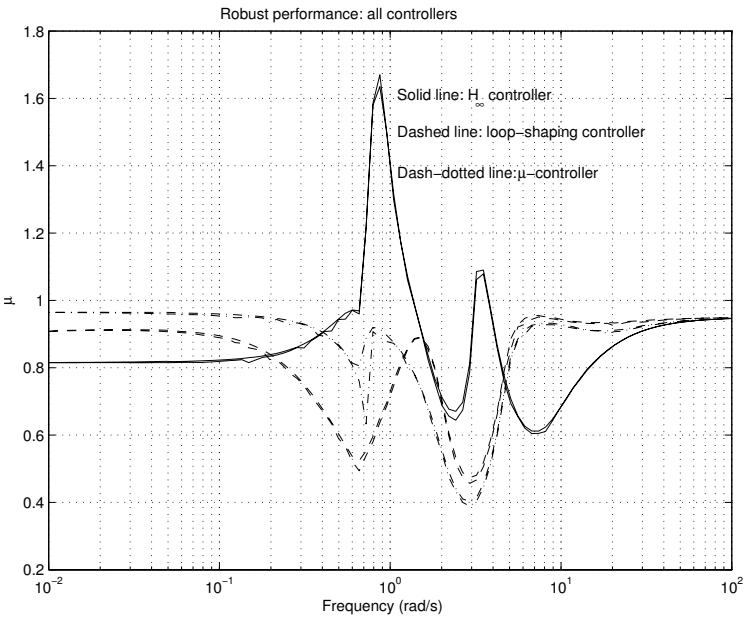

Fig. 8.45. Comparison of robust performance for 3 controllers

In summary, all three controllers ensure robust stability of the closed-loop system with respect to the parametric perturbations that are included in the 3×3 diagonal uncertainty matrix. However, the closed-loop system performance varies in a different way under the action of these diagonal perturbations. In the following file, `pdc_mds.m`, we use the function `wcperf`, which allows us to find the worst-case perturbation with respect to the performance, and to compare the performance of the three systems when the norm of perturbations increases. (The execution of this file may be accompanied by some warnings.)

File `pdc_mds.m`

```
omega = logspace(-2,3,100);
% Real perturbations
blks = [-1 1;-1 1;-1 1];
%
% H_infinity controller
clp_hin = starp(sys_ic,K_hin);
clp_hing = frsp(clp_hin,omega);
%
% Loop Shaping controller
clp_lsh = starp(sys_ic,K_lsh);
clp_lshg = frsp(clp_lsh,omega);
%
% mu-controller
clp_mu = starp(sys_ic,K_mu);
clp_mug = frsp(clp_mu,omega);
%
alpha = 0.1;
npts = 10;
[deltabadh,lowbndh,uppbndh] = wcperf(clp_hing,blks, ...
                                     alpha,npts);
[deltabadlsh,lowbndlsh,uppbndlsh] = wcperf(clp_lshg, ...
                                    blks,alpha,npts);
[deltabadmu,lowbndmu,uppbndmu] = wcperf(clp_mug,blks, ...
                                    alpha,npts);
figure(1)
vplot(lowbndh,'r-',uppbndh,'r-',lowbndlsh,'m--', ...
      uppbndlsh,'m--',lowbndmu,'c-.',uppbndmu,'c-.')
axis([0 1.8 0 2.0])
title('PERFORMANCE DEGRADATION CURVES FOR ALL CONTROLLERS')
xlabel('Size of Uncertainty')
text(1.0,0.6,'-H_\infty controller')
text(1.0,0.4,'-- Loop shaping controller')
text(1.0,0.2,'-. \mu-controller')
```

The results in Figure 8.46 show that the $\mathcal{H}_\infty$ loop-shaping controller and the μ-controller ensure robust performance for larger perturbations, with the former slightly outperforming the latter. The closed-loop performance deteriorates most rapidly with increasing perturbation magnitude in the case of the $\mathcal{H}_\infty$ controller.

The comparison results indicate that in the present exercise the $\mathcal{H}_\infty$ loop-shaping controller might be the best one to choose in terms of system robustness, though the μ-controller is not that far behind.

It is important to stress that in the above comparison the μ-controller is a reduced-order one of order 4. The order of the original μ-controller is actually

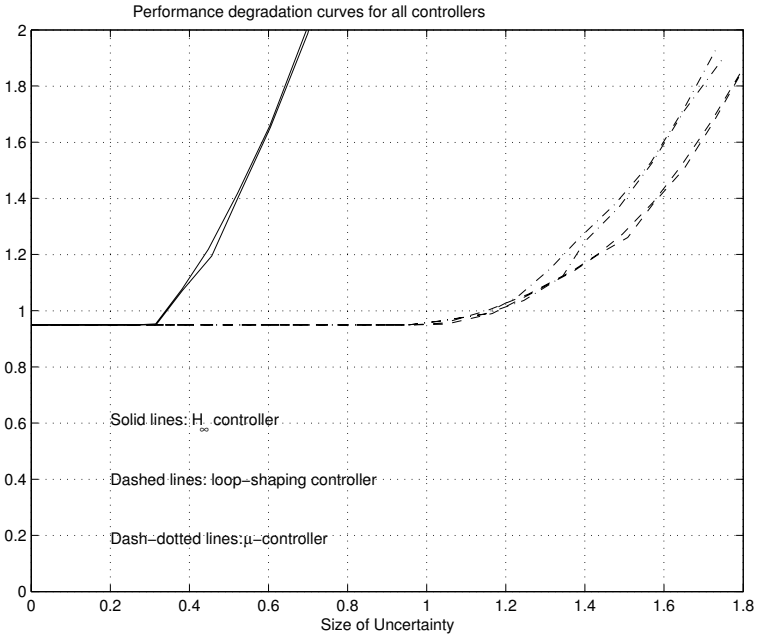

Fig. 8.46. Performance degradation for 3 controllers

20. However, the use of such a reduced-order μ-controller will be justified in the next section, which shows that the reduced-order controller does not seriously deteriorate the closed-loop system performance. It is also important to point out that for different design cases these three design approaches may well produce different results. That is, even the use of the $\mathcal{H}_\infty$ controller may lead to acceptable results in terms of performance and controller complexity. However, in general, in the case of structured uncertainty, the μ-synthesis will always produce more satisfactory and less conservative controllers.

8.12 Order Reduction of μ-controller

As shown in Section 8.9, the order of the μ-controller K_{mu} is 20, which makes it difficult in implementation. A reduced-order controller would be usually preferred. Various methods may be used to reduce the order, as discussed in Chapter 7. In this case study, the Hankel-norm approximation is used and implemented in the file `red_mds.m`. Two important commands in the file are `sysbal` and `hankmr`. The command `sysbal` generates the balanced realisation of a system (input argument) of the type `SYSTEM`. This command removes the unobservable and/or uncontrollable modes, if the system is not minimal. The command `sysbal` also returns the Hankel singular values of the system that

can be used to choose the order to be reduced. To use the file `red_mds.m`, first define

```
K = K_mu;
```

File `red_mds.m`

```
omega = logspace(-2,4,100);
K_g = frsp(K,omega);
[Kb,hsig] = sysbal(K);
Kred = hankmr(Kb,hsig,4,'d');
Kred_g = frsp(Kred,omega);
vplot('bode',K_g,'y-',Kred_g,'m--')
subplot(2,1,1)
title('BODE PLOTS OF FULL AND REDUCED ORDER CONTROLLERS')
subplot(2,1,2)
K = Kred;
```

In the present case the balanced realization Kb turns out to be of 20th order as well, which means that the state-space model of the μ-controller is already minimal. The Hankel singular values are

```
hsig =

  1.0e+003 *

   1.28877293261018
   0.01757808424290
   0.01413607705650
   0.00185159191695
   0.00043945590100
   0.00027713314731
   0.00013630163054
   0.00006894336934
   0.00002465391647
   0.00000787583669
   0.00000779094168
   0.00000247258791
   0.00000053897770
   0.00000023805949
   0.00000016178585
   0.00000008448505
   0.00000001681482
   0.00000000066695
   0.00000000021363
   0.00000000000201
```

Some of these values are very small, which suggests that the controller order can be greatly reduced. In this exercise this order is set equal to 4 in the command `hankmr` and the test with this reduced-order controller shows that the closed-loop system obtained is stable. Actually, a 3rd-order controller has been tried as well, but noticeable differences exist in the frequency responses in the range of $10^{-1} - 10^{1}$ rad/s. The system matrices of this 4th order controller are

```
[Ak,Bk,Ck,Dk] = unpck(K)

Ak =

  -5.94029444678383 -12.71890180361086  11.09659323806946
  15.39552256762868 -29.53184484831400 -16.41287136235254
                  0                   0  -6.84730630402175
                  0                   0                  0

                                          -0.04081607183541
                                           0.00507186515891
                                           0.03584524485830
                                          -0.00125108980521
Bk =

 -15.96860717359783
   7.91326562204500
  13.97349755769254
  -1.79576743717989


Ck =

 -12.96086158489860 -14.24741790999237   9.28057043520263
                                         -1.79885756979541


Dk =

   0.54044998732827
```

In Figure 8.47 we display the frequency responses of the full-order and reduced-order controllers. The responses plots practically coincide with each other, for frequencies up to 100 rad/s (up to about 1000 rad/s in magnitude) that ensures almost the same closed-loop performance for both controllers. In particular, the transient responses of the closed-loop systems with full-order and reduced-order controllers are practically indistinguishable (compare Figure 8.48 with Figure 8.38). Clearly, the 4th-order controller is implemented much easier compared to the 20th-order controller.

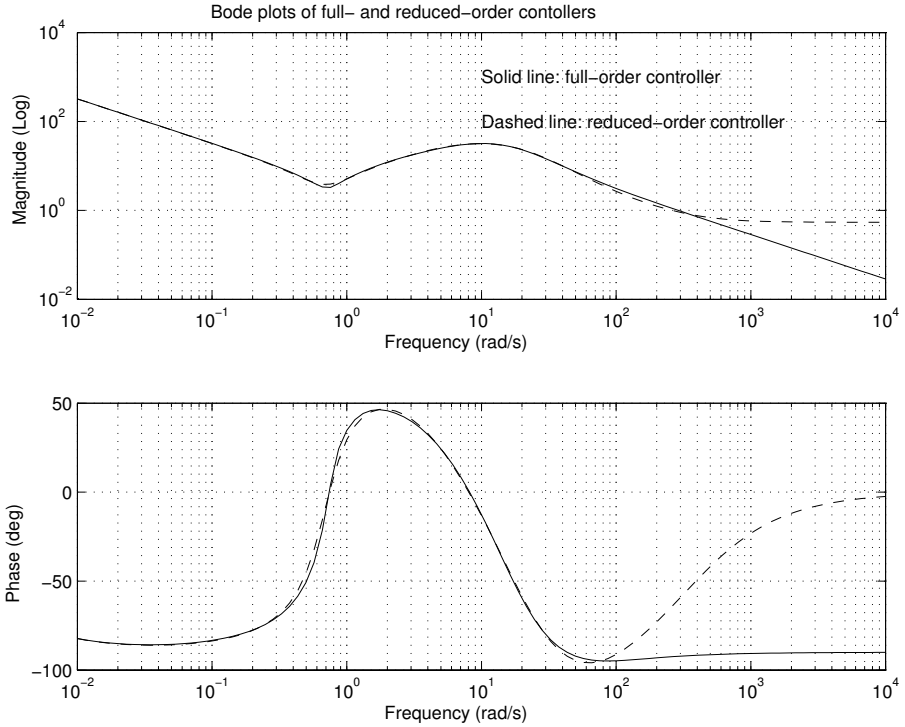

Fig. 8.47. Frequency responses of full- and reduced-order controllers

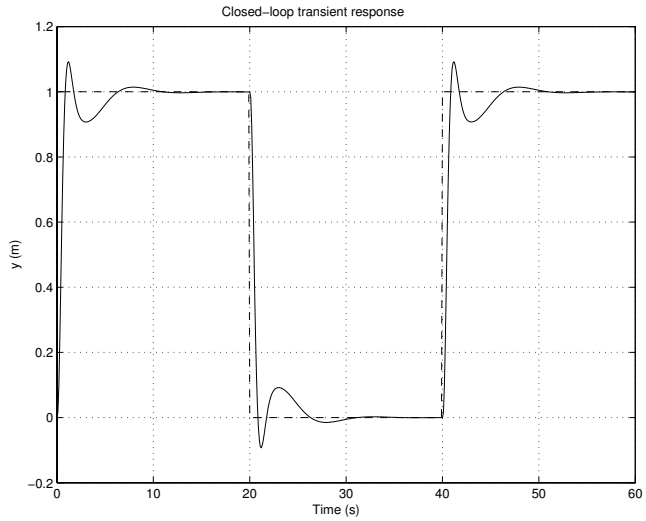

Fig. 8.48. Transient response for reduced-order controller

8.13 Conclusions

The design exercise of the mass-damper-spring system leads to the following conclusions.

- Even for a low-order plant such as the mass-damper-spring system the derivation of the uncertainty model may not be straightforward. For a system with parametric perturbations, it has to form a standard configuration in order to use the analysis and design commands from the Robust Control Toolbox. In this procedure, it may be convenient to consider separately the uncertain parameters, describe these perturbation influences by simple LFTs and construct the whole uncertainty model of the plant by using the function `sysic`.
- Finding appropriate weighting functions is a crucial step in robust control designs. It usually involves trial and error. Design experience and knowledge of the plants will help in choosing weighting functions.
- Best design results for this particular system are obtained by using the $\mathcal{H}_\infty$ loop-shaping design procedure and μ-synthesis. With nearly identical robustness properties, the μ-controller gives better transient responses with smaller overshoot than the $\mathcal{H}_\infty$ LSDP controller.
- Even for a second-order plant like this, the order of the μ-controller may be very high (20 in the given design). This makes it necessary to apply model reductions. Usually, the order may be reduced significantly without serious performance degradation.

Notes and References

The derivation of the uncertainty model of mass-damper-spring system is shown in [175, Chapter 10]. A model, obtained by using the function `sysic` and implemented by the file `sys_mds.m`, is presented in [9, Chapter 4].

9

A Triple Inverted Pendulum Control-system Design

Robust design of a triple inverted pendulum control system is discussed in this chapter.

The triple inverted pendulum is an interesting control system that resembles many features found in, for instance, walking robots and flexible space structures, and other industrial applications. This kind of pendulum system is difficult to control due to the inherent instability and nonlinear behaviour. Some of the pendulum parameters may not be known exactly in practice, which influences significantly the system dynamics.

In the design of a robust control system for triple inverted pendulums it is conventionally assumed that the system is affected by unstructured uncertainties and thus the robust properties of the closed-loop system could be achieved by using an $\mathcal{H}_\infty$ controller. In real cases, however, the uncertainties of such a pendulum system would be more reasonably considered to have some structures. For instance, because the moments of inertia and the friction coefficients are difficult to estimate precisely, it makes sense to assume unknown deviations in those parameters. Also, we would like to design the closed-loop control system to be more "robust" against those parameters that have a "larger" or more serious influence upon the system behaviour. For instance, the viscous friction in the joints may destroy the controllability of the linearised model. Hence, it would be important to treat uncertainties in such parameters individually rather than congregate them in an overall, unstructured uncertainty of the system dynamics. Consequently, it may be more suitable to apply the μ-synthesis technique that may lead to a less-conservative design to meet tighter design specifications.

In the pendulum control-system design we first model the uncertainties as a mixed type that consists of complex uncertainties in the actuators, real uncertainties in the moments of inertia and in the viscous friction coefficients. A two-degree-of-freedom (2DOF) design framework is adopted. Both $\mathcal{H}_\infty$ suboptimal and μ-controllers are designed. The $\mathcal{H}_\infty$ controller shows better transient and disturbance responses but does not ensure robust stability nor robust performance. The μ-controller achieves both robust stability and robust per-

formance, however, at the price of poorer time responses. The μ-controller designed is initially of quite high order, which makes it unsuitable for implementation in practice. A model reduction is then conducted that leads to a reduced-order controller maintaining the required robust stability and robust performance of the closed-loop system.

9.1 System Description

The triple inverted pendulum considered is the experimental setup realized by Furuta *et al.* [41] (Figure 9.1). The pendulum consists of three arms that are hinged by ball bearings and can rotate in the vertical plane. The torques of the two upper hinges are controlled by motors, with the lowest hinge made free for rotation. By controlling the angles of the two upper arms around specified values, the pendulum can be stabilised inversely with the desired angle attitudes. A horizontal bar is fixed to each of the arms to ease the control by increasing the moment of inertia. Two dc motors, M_1 and M_2, are mounted on the first and third arm, respectively, acting as actuators that provide torques to the two upper hinges through timing belts. The potentiometers P_1, P_2 and P_3 are fixed to the hinges to measure the corresponding angles.

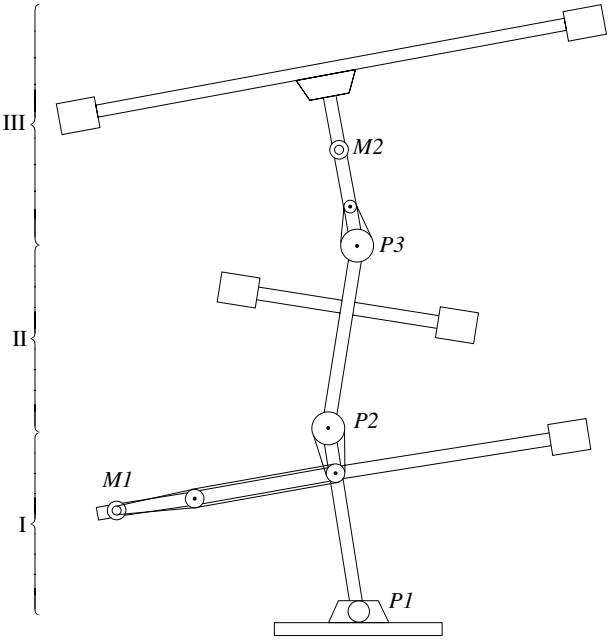

Fig. 9.1. Triple inverted pendulum

Let Θ_i denote the angle of the ith arm. The first potentiometer measures the angle Θ_1, and the second and third potentiometers measure the angles $\Theta_2 - \Theta_1$ and $\Theta_3 - \Theta_2$, respectively (Figure 9.2).

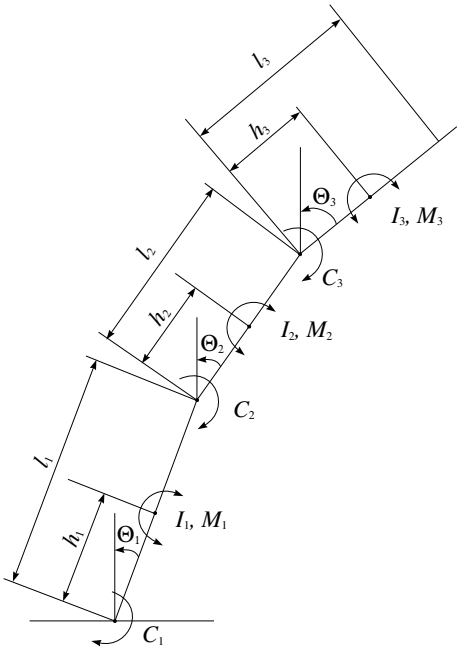

Fig. 9.2. Geometric relationship of potentiometers

The mathematical description of the triple inverted pendulum is derived under the following assumptions:

(a) each arm is a rigid body;
(b) the lengths of the belts remain constant during the operation of the system;
(c) the friction force in the bottom hinge is proportional to the velocity of the bottom arm and the friction forces in the upper hinges are proportional to the differences of the respective velocities of two neighbouring arms.

We shall first consider the mathematical model of the pendulum itself, without the actuators. The pendulum model is constructed using the Lagrange differential equations [41] that yield the following nonlinear vector-matrix differential equation

$$M(\Theta)\begin{bmatrix}\ddot{\Theta}_1\\ \ddot{\Theta}_2\\ \ddot{\Theta}_3\end{bmatrix} + N\begin{bmatrix}\dot{\Theta}_1\\ \dot{\Theta}_2\\ \dot{\Theta}_3\end{bmatrix} + \begin{bmatrix}q_1\\ q_2\\ q_3\end{bmatrix} + G\begin{bmatrix}t_{m_1}\\ t_{m_2}\end{bmatrix} = T\begin{bmatrix}\tau_1\\ \tau_2\\ \tau_3\end{bmatrix} \tag{9.1}$$

where, $\Theta = \begin{bmatrix} \Theta_1 \\ \Theta_2 \\ \Theta_3 \end{bmatrix}$

$$M(\Theta) =$$

$$\begin{bmatrix} J_1 + I_{p_1} & l_1 M_2 \cos(\Theta_1 - \Theta_2) - I_{p_1} & l_1 M_3 \cos(\Theta_1 - \Theta_3) \\ l_1 M_2 \cos(\Theta_1 - \Theta_2) - I_{p_1} & J_2 + I_{p_1} + I_{p_2} & l_2 M_3 \cos(\Theta_2 - \Theta_3) - I_{p_2} \\ l_1 M_3 \cos(\Theta_1 - \Theta_3) & l_2 M_3 \cos(\Theta_2 - \Theta_3) - I_{p_2} & J_3 + I_{p_2} \end{bmatrix}$$

$$N = \begin{bmatrix} C_1 + C_2 + C_{p_1} & -C_2 - C_{p_1} & 0 \\ -C_2 - C_{p_1} & C_{p_1} + C_{p_2} + C_2 + C_3 & -C_3 - C_{p_2} \\ 0 & -C_3 - C_{p_2} & C_3 + C_{p_2} \end{bmatrix}$$

$$q_1 = l_1 M_2 \sin(\Theta_1 - \Theta_2)\dot{\Theta}_2^2 + l_1 M_3 \sin(\Theta_1 - \Theta_3)\dot{\Theta}_3^2 - M_1 g \sin(\Theta_1)$$

$$q_2 = l_1 M_2 \sin(\Theta_1 - \Theta_2)\dot{\Theta}_1^2 + l_2 M_3 \sin(\Theta_2 - \Theta_3)\dot{\Theta}_3^2 - M_2 g \sin(\Theta_2)$$

$$q_3 = l_1 M_3 \sin(\Theta_1 - \Theta_3)(\dot{\Theta}_1^2 - 2\dot{\Theta}_1\dot{\Theta}_3) + l_2 M_3 \sin(\Theta_2 - \Theta_3)(\dot{\Theta}_2^2 - 2\dot{\Theta}_2\dot{\Theta}_3)$$
$$- M_3 g \sin(\Theta_3),$$

$$G = \begin{bmatrix} K_1 & 0 \\ -K_1 & K_2 \\ 0 & -K_2 \end{bmatrix},\ T = \begin{bmatrix} 1 & -1 & 0 \\ 0 & 1 & -1 \\ 0 & 0 & 1 \end{bmatrix}$$

$$C_{p_i} = C_{p_i'} + K_i^2 C_{m_i},\ I_{p_i} = I_{p_i'} + K_i^2 I_{m_i},$$

$$M_1 = m_1 h_1 + m_2 l_1 + m_3 l_1,\ M_2 = m_2 h_2 + m_3 l_2,\ M_3 = m_3 h_3$$

$$J_1 = I_1 + m_1 h_1^2 + m_2 l_1^2 + m_3 l_1^2,\ J_2 = I_2 + m_2 h_2^2 + m_3 l_2^2$$

$$J_3 = I_3 + m_3 h_3^2$$

and all other parameters and variables are defined in Table 9.1.

After linearisation of (9.1) under the assumptions of small deviations of the pendulum from the vertical position and of small velocities, one obtains the following equation

$$M \begin{bmatrix} \ddot{\Theta}_1 \\ \ddot{\Theta}_2 \\ \ddot{\Theta}_3 \end{bmatrix} + N \begin{bmatrix} \dot{\Theta}_1 \\ \dot{\Theta}_2 \\ \dot{\Theta}_3 \end{bmatrix} + P \begin{bmatrix} \Theta_1 \\ \Theta_2 \\ \Theta_3 \end{bmatrix} + G \begin{bmatrix} t_{m_1} \\ t_{m_2} \end{bmatrix} = T \begin{bmatrix} \tau_1 \\ \tau_2 \\ \tau_3 \end{bmatrix} \tag{9.2}$$

where

$$M = \begin{bmatrix} J_1 + I_{p_1} & l_1 M_2 - I_{p_1} & l_1 M_3 \\ l_1 M_2 - I_{p_1} & J_2 + I_{p_1} + I_{p_2} & l_2 M_3 - I_{p_2} \\ l_1 M_3 & l_2 M_3 - I_{p_2} & J_3 + I_{p_2} \end{bmatrix}$$

$$P = \begin{bmatrix} M_1 g & 0 & 0 \\ 0 & -M_2 g & 0 \\ 0 & 0 & -M_3 g \end{bmatrix}$$

By introducing the control torques vector $t_m = [t_{m_1}\ t_{m_2}]^T$ and the vector of disturbance torques $d = [\tau_1,\ \tau_2,\ \tau_3]^T$, (9.2) can be rewritten in the form

Table 9.1. System nomenclature

Symbol	Description
u_j	input voltage to the jth motor
t_{m_j}	control torque of the jth motor
τ_i	disturbance torque to the ith arm
l_i	length of the ith arm
h_i	the distance from the bottom to the centre of gravity of the ith arm
m_i	mass of the ith arm
I_i	moment of inertia of the i-th arm around the centre of gravity
C_i	coefficient of viscous friction of the ith hinge
Θ_i	angle of the ith arm from vertical line
C_{m_i}	viscous friction coefficient of the ith motor
I_{m_i}	moment of inertia of the ith motor
K_i	ratio of teeth of belt-pulley system of the ith hinge
$C_{p_i'}$	viscous friction coefficient of the belt-pulley system of the ith hinge
$I_{p_i'}$	moment of inertia of the belt-pulley system of the ith hinge
α_i	gain of the ith potentiometer
g	acceleration of gravity

$$M\ddot{\Theta} + N\dot{\Theta} + P\Theta + Gt_m = Td$$

i.e.,

$$\ddot{\Theta} = -M^{-1}N\dot{\Theta} - M^{-1}P\Theta - M^{-1}Gt_m + M^{-1}Td.$$

The block-diagram of the pendulum system is shown in Figure 9.3 and the nominal values of the parameters are given in Table 9.2.

9.2 Modelling of Uncertainties

Based on practical considerations, we in particular consider the variations of the moments of inertia I_1, I_2 and I_3 of the three arms and the variations of the viscous friction coefficients C_1, C_2, C_3 and C_{p_1}, C_{p_2}. It is assumed that the moments of inertia are constants but with possible relative error of 10% around the nominal values; similarly, the friction coefficients may have with 15% relative errors.

Notice that in the rest of the chapter, a parameter with a bar above denotes its nominal value.

Therefore, the actual moments of inertia are presented as

$$I_i = \overline{I}_i(1 + p_i\delta_{I_i}),\ i = 1,\ 2,\ 3$$

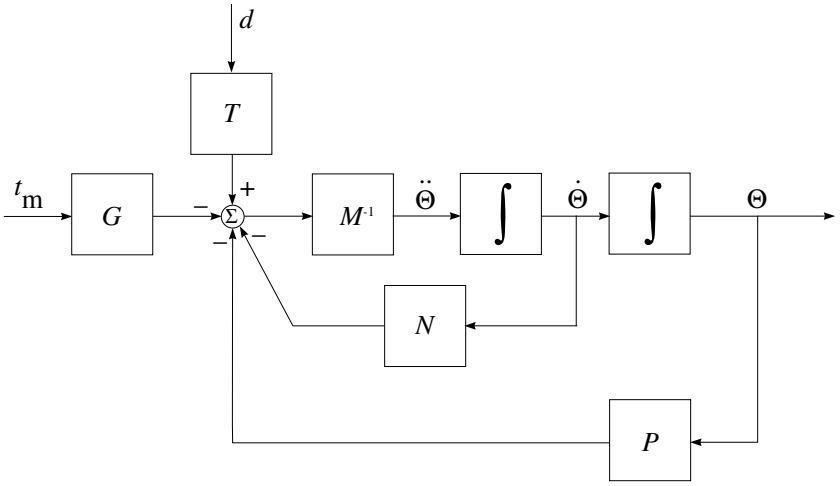

Fig. 9.3. Block diagram of the triple inverted pendulum system

Table 9.2. Nominal values of the parameters

Symbol (unit)	value	Symbol (unit)	value
l_1 (m)	0.5	α_1 (V/rad)	1.146
l_2 (m)	0.4	α_2 (V/rad)	1.146
h_1 (m)	0.35	α_3 (V/rad)	0.9964
h_2 (m)	0.181	C_{m_1} (N m s)	2.19×10^{-3}
h_3 (m)	0.245	C_{m_2} (N m s)	7.17×10^{-4}
m_1 (kg)	3.25	I_{m_1} (kg m^2)	2.40×10^{-5}
m_2 (kg)	1.90	I_{m_2} (kg m^2)	4.90×10^{-6}
m_3 (kg)	2.23	$C_{p_1'}$ (N m s)	0
I_1 (kg m^2)	0.654	$C_{p_2'}$ (N m s)	0
I_2 (kg m^2)	0.117	$I_{p_1'}$ (kg m^2)	7.95×10^{-3}
I_3 (kg m^2)	0.535	$I_{p_2'}$ (kg m^2)	3.97×10^{-3}
C_1 (N m s)	6.54×10^{-2}	K_1	30.72
C_2 (N m s)	2.32×10^{-2}	K_2	27.00
C_3 (N m s)	8.80×10^{-3}		

where $\overline{I}_i$ is the nominal value of the corresponding moment of inertia, $p_i = 0.10$ is the maximum relative uncertainty in each of these moments and $-1 \leq \delta_{I_i} \leq 1$, $i = 1, 2, 3$. As a result, the matrix M is obtained in the form

$$M = \overline{M} + M_p \Delta_I$$

where the elements of $\overline{M}$ are determined by the nominal values of the moments of inertia,

$$\overline{M} = \begin{bmatrix} \overline{J}_1 + \overline{I}_{p_1} & \overline{l}_1\overline{M}_2 - \overline{I}_{p_1} & \overline{l}_1\overline{M}_3 \\ \overline{l}_1\overline{M}_2 - \overline{I}_{p_1} & \overline{J}_2 + \overline{I}_{p_1} + \overline{I}_{p_2} & \overline{l}_2\overline{M}_3 - \overline{I}_{p_2} \\ \overline{l}_1\overline{M}_3 & \overline{l}_2\overline{M}_3 - \overline{I}_{p_2} & \overline{J}_3 + \overline{I}_{p_2} \end{bmatrix}$$

and

$$M_p = \begin{bmatrix} \overline{I}_1 p_1 & 0 & 0 \\ 0 & \overline{I}_2 p_2 & 0 \\ 0 & 0 & \overline{I}_3 p_3 \end{bmatrix},\ \Delta_I = \begin{bmatrix} \delta_{I_1} & 0 & 0 \\ 0 & \delta_{I_2} & 0 \\ 0 & 0 & \delta_{I_3} \end{bmatrix}$$

Next we calculate the matrix M^{-1}. We have that

$$M^{-1} = (M_p^{-1}\overline{M} + \Delta_I)^{-1} M_p^{-1}$$

Using the Matrix Inversion Lemma, we obtain

$$(M_p^{-1}\overline{M} + \Delta_I)^{-1} = \overline{M}^{-1} M_p - \overline{M}^{-1} M_p \Delta_I (\overline{M}^{-1} M_p \Delta_I + I_3)^{-1} \overline{M}^{-1} M_p$$

where I_3 is the 3×3 unit matrix. Therefore, we have

$$M^{-1} = \overline{M}^{-1} - \overline{M}^{-1} M_p \Delta_I (I_3 + \overline{M}^{-1} M_p \Delta_I)^{-1} \overline{M}^{-1}$$

The matrix M^{-1} can be represented as an upper linear fractional transformation (LFT)

$$M^{-1} = F_U(Q_I, \Delta_I) = Q_{I_{22}} + Q_{I_{21}} \Delta_I (I_3 - Q_{I_{11}} \Delta_I)^{-1} Q_{I_{12}}$$

where

$$Q_{I_{11}} = -\overline{M}^{-1} M_p,\ Q_{I_{12}} = \overline{M}^{-1}$$
$$Q_{I_{21}} = -\overline{M}^{-1} M_p,\ Q_{I_{22}} = \overline{M}^{-1}$$

such that

$$Q_I = \begin{bmatrix} Q_{I_{11}} & Q_{I_{12}} \\ Q_{I_{21}} & Q_{I_{22}} \end{bmatrix} = \begin{bmatrix} -\overline{M}^{-1} M_p & \overline{M}^{-1} \\ -\overline{M}^{-1} M_p & \overline{M}^{-1} \end{bmatrix}$$

Let us now consider the uncertainties in the friction coefficients. It can be seen that C_{p_1} and C_2 always appear together and so do C_{p_2} and C_3, in the matrix N. Further, the magnitude of C_{p_1} and C_{p_2} is much smaller in comparison to that of C_2 and C_3, Hence, the related uncertainties in C_{p_1} and C_{p_2} have much less influence with regard to the system dynamics. We may therefore assume

$$C_2 + C_{p_1} = (\overline{C}_2 + \overline{C}_{p_1})(1 + s_2 \delta_{C_2})$$

$$C_3 + C_{p_2} = (\overline{C}_3 + \overline{C}_{p_2})(1 + s_3 \delta_{C_3})$$

where $s_2 = s_3 = 0.15$ and $-1 \leq \delta_{C_2},\ \delta_{C_3} \leq 1$. Similarly, we set

$$C_1 = \overline{C}_1(1 + s_1 \delta_{C_1})$$

where $s_1 = 0.15$ and $-1 \leq \delta_{C_1} \leq 1$.

Taking into account the uncertainties in the friction coefficients, we obtain

$$N = \overline{N} + \Delta N$$

where

$$\overline{N} = \begin{bmatrix} \overline{C}_1 + \overline{C}_2 + \overline{C}_{p_1} & -\overline{C}_2 - \overline{C}_{p_1} & 0 \\ -\overline{C}_2 - \overline{C}_{p_1} & \overline{C}_2 + \overline{C}_{p_1} + \overline{C}_3 + \overline{C}_{p_2} & -\overline{C}_3 - \overline{C}_{p_2} \\ 0 & -\overline{C}_3 - \overline{C}_{p_2} & \overline{C}_3 + \overline{C}_{p_2} \end{bmatrix}$$

and

$$\Delta N = \begin{bmatrix} \overline{C}_1 s_1 \delta_{C_1} + (\overline{C}_2 + \overline{C}_{p_1}) s_2 \delta_{C_2} & -(\overline{C}_2 + \overline{C}_{p_1}) s_2 \delta_{C_2} & 0 \\ -(\overline{C}_2 + \overline{C}_{p_1}) s_2 \delta_{C_2} & (\overline{C}_2 + \overline{C}_{p_1}) s_2 \delta_{C_2} + (\overline{C}_3 + \overline{C}_{p_2}) s_3 \delta_{C_3} & -(\overline{C}_3 + \overline{C}_{p_2}) s_3 \delta_{C_3} \\ 0 & -(\overline{C}_3 + \overline{C}_{p_2}) s_3 \delta_{C_3} & (\overline{C}_3 + \overline{C}_{p_2}) s_3 \delta_{C_3} \end{bmatrix}$$

The matrix ΔN may be represented as

$$\Delta N = N_1 \Delta_C N_2$$

where

$$N_1 = \begin{bmatrix} \overline{C}_1 s_1 & -(\overline{C}_2 + \overline{C}_{p_1}) s_2 & 0 \\ 0 & (\overline{C}_2 + \overline{C}_{p_1}) s_2 & -(\overline{C}_3 + \overline{C}_{p_2}) s_3 \\ 0 & 0 & (\overline{C}_3 + \overline{C}_{p_2}) s_3 \end{bmatrix}$$

$$N_2 = \begin{bmatrix} 1 & 0 & 0 \\ -1 & 1 & 0 \\ 0 & -1 & 1 \end{bmatrix}, \ \Delta_C = \begin{bmatrix} \delta_{C_1} & 0 & 0 \\ 0 & \delta_{C_2} & 0 \\ 0 & 0 & \delta_{C_3} \end{bmatrix}$$

In turn, the matrix $N = \overline{N} + N_1 \Delta_C N_2$ can be rewritten as an upper LFT

$$N = F_U(Q_C, \Delta_C) = Q_{C_{22}} + Q_{C_{21}} \Delta_C (I_3 - Q_{C_{11}} \Delta_C)^{-1} Q_{C_{12}}$$

where

$$Q_{C_{11}} = 0_{3\times 3}, \ Q_{C_{12}} = N_2, \ Q_{C_{21}} = N_1, \ Q_{C_{22}} = \overline{N}$$

such that

$$Q_C = \begin{bmatrix} Q_{C_{11}} & Q_{C_{12}} \\ Q_{C_{21}} & Q_{C_{22}} \end{bmatrix} = \begin{bmatrix} 0_{3\times 3} & N_2 \\ N_1 & \overline{N} \end{bmatrix}$$

To represent the pendulum model as an LFT of the real uncertain parameters δ_{I_1}, δ_{I_2}, δ_{I_3}, and δ_{C_1}, δ_{C_2}, δ_{C_3}, we first extract out the uncertain parameters and then denote the inputs and outputs of Δ_I and Δ_C as y_I, y_C and u_I, u_C, respectively, as shown in Figure 9.4.

The dynamic equation of the pendulum system is then rearranged as

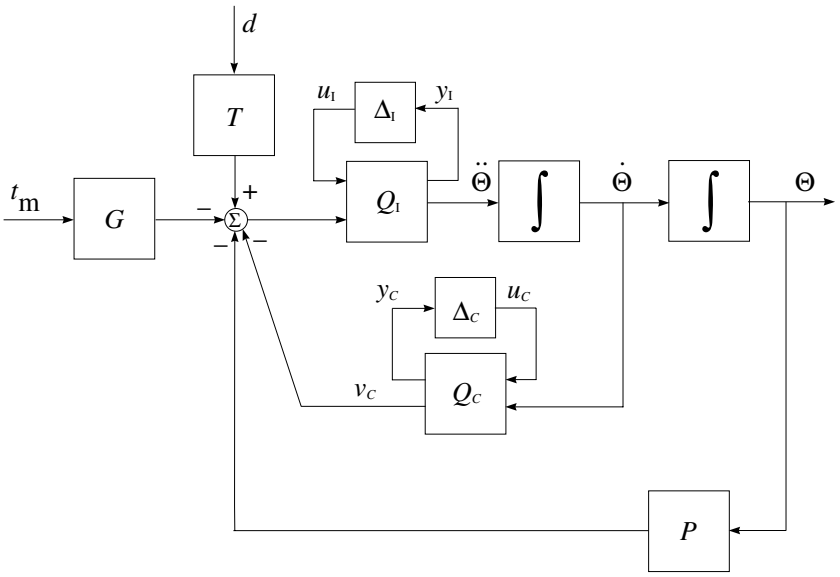

Fig. 9.4. System block diagram with uncertain parameters

$$\begin{bmatrix} y_I \\ \ddot{\Theta} \end{bmatrix} = \begin{bmatrix} -\overline{M}^{-1} M_p \, \overline{M}^{-1} \\ -\overline{M}^{-1} M_p \, \overline{M}^{-1} \end{bmatrix} \begin{bmatrix} u_I \\ Td - (Gt_m + v_C + P\Theta) \end{bmatrix}$$

$$\begin{bmatrix} y_c \\ v_c \end{bmatrix} = \begin{bmatrix} 0_{3\times 3} & N_2 \\ N_1 & \overline{N} \end{bmatrix} \begin{bmatrix} u_c \\ \dot{\Theta} \end{bmatrix}$$
$$u_I = \Delta_I y_I$$
$$u_C = \Delta_C y_C$$

The pendulum state vector $x = [x_1 \; x_2 \; x_3 \; x_4 \; x_5 \; x_6]^T$ is defined by

$$x_1 = \Theta_1, \; x_2 = \Theta_2, \; x_3 = \Theta_3, \; x_4 = \dot{\Theta}_1, \; x_5 = \dot{\Theta}_2, \; x_6 = \dot{\Theta}_3$$

Hence

$$\begin{bmatrix} \dot{x}_1 \; \dot{x}_2 \; \dot{x}_3 \end{bmatrix}^T = \dot{\Theta}$$

and

$$\begin{bmatrix} \dot{x}_4 \; \dot{x}_5 \; \dot{x}_6 \end{bmatrix}^T = \ddot{\Theta}$$

As for the output vector, we define

$$y = [\Theta_1 \; \Theta_2 \; \Theta_3]^T$$

The outputs are measured by linear potentiometers, whose voltages are given by

$$y_{p_1} = \alpha_1 \Theta_1, \; y_{p_2} = \alpha_2(\Theta_2 - \Theta_1), \; y_{p_3} = \alpha_3(\Theta_3 - \Theta_2)$$

By introducing the vector of the measured outputs

$$y_p = [y_{p_1}\ y_{p_2}\ y_{p_3}]^T$$

we obtain that

$$y_p = C_p\Theta,\ \ C_p = \begin{bmatrix} \alpha_1 & 0 & 0 \\ -\alpha_2 & \alpha_2 & 0 \\ 0 & -\alpha_3 & \alpha_3 \end{bmatrix}$$

As a result, we obtain the equations of the system

$$\begin{bmatrix} \dot{x}_1 \\ \dot{x}_2 \\ \dot{x}_3 \end{bmatrix} = \dot{\Theta}$$

$$\begin{bmatrix} \dot{x}_4 \\ \dot{x}_5 \\ \dot{x}_6 \end{bmatrix} = -\overline{M}^{-1}M_p u_I + \overline{M}^{-1}Td - \overline{M}^{-1}(Gt_m + v_C + P\Theta)$$

$$\begin{aligned} y_I &= -\overline{M}^{-1}M_p u_I + \overline{M}^{-1}Td - \overline{M}^{-1}(Gt_m + v_C + P\Theta) \\ y_C &= N_2\dot{\Theta} \\ v_C &= N_1 u_C + \overline{N}\dot{\Theta} \\ y &= \Theta \\ y_p &= C_p\Theta \\ u_I &= \Delta_I y_I \\ u_C &= \Delta_C y_C \end{aligned}$$

By substituting the variable v_C in the equations of $\ddot{\Theta}$ and y_I, respectively, the system equations are summarised as

$$\begin{bmatrix} \dot{x}_1 \\ \dot{x}_2 \\ \dot{x}_3 \\ \dot{x}_4 \\ \dot{x}_5 \\ \dot{x}_6 \\ -- \\ y_I \\ y_C \\ -- \\ y \\ y_p \end{bmatrix} = \Pi \begin{bmatrix} x_1 \\ x_2 \\ x_3 \\ x_4 \\ x_5 \\ x_6 \\ -- \\ u_I \\ u_C \\ -- \\ d \\ t_m \end{bmatrix} \tag{9.3}$$

$$\begin{bmatrix} u_I \\ u_C \end{bmatrix} = \begin{bmatrix} \Delta_I & 0 \\ 0 & \Delta_C \end{bmatrix} \begin{bmatrix} y_I \\ y_C \end{bmatrix} \tag{9.4}$$

where

$$\Pi =$$

$$\left[\begin{array}{cc|cc|cc}
0_{3\times3} & I_{3\times3} & 0_{3\times3} & 0_{3\times3} & 0_{3\times3} & 0_{3\times2} \\
-\overline{M}^{-1}P & -\overline{M}^{-1}\overline{N} & -\overline{M}^{-1}M_p & -\overline{M}^{-1}N_1 & \overline{M}^{-1}T & -\overline{M}^{-1}G \\
\hline
-\overline{M}^{-1}P & -\overline{M}^{-1}\overline{N} & -\overline{M}^{-1}M_p & -\overline{M}^{-1}N_1 & \overline{M}^{-1}T & -\overline{M}^{-1}G \\
0_{3\times3} & N_2 & 0_{3\times3} & 0_{3\times3} & 0_{3\times3} & 0_{3\times2} \\
\hline
I_{3\times3} & 0_{3\times3} & 0_{3\times3} & 0_{3\times3} & 0_{3\times3} & 0_{3\times2} \\
C_p & 0_{3\times3} & 0_{3\times3} & 0_{3\times3} & 0_{3\times3} & 0_{3\times2}
\end{array}\right]$$

Thus, the open-loop, pendulum model

$$\begin{bmatrix} y_I \\ y_C \\ y \\ y_p \end{bmatrix} = G_{\text{pend}} \begin{bmatrix} u_I \\ u_C \\ d \\ t_m \end{bmatrix}$$

is an eleven-input, twelve-output system with six states, where

$$G_{\text{pend}} = \left[\begin{array}{c|cc} A & B_1 & B_2 \\ \hline C_1 & D_{11} & D_{12} \\ C_2 & D_{21} & D_{22} \end{array}\right]$$

and

$$A = \begin{bmatrix} 0_{3\times3} & I_{3\times3} \\ -\overline{M}^{-1}P & -\overline{M}^{-1}\overline{N} \end{bmatrix},\ B_1 = \begin{bmatrix} 0_{3\times3} & 0_{3\times3} \\ -\overline{M}^{-1}M_p & -\overline{M}^{-1}N_1 \end{bmatrix}$$

$$B_2 = \begin{bmatrix} 0_{3\times3} & 0_{3\times2} \\ \overline{M}^{-1}T & -\overline{M}^{-1}G \end{bmatrix}$$

$$C_1 = \begin{bmatrix} -\overline{M}^{-1}P & -\overline{M}^{-1}\overline{N} \\ 0_{3\times3} & N_2 \end{bmatrix},\ D_{11} = \begin{bmatrix} -\overline{M}^{-1}M_p & -\overline{M}^{-1}N_1 \\ 0_{3\times3} & 0_{3\times3} \end{bmatrix}$$

$$D_{12} = \begin{bmatrix} \overline{M}^{-1}T & -\overline{M}^{-1}G \\ 0_{3\times3} & 0_{3\times2} \end{bmatrix}$$

$$C_2 = \begin{bmatrix} I_{3\times3} & 0_{3\times3} \\ C_p & 0_{3\times3} \end{bmatrix},\ D_{21} = 0_{6\times6},\ D_{22} = 0_{6\times5}$$

This pendulum model is implemented by the M-file `mod_pend.m`. (Note that the system matrix G_{pend} may be obtained by using the function `sysic`, too.)

The input/output relation of the perturbed, pendulum system is described by the upper LFT

$$\begin{bmatrix} y \\ y_p \end{bmatrix} = F_U(G_{\text{pend}}, \Delta_{\text{pend}}) \begin{bmatrix} d \\ t_m \end{bmatrix}$$

with the diagonal, uncertain matrix

$$\Delta_{pend} = \begin{bmatrix} \Delta_I & 0 \\ 0 & \Delta_C \end{bmatrix}$$

as depicted in Figure 9.5.

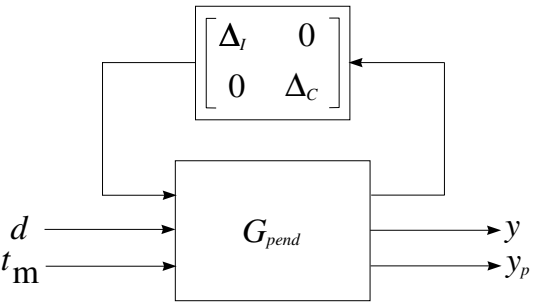

Fig. 9.5. The LFT representation of the perturbed triple inverted pendulum

The singular value plot of the triple, inverted pendulum system (the nominal system) is shown in Figure 9.6.

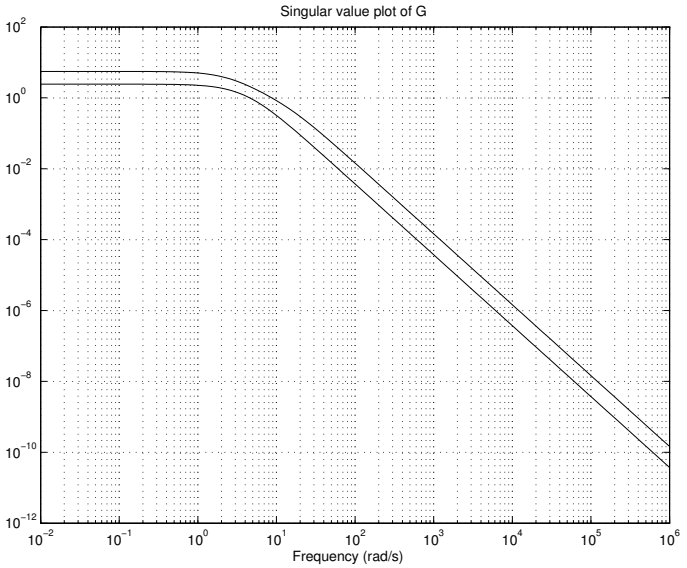

Fig. 9.6. Singular values of the pendulum system

We now consider the models of the actuators. The nominal transfer functions of the actuators are taken as first-order, phase-lag models of

$$\overline{G}_{m_1} = \frac{\overline{K}_{m_1}}{\overline{T}_{m_1}s+1},\ \ \overline{G}_{m_2} = \frac{\overline{K}_{m_2}}{\overline{T}_{m_2}s+1}$$

with parameters

$$\overline{K}_{m_1} = 1.08,\ \overline{T}_{m_1} = 0.005,\ \overline{K}_{m_2} = 0.335,\ \overline{T}_{m_2} = 0.002$$

It is assumed that the actual gain coefficients $(K_{m_1},\ K_{m_2})$ are constants with relative error 10% around their nominal values and the time constants $(T_{m_1},\ T_{m_2})$ with relative error 20%. The uncertain frequency responses of the actuators are shown in Figure 9.7.

In order to account for unmodelled dynamics and nonlinear effects, the uncertainties in the actuator models are approximated by input multiplicative uncertainties that give rise to the perturbed transfer functions

$$G_{m_1} = (1 + W_{m_1}\delta_{m_1})\overline{G}_{m_1},\ \ G_{m_2} = (1 + W_{m_2}\delta_{m_2})\overline{G}_{m_2}$$

where

$$|\delta_{m_1}| \le 1,\ \ |\delta_{m_2}| \le 1$$

and the uncertainty weights $W_{m_1},\ W_{m_2}$ are so chosen that

$$\frac{\left|G_{m_1}(j\omega) - \overline{G}_{m_1}(j\omega)\right|}{\left|\overline{G}_{m_1}(j\omega)\right|} < |W_{m_1}(j\omega)|\,,\ \ \frac{\left|G_{m_2}(j\omega) - \overline{G}_{m_2}(j\omega)\right|}{\left|\overline{G}_{m_2}(j\omega)\right|} < |W_{m_2}(j\omega)|\,.$$

The frequency responses of $W_{m_1},\ W_{m_2}$ are found graphically as shown in Figure 9.8 and then approximated by first-order transfer functions using the file `wfit.m`. As a result, we obtain

$$W_{m_1} = \frac{0.3877s + 25.6011}{1.0000s + 246.3606},\ \ W_{m_2} = \frac{0.3803s + 60.8973}{1.0000s + 599.5829}$$

By introducing the vector $u = [u_1,\ u_2]^T$, the equations of the actuators are rewritten as

$$t_m = \overline{G}_m(I_2 + W_m\Delta_m)u$$

where

$$\overline{G}_m = \begin{bmatrix} \overline{G}_{m_1} & 0 \\ 0 & \overline{G}_{m_2} \end{bmatrix},\ \ W_m = \begin{bmatrix} W_{m_1} & 0 \\ 0 & W_{m_2} \end{bmatrix},\ \ \Delta_m = \begin{bmatrix} \delta_{m_1} & 0 \\ 0 & \delta_{m_2} \end{bmatrix}$$

The block diagram of the actuators with the input multiplicative uncertainty is shown in Figure 9.9.

Let the inputs and outputs of the uncertain blocks $(\delta_{m_1},\ \delta_{m_2})$ be denoted by $y_{m_1},\ y_{m_2}$ and $u_{m_1},\ u_{m_2}$, respectively. Defining the vectors $u_m = [u_{m_1}\ u_{m_2}]^T$ and $y_m = [y_{m_1}\ y_{m_2}]^T$, we may rearrange the actuator models as

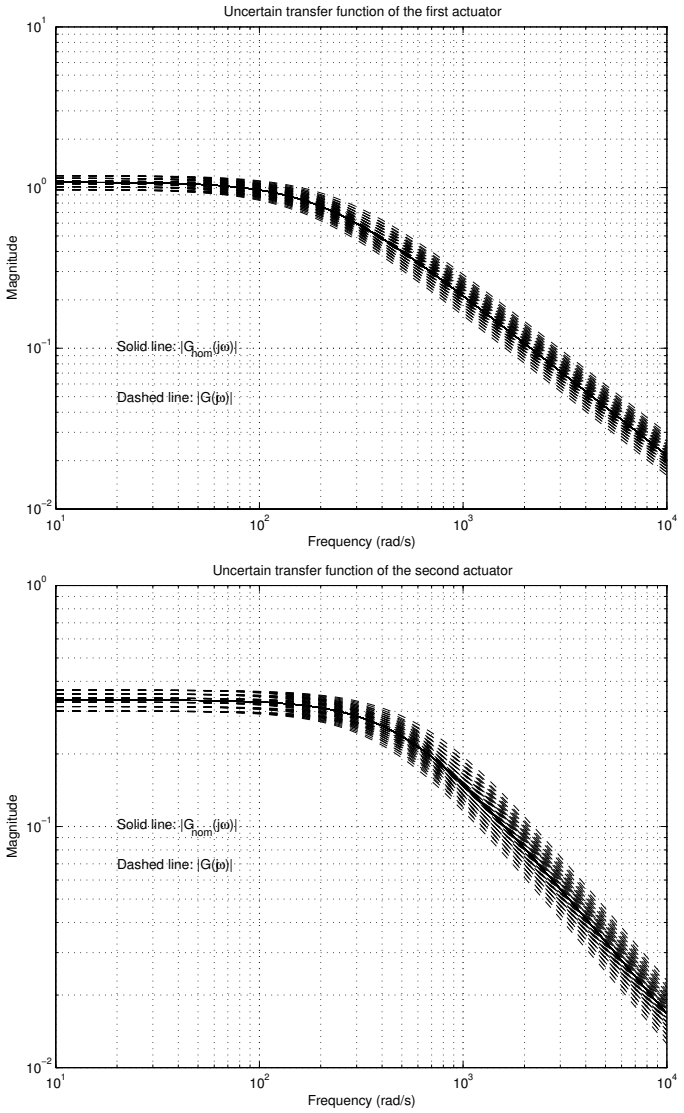

Fig. 9.7. Uncertain frequency responses of the actuators

$$\begin{bmatrix} y_m \\ t_m \end{bmatrix} = G_{\text{act}} \begin{bmatrix} u_m \\ u \end{bmatrix} \tag{9.5}$$

$$u_m = \Delta_m y_m \tag{9.6}$$

where

$$G_{\text{act}} = \begin{bmatrix} 0_{2\times 2} & W_m \\ \overline{G}_m & \overline{G}_m \end{bmatrix}$$

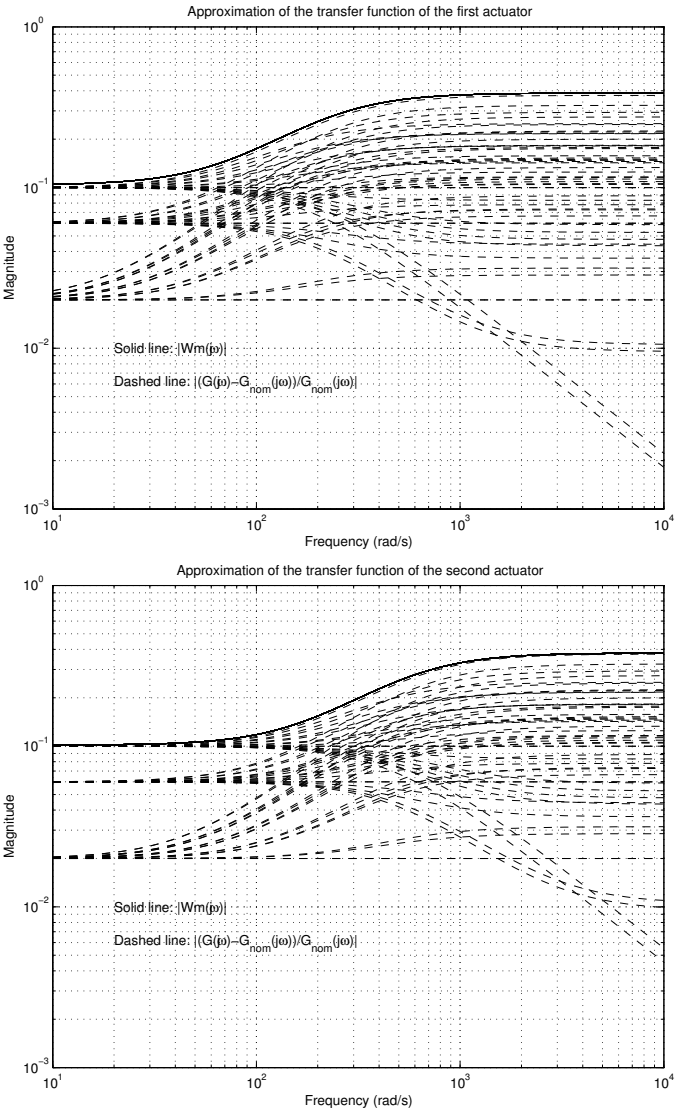

Fig. 9.8. Actuators uncertainty approximations

The perturbed actuators can be described by the following upper LFT and shown in Figure 9.10,

$$t_m = F_U(G_{act}, \Delta_m)u$$

Having modelled both the pendulum and the actuators with consideration of possible perturbations, the block-diagram of the whole system is seen as in Figure 9.11. Note that Δ_m is a complex uncertainty, while Δ_I and Δ_C are real

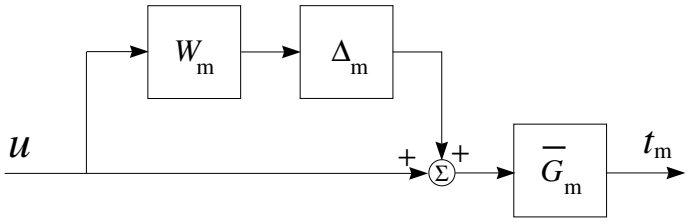

Fig. 9.9. Block diagram of the perturbed actuators

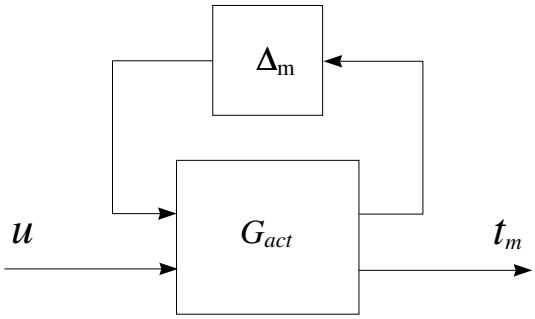

Fig. 9.10. LFT representation of the perturbed actuators

uncertainties. We thus have a case of a mixed, real and complex, uncertainty configuration.

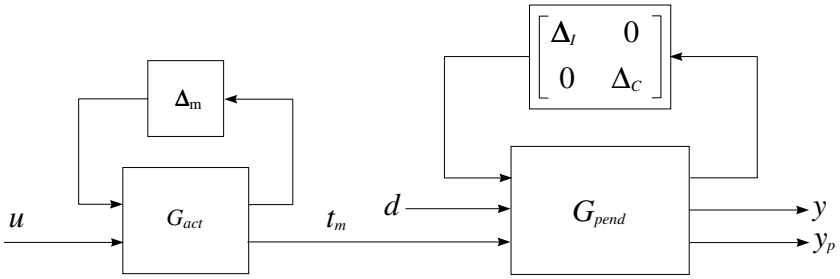

Fig. 9.11. Triple inverted pendulum system with uncertainties

The model of the whole triple inverted pendulum system is given by the equations

$$\begin{bmatrix} y_m \\ y_I \\ y_C \\ y \\ y_p \end{bmatrix} = G_{\text{sys}} \begin{bmatrix} u_m \\ u_I \\ u_C \\ d \\ u \end{bmatrix} \tag{9.7}$$

where the transfer matrix G_{sys} is determined by the matrices G_{act} and G_{pend}, and can be easily obtained by using the function `sysic`.

The whole, perturbed, triple inverted pendulum system can be described by the following upper LFT, as shown in Figure 9.12,

$$\begin{bmatrix} y \\ y_p \end{bmatrix} = F_U(G_{\text{sys}}, \Delta) \begin{bmatrix} d \\ u \end{bmatrix}$$

with the diagonal, uncertainty matrix

$$\Delta = \begin{bmatrix} \Delta_m & 0 & 0 \\ 0 & \Delta_I & 0 \\ 0 & 0 & \Delta_C \end{bmatrix} \tag{9.8}$$

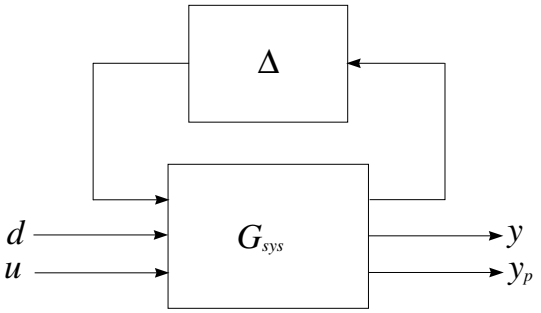

Fig. 9.12. LFT representation of triple inverted pendulum system with uncertainty

9.3 Design Specifications

The block diagram of the closed-loop system, which includes the triple inverted pendulum model, the feedback structure and the controller, as well as the elements reflecting the model uncertainty and the performance objectives, is depicted in Figure 9.13. In order to achieve better performance, we shall make use of the configuration of a two-degree-of-freedom (2DOF) controller.

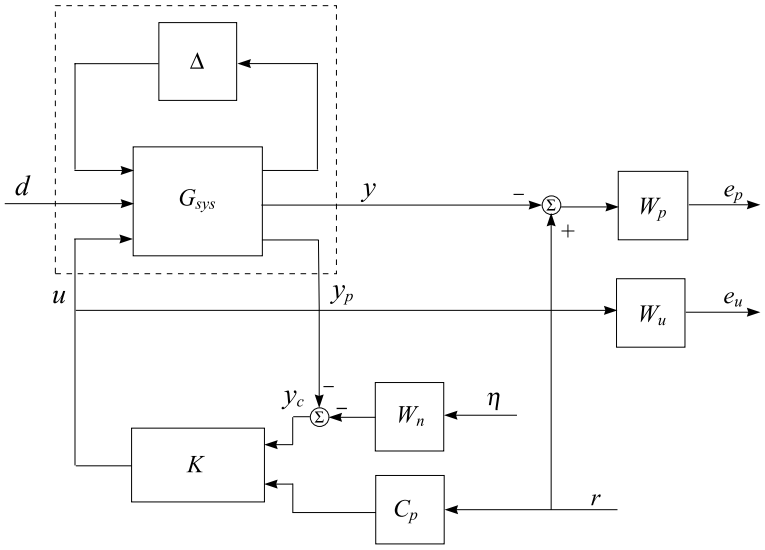

Fig. 9.13. Interconnection structure of the closed-loop system

The model of the triple inverted pendulum system represents an upper LFT in the form $G = F_U(G_{sys}, \Delta)$. The rectangle, shown with dashed lines, represents the transfer function matrix G. Inside the rectangle is the nominal model G_{sys} and the block Δ, which parametrises the model uncertainties. The matrix Δ is unknown, but with the structure defined in (9.8) and with the norm bound $\|\Delta\|_\infty < 1$.

The feedback signal is generated on the basis of the potentiometers output $y_p = C_p y$, which requires the reference r to be multiplied by the matrix C_p (the other way to deal with the situation is to multiply y_p by C_p^{-1}). The measurement of the arm angles is accompanied by introduction of frequency-dependent noises that are inevitable in practice and are thus added to the corresponding measurements. This is why at the outputs of the potentiometers one obtains the signal $y_c = -(y_p + W_n\eta)$, where W_n is a weighting function (shaping filter on the measurement noise) and $\eta = [\eta_1\ \eta_2\ \eta_3]^T$ is an arbitrary noise signal satisfying $\|\eta\|_2 \leq 1$. By choosing an appropriate W_n it is possible

to form the desired spectral contents of the actual noise signal (in the form of $W_n\eta$).

In the given case the matrix W_n is chosen as

$$W_n(s) = \begin{bmatrix} w_n(s) & 0 & 0 \\ 0 & w_n(s) & 0 \\ 0 & 0 & w_n(s) \end{bmatrix}$$

where the weighting transfer function $w_n = 2 \times 10^{-5} \frac{10s+1}{0.1s+1}$ is a high pass filter that shapes the noise spectral density for the type of potentiometers under consideration. The magnitude plot of this filter is shown in Figure 9.14. This transfer function means that in the low-frequency range the magnitude of the measurement error is about 2×10^{-5} V, and in the high-frequency range, about 2×10^{-3} V.

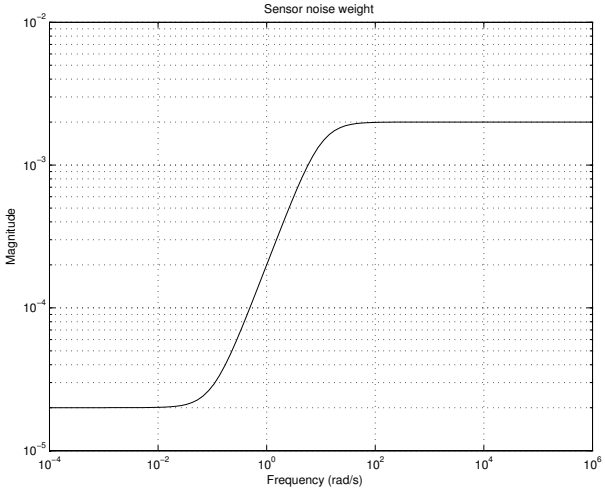

Fig. 9.14. Measurement noise weighting function

The closed-loop system error $e_y = r - y$ may be determined by

$$e_y = S \begin{bmatrix} r \\ d \\ \eta \end{bmatrix}$$

where the matrix $S = S(G_{\text{sys}})$ is considered as the nominal sensitivity function with respect to the inputs r, d and η. As for feedback signals, we shall use $y_c = -(y_p + W_n\eta)$ and $C_p r$.

The performance objective requires the transfer function matrices from r, d and η to e_y and e_u to be small in the sense of $\|\cdot\|_\infty$, for all possible (stable)

uncertainty matrices Δ. The transfer function matrices W_p and W_u are used to reflect the relative significance over different frequency ranges for which the performance is required.

The design problem for the triple inverted pendulum system is to find a linear, output controller $K(s)$ to generate the output feedback

$$u(s) = K(s) \begin{bmatrix} y_c(s) \\ C_p r(s) \end{bmatrix}$$

to ensure the following properties of the closed-loop system.

Nominal performance:

The closed-loop system achieves nominal performance if the following performance objective is satisfied for the nominal plant model G_{sys},

$$\left\| \begin{bmatrix} W_p S(G_{\text{sys}}) \\ W_u K S(G_{\text{sys}}) \end{bmatrix} \right\|_\infty < 1 \tag{9.9}$$

where W_p and W_u are appropriately chosen weighting functions. This objective corresponds to the mixed S/KS sensitivity optimisation.

Robust stability:

The closed-loop system achieves robust stability if the closed-loop system is internally stable for each possible, perturbed plant dynamics $G = F_U(G_{\text{sys}}, \Delta)$.

Robust performance:

The closed-loop system must maintain, for each $G = F_U(G_{\text{sys}}, \Delta)$, the performance objective

$$\left\| \begin{bmatrix} W_p S(G) \\ W_u K S(G) \end{bmatrix} \right\|_\infty < 1 \tag{9.10}$$

where $S(G)$ is the perturbed sensitivity function of $G = F_U(G_{\text{sys}}, \Delta)$.

In addition to the above requirements, it is desirable that the controller designed would have acceptable complexity, *i.e.* it is of reasonably low order.

9.4 System Interconnections

The internal structure of the nineteen-input, nineteen-output open-loop system, which is saved as the variable `pend_ic`, is shown in Figure 9.15. The inputs and outputs of the uncertainties are saved in the variables `pertin` and `pertout`, respectively, and the reference, the disturbance and the noise in the

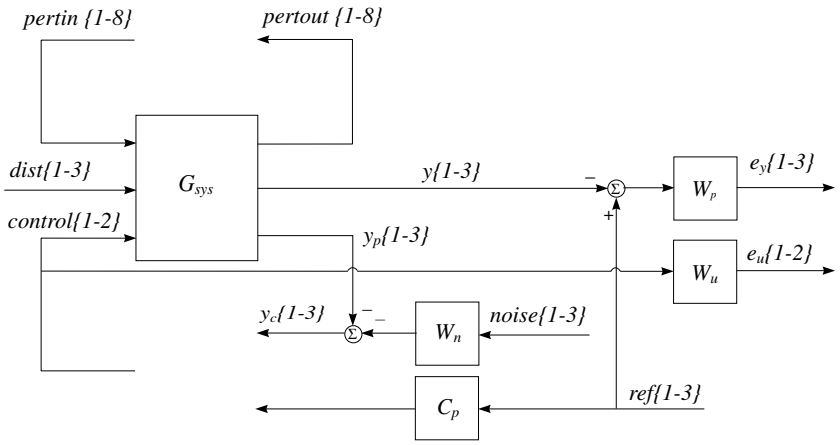

Fig. 9.15. Open-Loop interconnection of the triple inverted pendulum system

variables `ref`, `dist`, `noise`, respectively. The control signal is saved in the variable `control`.

The variables `pertin` and `pertout` each have eight elements. The variables `ref, dist, noise, y, y_p, y_c, e_y` have all three elements and the variables `control, e_u` have two elements. The open-loop connection is assigned by the M-file `olp_pend`. The schematic diagram showing the specific input/output ordering for the variable `pend_ic` is shown in Figure 9.16.

The block-diagram used in the closed-loop system simulation is shown in Figure 9.17. The corresponding closed-loop interconnection, which is saved in the variable `pend_sm`, is obtained by the M-file `sim_pend`.

Figure 9.18 shows the schematic diagram of the specific input/output ordering for the variable `pend_sm`.

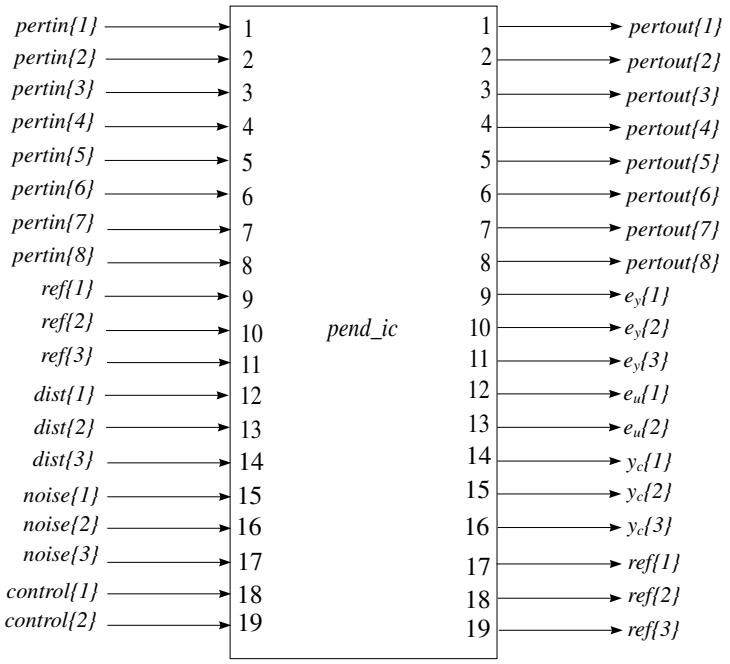

Fig. 9.16. Schematic diagram of the open-loop system

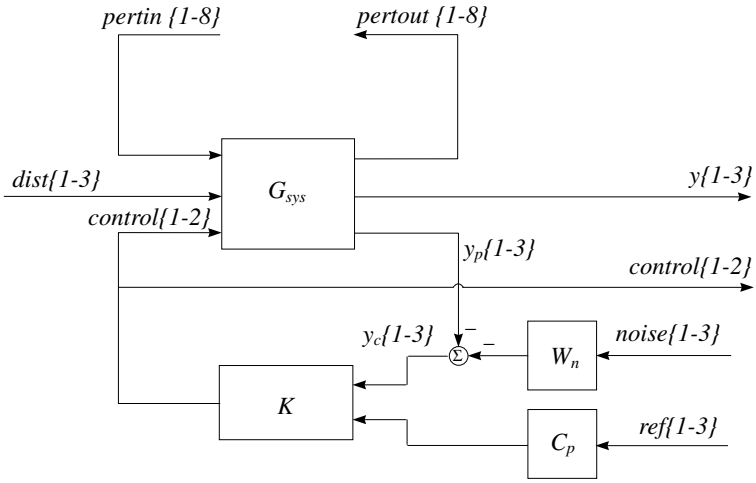

Fig. 9.17. Closed-loop interconnection structure of the pendulum system

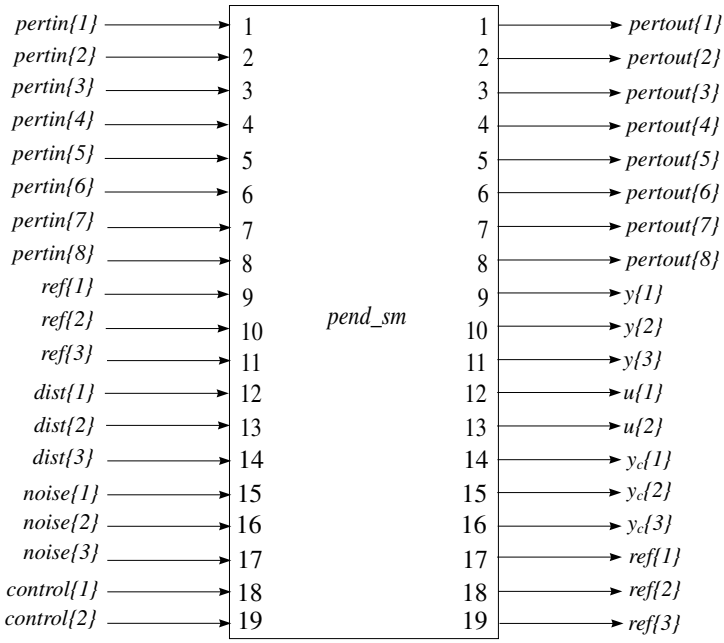

Fig. 9.18. Schematic diagram of the closed-loop system

9.5 $\mathcal{H}_\infty$ Design

The design goal in this case is to find an $\mathcal{H}_\infty$ (sub)optimal control law for the interconnection shown in Figure 9.19, in which we neglect the uncertainty inputs and outputs. The variable `hin_ic`, which corresponds to the transfer function matrix of the augmented system, may be obtained by the command line

```
hin_ic = sel(pend_ic,[9:19],[9:19])
```

The $\mathcal{H}_\infty$ optimal control minimises the $\|\cdot\|_\infty$ norm of $F_L(P,K)$ over the stabilising controller transfer matrix K, where P is the transfer function matrix of the augmented system. In the given case $F_L(P,K)$ is the nominal closed-loop system transfer matrix from the references, disturbances and noises (the signals r, d and η) to the weighted outputs e_y and e_u (Figure 9.19).

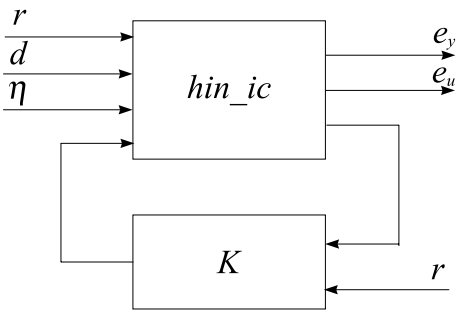

Fig. 9.19. Block diagram for $\mathcal{H}_\infty$ design

In the given case the weighting performance functions are chosen in the forms of

$$W_p(s) = \begin{bmatrix} w_{p1}(s) & 0 & 0 \\ 0 & w_{p2}(s) & 0 \\ 0 & 0 & w_{p3}(s) \end{bmatrix}, \quad W_u(s) = \begin{bmatrix} w_u(s) & 0 \\ 0 & w_u(s) \end{bmatrix}$$

where

$$w_{p1}(s) = 10^{-6} \frac{s^4 + 12s^3 + 80s^2 + 80s + 65}{s^4 + 1500s^3 + 13000s^2 + 12000s + 0.005}$$

$$w_{p2}(s) = \frac{s^4 + 12s^3 + 80s^2 + 80s + 65}{s^4 + 1500s^3 + 13000s^2 + 12000s + 0.005}$$

$$w_{p3}(s) = \frac{s^4 + 12s^3 + 80s^2 + 80s + 65}{s^4 + 1500s^3 + 13000s^2 + 12000s + 0.005}$$

and $w_u(s) = 10^{-6}$.

The small gain in the first weighting function (w_{p1}) indicates that the first error may be allowed to be large. This is due to the fact that the requirement on precision position of the first arm may be relaxed a little in this case.

The weighting functions are set in the M-file `wts_pend.m`.

The $\mathcal{H}_\infty$ design is conducted by using the M-file `hinf_pend.m`. It utilises the function `hinfsyn`, which determines a (sub)optimal $\mathcal{H}_\infty$ control law, based on the prescribed open-loop interconnection. The interval for γ iteration is chosen between 0 and 10 with a tolerance tol = 0.001. The controller obtained is of 28th order and for this controller the closed-loop system achieves $\mathcal{H}_\infty$ norm equal to 1.0005. An undesired property of the controller is that it has a pole at 33.6, *i.e.* this controller is unstable, which makes it less favourable in practice.

The singular value plot of the $\mathcal{H}_\infty$ controller transfer matrix is shown in Figure 9.20.

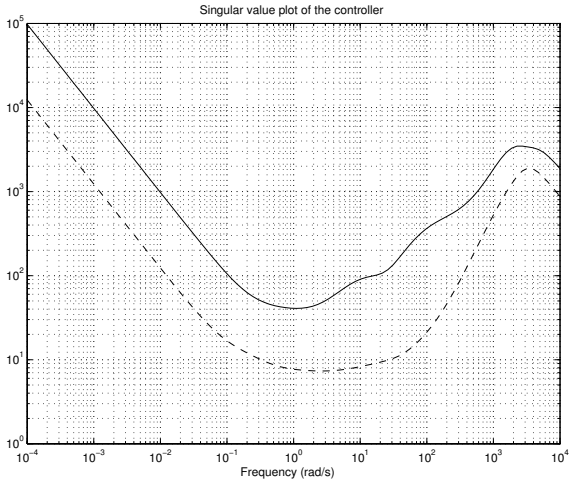

Fig. 9.20. Singular values of the $\mathcal{H}_\infty$ controller

The closed-loop, transient responses (reference tracking) are obtained by using the file `clp_pend`. The transient response of the closed-loop system with $\mathcal{H}_\infty$ controller for the reference vector

$$r = \begin{bmatrix} 0 \\ -0.1 \\ 0.2 \end{bmatrix}$$

(the references are measured in radians) is shown in Figure 9.21. The response is fast (settling time approximately equal to 6 s) with small overshoots of the output variables. The steady-state errors are small, except for a small error on the position of the first arm.

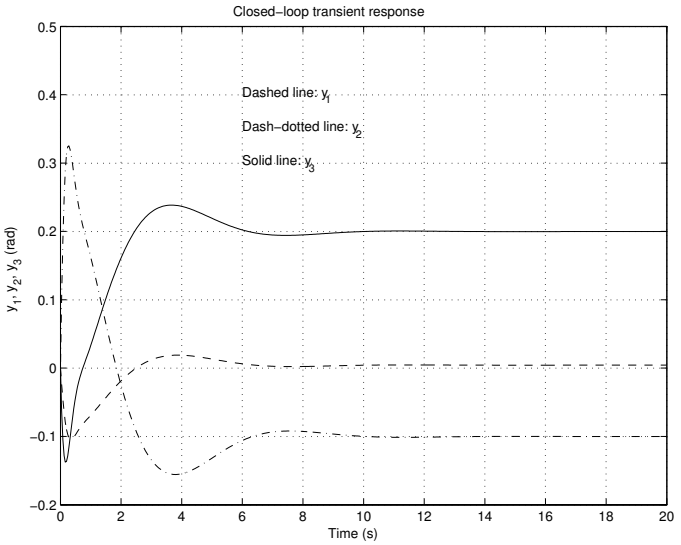

Fig. 9.21. Closed-loop transient response of $\mathcal{H}_\infty$ controller

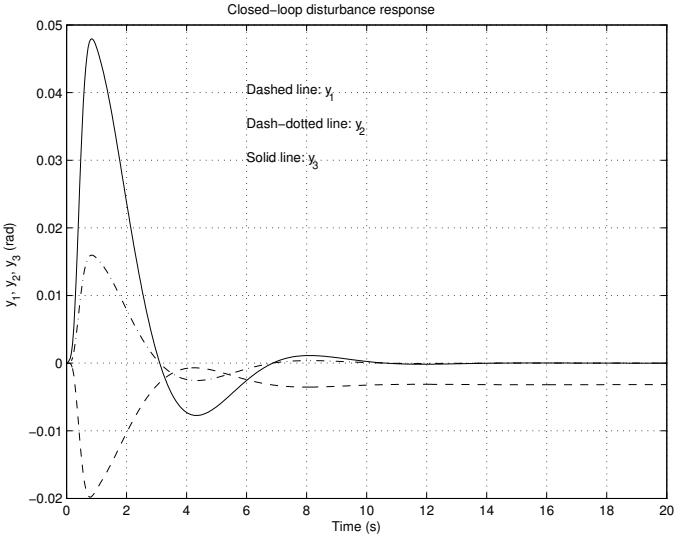

Fig. 9.22. Disturbance rejection of $\mathcal{H}_\infty$ controller

The disturbance rejection of the closed-loop system with the $\mathcal{H}_\infty$ controller is shown in Figure 9.22. The disturbance vector is set to

$$d = \begin{bmatrix} 0.1 \\ 0.1 \\ 0.1 \end{bmatrix}$$

and measured in N m.

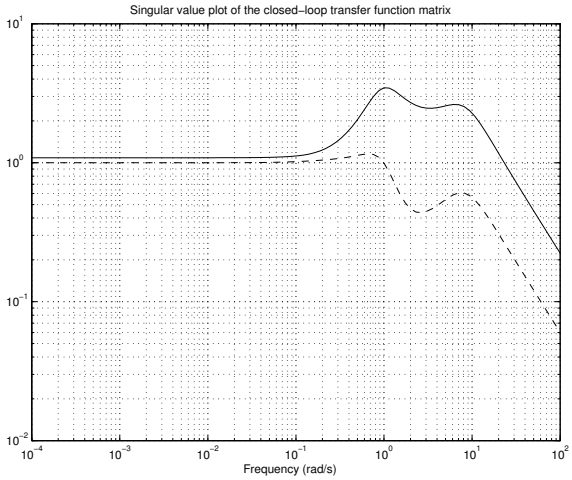

Fig. 9.23. Closed-loop singular values with $\mathcal{H}_\infty$ controller

In Figure 9.23 we show the singular values plot of the closed-loop transfer matrix with the $\mathcal{H}_\infty$ controller.

The test for robust stability is based on the μ values of the upper 8×8 block of the closed-loop transfer function matrix. The block structure of the uncertainty is set as

```
blks = [1 1;1 1;-1 1;-1 1;-1 1;-1 1;-1 1;-1 1]
```

The upper and lower bounds of the structured singular value μ (over the frequency range) are shown in Figure 9.24. It is clear that the closed-loop system with $\mathcal{H}_\infty$ controller does not achieve robust stability, since the maximum value of μ is equal to 1.666.

The robust performance of the closed-loop system with $\mathcal{H}_\infty$ controller is checked with the μ-analysis, too. The block-structure of the uncertainty Δ_P consists of an 8×8 diagonal uncertainty block and a 9×5 full (complex) uncertainty performance block, i.e.,

$$\Delta_P := \left\{ \begin{bmatrix} \Delta & 0 \\ 0 & \Delta_F \end{bmatrix} : \Delta \in \mathcal{C}^{8\times 8},\ \Delta_F \in \mathcal{C}^{9\times 5} \right\}$$

The μ values corresponding to the case of robust performance analysis are shown in Figure 9.25. Again, the closed-loop system does not achieve robust performance either, because the maximum value of μ is equal to 1.673.

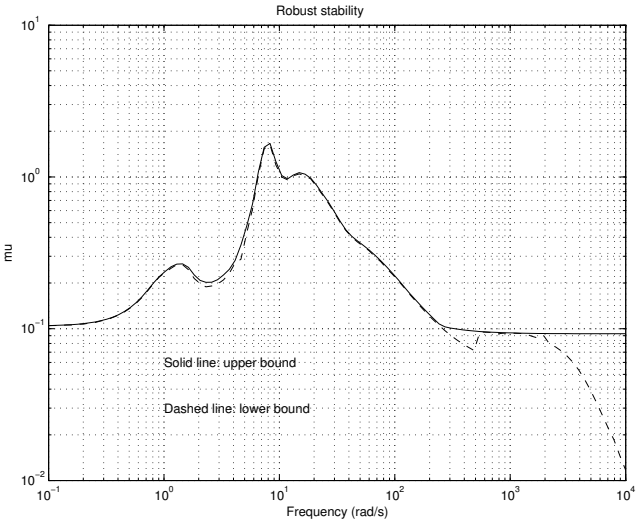

Fig. 9.24. Robust stability test of $\mathcal{H}_\infty$ controller

Hence, it is concluded that the designed $\mathcal{H}_\infty$ controller leads to good closed-loop transient responses, but does not ensure the necessary robustness of the closed-loop system as required.

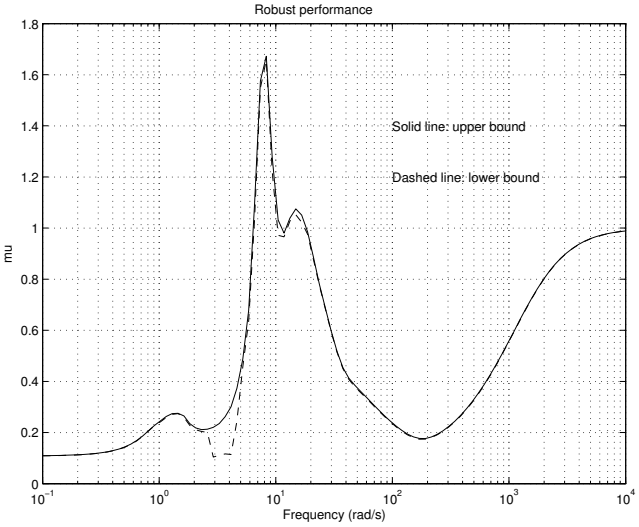

Fig. 9.25. Robust performance of $\mathcal{H}_\infty$ controller

9.6 μ-Synthesis

Let us denote by $P(s)$ the transfer function matrix of the nineteen-input, sixteen-output, open-loop system consisting of the pendulum system model plus the weighting functions, and let the block structure Δ_P of uncertainties be defined by

$$\Delta_P := \left\{ \begin{bmatrix} \Delta & 0 \\ 0 & \Delta_F \end{bmatrix} : \Delta \in \mathcal{R}^{8\times 8},\ \Delta_F \in \mathcal{C}^{9\times 5} \right\}$$

The first block of the matrix Δ_P, the uncertainty block Δ, corresponds to the parametric uncertainties modelled in the triple inverted pendulum system. The second block, Δ_F, is a fictitious uncertainty block, introduced to include the performance objectives in the framework of the μ-approach.

To meet the design objectives a stabilising controller K is to be found such that, at each frequency $\omega \in [0, \infty]$, the structured singular value μ satisfies the condition

$$\mu_{\Delta_P}[F_L(P, K)(j\omega)] < 1$$

The fulfillment of this condition guarantees robust performance of the closed-loop system, *i.e.*,

$$\left\| \begin{bmatrix} W_p S(G) \\ W_u K S(G) \end{bmatrix} \right\|_\infty < 1$$

where $G = F_U(G_{\text{sys}}, \Delta)$, for all stable perturbations Δ with $\|\Delta\|_\infty < 1$.

The μ-synthesis is conducted by using the M-file `ms_pend.m`. The uncertainty structure and other parameters used in the D-K iteration are assigned in the auxiliary file `dk_pend.m`.

The experiments with μ-synthesis show that the use of the weighting functions, used in the $\mathcal{H}_\infty$ design, leads to very slow transient responses. Hence, these functions are appropriately modified to

$$w_{p1}(s) = 10^{-6} \frac{s^4 + 12s^3 + 80s^2 + 80s + 65}{15s^4 + 1500s^3 + 13000s^2 + 12000s + 0.005}$$

$$w_{p2}(s) = 2.5 \frac{s^4 + 12s^3 + 80s^2 + 80s + 65}{15s^4 + 1500s^3 + 13000s^2 + 12000s + 0.005}$$

$$w_{p3}(s) = 10 \frac{s^4 + 12s^3 + 80s^2 + 80s + 65}{15s^4 + 1500s^3 + 13000s^2 + 12000s + 0.005}$$

The control weighting functions are again taken as $w_u(s) = 10^{-6}$.

The progress of the D-K iteration is shown in Table 9.3.

It can be seen from the table that after the third iteration the maximum value of μ is equal to 0.960, which indicates that the robust performance has been achieved. The final controller obtained is of 84th order. Note that this controller is stable.

Table 9.3. D-K iterations results in μ-synthesis

Iteration	Controller order	Maximum value of μ
1	28	13.852
2	84	1.422
3	84	0.960

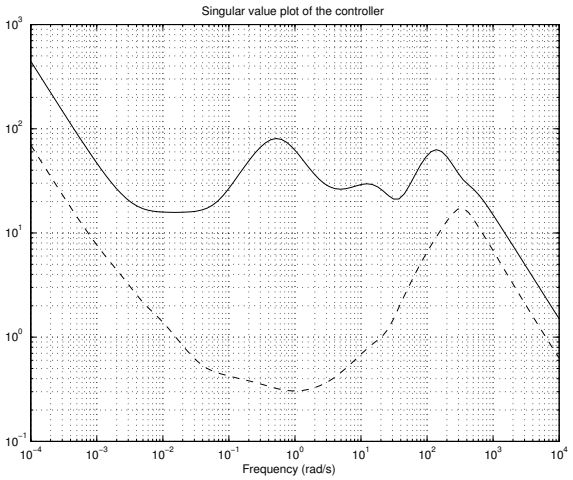

Fig. 9.26. Singular values of the μ-controller

The singular value plot of the μ-controller is shown in Figure 9.26. Similar to the $\mathcal{H}_\infty$ controller, the μ-controller has an integrating action in the low frequency range.

The structured singular values for the robust stability study (over the frequency range) are shown in Figure 9.27. The maximum value of μ is 0.626 which means that the stability of the system is preserved under perturbations that satisfy $\|\Delta\|_\infty < \frac{1}{0.626}$.

The μ values over the frequency range for the case of robust performance analysis are shown in Figure 9.28. The closed-loop system achieves robust performance, since the maximum value of μ is equal to 0.820.

Consider now the closed-loop transient responses obtained by using the M-file `clp_pend`. The same reference signal as used in the $\mathcal{H}_\infty$ simulation is used here. That is,

$$r = \begin{bmatrix} 0 \\ -0.1 \\ 0.2 \end{bmatrix}$$

The transient response is shown in Figure 9.29. To compare with those of the

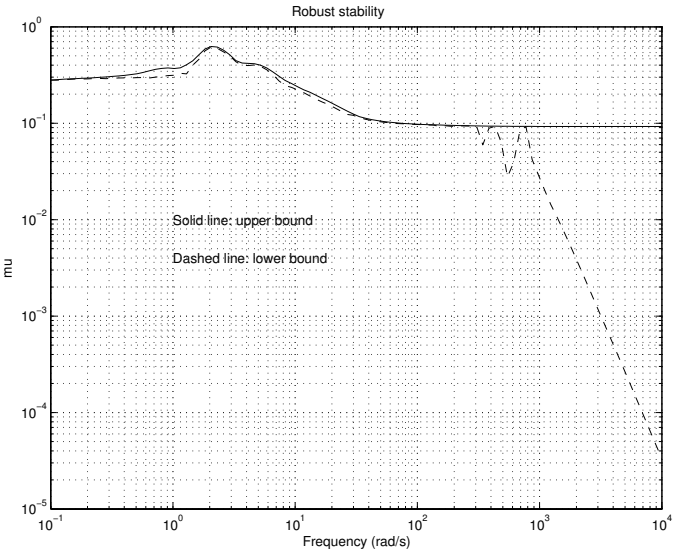

Fig. 9.27. Robust stability of μ controller

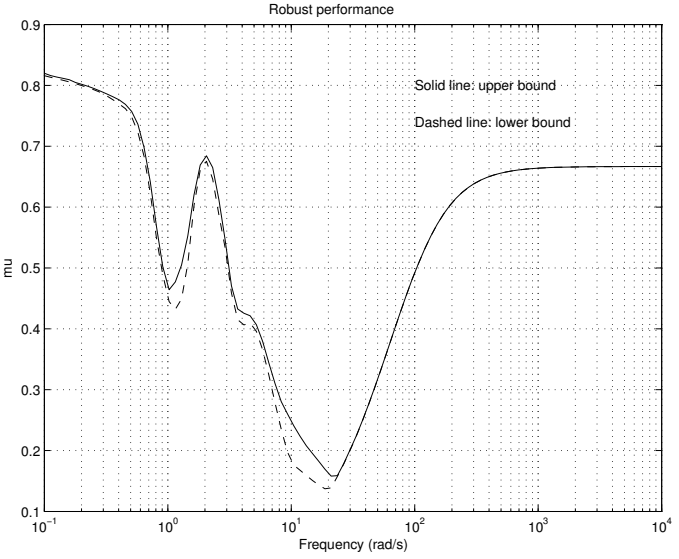

Fig. 9.28. Robust performance of μ controller

$\mathcal{H}_\infty$ controller, it can be seen that the transient response (reference tracking) of the μ-controller is slower and the steady-state errors are slightly larger, though with less overshoot (undershoot).

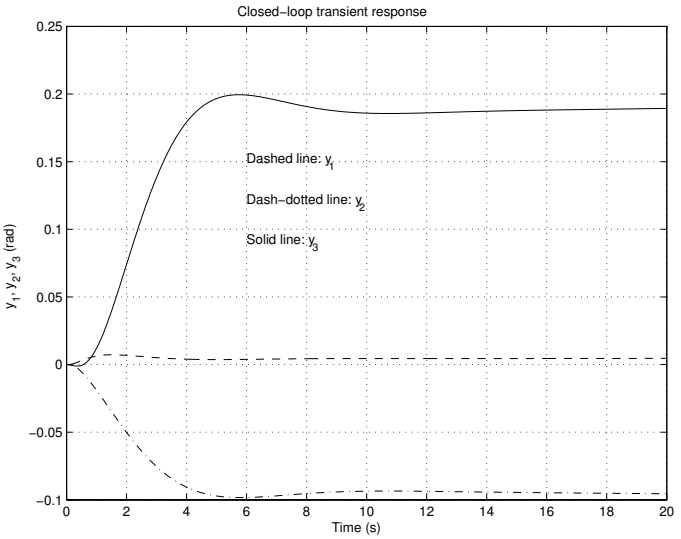

Fig. 9.29. Closed-loop transient response of μ-controller

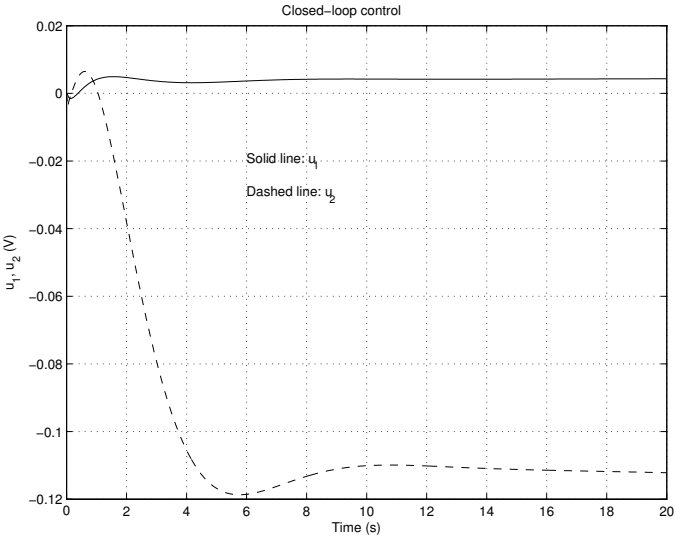

Fig. 9.30. Control action of μ-controller

The control action in the case of a μ-controller is shown in Figure 9.30. The motor voltages are kept within 0.12 V.

The disturbance rejection of the closed-loop system with the μ-controller is shown in Figure 9.31. We see that the overshoot of the third output is almost 7 times larger than in the case of the $\mathcal{H}_\infty$ controller.

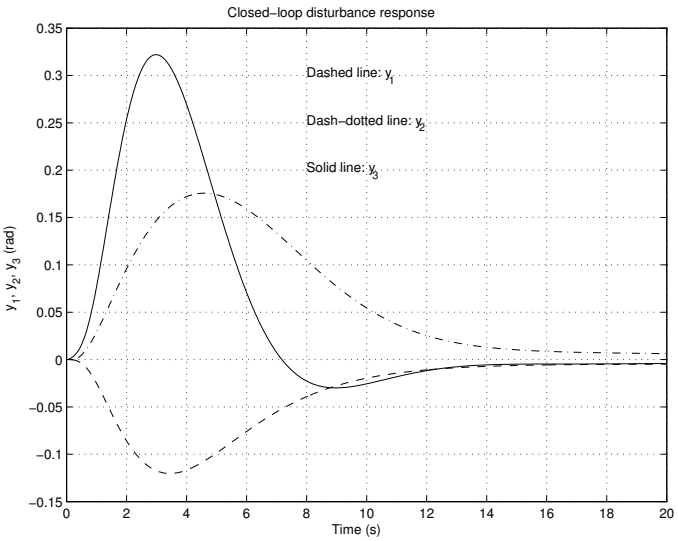

Fig. 9.31. Disturbance rejection of μ-controller

Hence, it is clear that the (nominal) transient responses in terms of reference tracking and disturbance attenuation are worse in the case of the μ-controller. This is the price that has to be paid to ensure the robust stability and robust performance of the closed-loop system.

In Figure 9.32, we show the noise $w_n\eta_3$ that acts at the output of the third potentiometer, and the corresponding response of the output y_3. From the magnitudes of $w_n\eta_3$ and y_3, one may conclude that the closed-loop system is susceptible to noises.

The closed-loop frequency responses are obtained by the M-file `frs_pend.m`. The singular values of the closed-loop transfer matrix with the μ-controller are plotted in Figure 9.33. The comparison with the plot shown in Figure 9.23 reveals that the closed-loop bandwidth in the case of a μ-controller is smaller, which leads to a slower response and worse disturbance attenuation.

The singular values of the transfer function matrix concerning disturbance rejection are shown in Figure 9.34. We see that the disturbance attenuation is worst for frequencies around 1 rad/s.

From the singular values plot of the transfer function matrix concerning noise attenuation, shown in Figure 9.35, we see that the influence of noises on the system output would be maximal for frequencies between 1 rad/s and 10 rad/s.

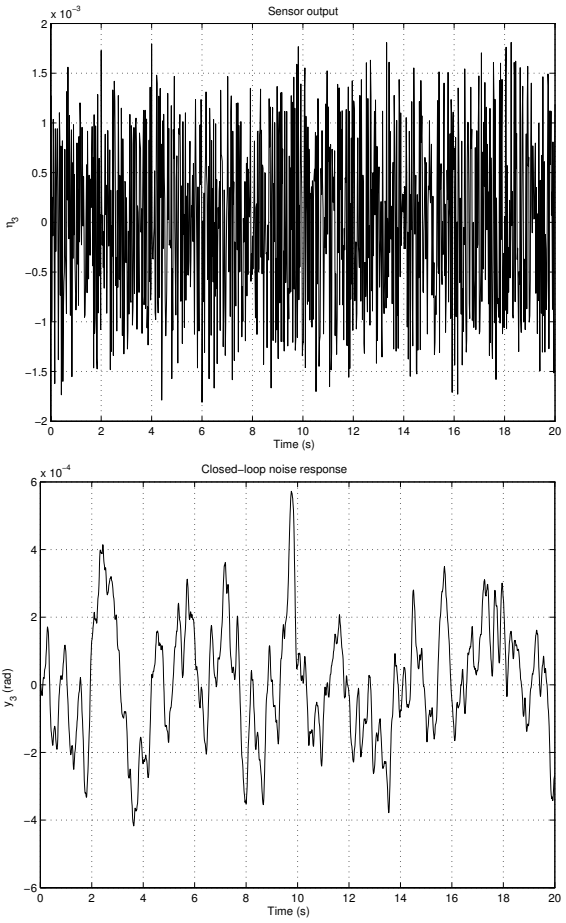

Fig. 9.32. Sensor noise and closed-loop noise response

As mentioned earlier, the controller obtained by μ-synthesis is initially of 80th order, which makes its implementation in practice very difficult. Therefore, it is necessary to reduce the controller order. For this purpose, we implements the M-file `red_pend.m`. We use the model reduction algorithm based on system balancing followed by optimal Hankel approximation. This algorithm allows us to reduce the controller order to 27. Further reduction of the controller order leads to deterioration of the closed-loop transient responses and would even cause the instability of the closed-loop system.

In Figure 9.36 we compare the frequency responses (the maximum singular values) of the full-order and reduced-order μ-controllers. Up to the frequency 10^4 rad/s the frequency plots of both controllers coincide with each other, which implies very similar performance of the closed-loop systems. In fact,

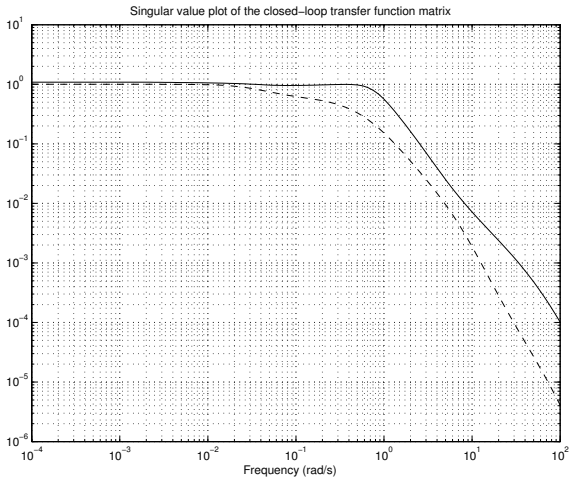

Fig. 9.33. Closed-loop singular value plot

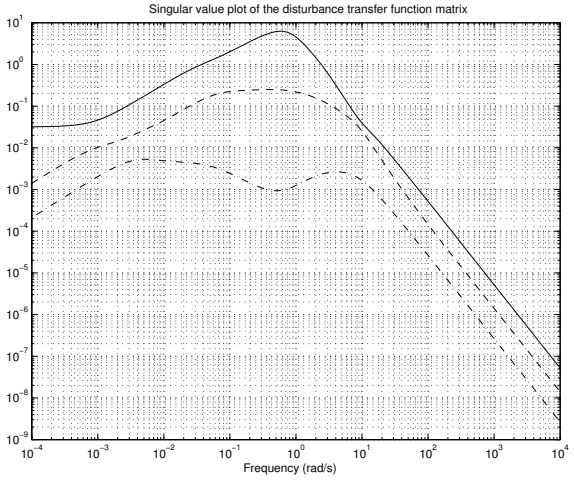

Fig. 9.34. Singular values of the disturbance rejection transfer function matrix

the closed-loop transient responses with the full-order controller and those with the reduced-order controller (not included in the book) are practically undistinguishable.

A discrete-time controller may be obtained by sampling the already designed continuous-time controller for a sampling frequency $f_\mathrm{s} = 1/T_\mathrm{s}$. This can be conducted by the M-file `dcl_pend.m` that utilises the Robust Control Toolbox function `samhld`. The resulting, sampled-data closed-loop system can be simulated by using the function `sdtrsp`. Since the inverted pendu-

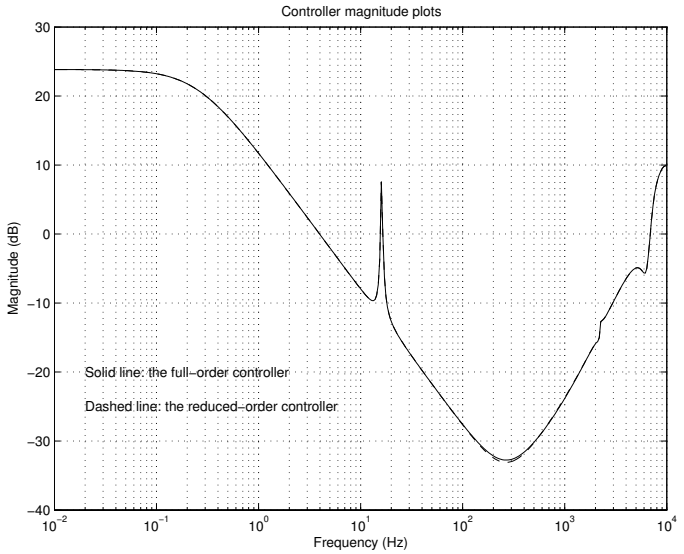

Fig. 10.37. Magnitude plots of full- and reduced-order μ-controllers

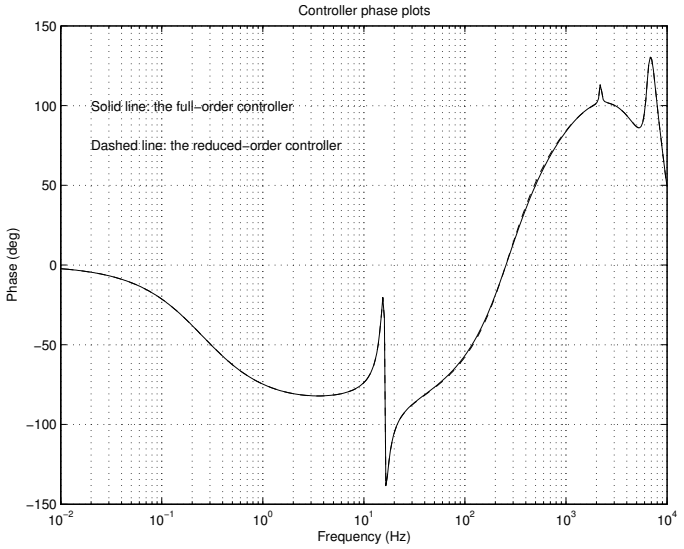

Fig. 10.38. Phase plots of full- and reduced-order μ-controllers

10.8 Design of Discrete-time Controller

In general, there are two approaches to designing a discrete-time servo controller.

The first approach is to sample the already designed continuous-time controller at a given sampling frequency $f_s = 1/T_s$. This may be accomplished by the M-file `dcl_hdd.m` that utilises the Robust Control Toolbox function `samhld`. It is assumed that the control-action calculation requires one sampling period T_s. This introduces a pure delay equal to T_s that is approximated by a rational transfer function using the command `pade`. The resultant sampled-data, closed-loop system is simulated by using the function `sdtrsp`. This approach gives satisfactory results for a sufficiently high sampling frequency (say, 100 kHz in the given case).

The second method is to sample the continuous-time, open-loop system (including the weighting filters) and to design directly a discrete-time controller by using $\mathcal{H}_\infty$ optimisation (implementing the function `dhinfsyn`) or μ-synthesis (implementing the function `dkit`).

The choice of the sampling frequency in the discrete-time case has a strong influence on the closed-loop system performance. A low sampling frequency limits the system bandwidth and would deteriorate the transient performance such as the disturbance rejection. On the other hand, the increase of the sampling frequency would complicate the controller implementation and raise the cost of the HDD.

Later we consider the μ-synthesis of the discrete-time controller for two sampling rates – 24 kHz and 36 kHz. In both cases we use the same performance weighting function

$$W_{p2}(s) = 10^{-4} \frac{s^2 + 4 \times 10^5 s + 2.5 \times 10^9}{s^2 + 3.9 \times 10^5 s + 6.25 \times 10^5}$$

utilised already in the continuous-time design. Depending on the sample rate we use two different control weighting functions

$$W_{u1}(s) = 10^{-6} \frac{4s^2 + 2s + 1}{2 \times 10^{-3} s^2 + 2 \times 10^{-3} s + 1}$$

(for $f_s = 24$ kHz) and

$$W_{u2}(s) = 10^{-6} \frac{1.04s^2 + 2s + 1}{7.5^{-5} s^2 + 2 \times 10^{-3} s + 1}.$$

(for $f_s = 36$ kHz). This allows, in both cases, to obtain control signals that do not exceed 1.2 V.

The noise shaping filter is the same as in the continuous-time case.

The sampling of the extended open-loop system for the given sampling rate is conducted by the M-file `dlp_hdd.m`. The discrete-time μ-synthesis is

accomplished by the file `dms_hdd.m` that is used in conjunction with the auxiliary file `ddk_hdd.m`. The file `ddk_hdd.m` sets the structure of the uncertainty and the parameter values of the $D-K$ iteration. As in the continuous-time μ-synthesis, only the rigid-body uncertain parameters are taken into account. The frequency is set on the unit circle in the interval $[0, \pi]$. In the discrete-time case it is also necessary to add the operator

```
DISCRETE_DK = 1;
```

in the file `ddk_hdd.m`.

The results from the μ-synthesis for $f_s = 24$ kHz show that for the chosen weighting functions the closed-loop system almost achieves robust performance at the fifth $D-K$ iteration ($\mu_{\max} = 1.06$) but the closed-loop response is relatively slow and the undershoot is large (44%). The maximum control amplitude is 1.19 V. To obtain better results it is necessary to increase the sampling frequency.

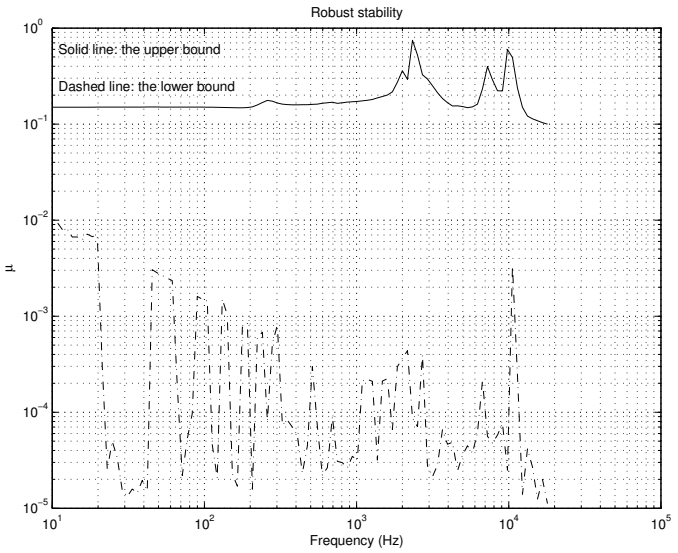

Fig. 10.39. Robust stability of $f_s = 36$ kHz design

We now present in more detail the results from the μ-synthesis at $f_s = 36$ kHz. In this case an appropriate controller is obtained after three $D-K$ iterations and the maximum robust performance achieved is $\mu_{\max} = 1.071$. In Figures 10.39 and 10.40, we show the μ-plots, obtained by the M-file `dmu_hdd.m`, for robust stability analysis and robust performance analysis, respectively. In both plots the worst results are seen around the second resonant frequency of 2.2 kHz.

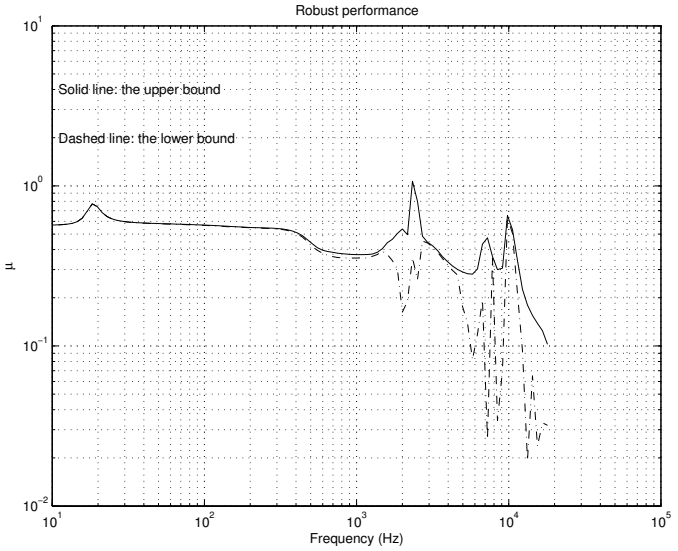

Fig. 10.40. Robust performance of $f_s = 36$ kHz design

The closed-loop transient response is obtained by the file `dsl_hdd.m` that uses the function `sdtrsp`. The function `sdtrsp` also computes the control signal obtained at the output of the digital-to-analogue converter. The closed-loop transient response is shown in Figure 10.41 and the corresponding control action in Figure 10.42. The undershoot of the transient response is less than 36% and the peak amplitude of the control is less than 1.05 V.

The transient response to disturbance is shown in Figure 10.43. Overall, the results obtained are almost as good as the results obtained with the continuous-time, μ-controller.

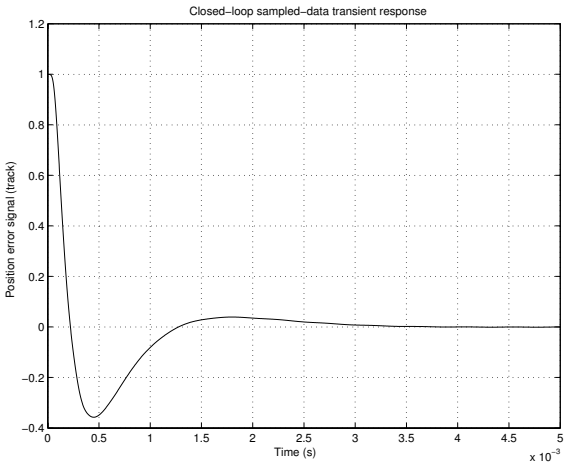

Fig. 10.41. Transient response of $f_s = 36$ kHz design

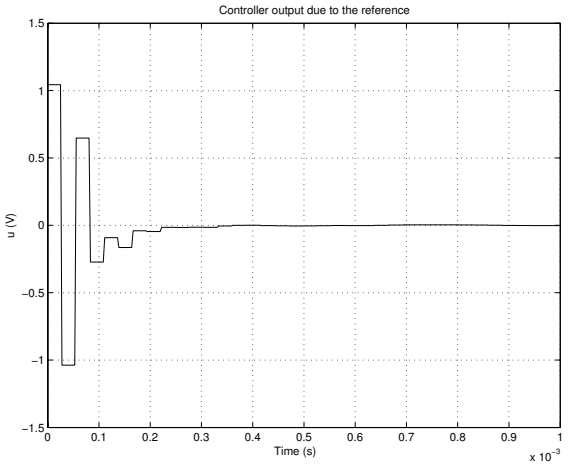

Fig. 10.42. Control action of $f_s = 36$ kHz design

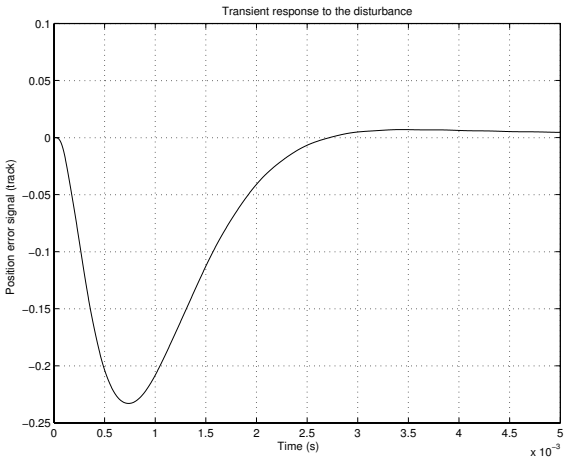

Fig. 10.43. Transient response to disturbance of $f_s = 36$ kHz design

10.9 Nonlinear System Simulation

In order to obtain a realistic idea about the behaviour of the designed system, the nonlinear, closed-loop servo system is simulated by using Simulink®. For this aim, two models are developed, namely `c_hdd.mdl` for the continuous-time system and `d_hdd.mdl` for the sampled-data system. In the simulation we take into account the amplifier saturation, which was neglected in the design so far. Both models allow us to simulate the closed-loop system for different reference, disturbance and noise signals.

Before simulating the continuous-time system it is necessary to assign the model parameters by using the M-file `init_c_hdd.m`.

The sampled-data model involves the discrete-time controller, 16-bit analogue-to-digital converter with maximum input voltage 2.5 V and 16-bit digital-to-analogue converter with maximum output voltage 10 V. It is assumed that the discrete-time controller is implemented on a *digital signal processor(DSP)* with word length of 64 bits. These parameters are set prior to the simulation by using the M-file `init_d_hdd.m`. It is assumed that the control action calculation requires one sampling period T_s.

In Figure 10.44 we show the Simulink® model `d_hdd.mdl` of the nonlinear, sampled-data, closed-loop system.

As in the linear case, the transient responses of the nonlinear closed-loop system are obtained for a simulated runout of 1 track width (1μm) and torque disturbance $t_d = 0.0005$ N m.

In Figure 10.45 and in Figure 10.46 we compare the results from the simulation of the continuous-time and discrete-time nonlinear systems. The continuous-time controller is the reduced-order μ-controller in Section 10.7 and the discrete-time controller is the controller designed at the sampling frequency of 36 kHz.

The transient responses of the nonlinear system are close to the corresponding responses of the linear system due to the small input signals (amplitude less than 1.2 V).

It should be mentioned that the controllers designed are appropriate for small reference signals (equivalent to one track). For larger references the amplifier saturates and it is necessary to implement an appropriate seeking algorithm.

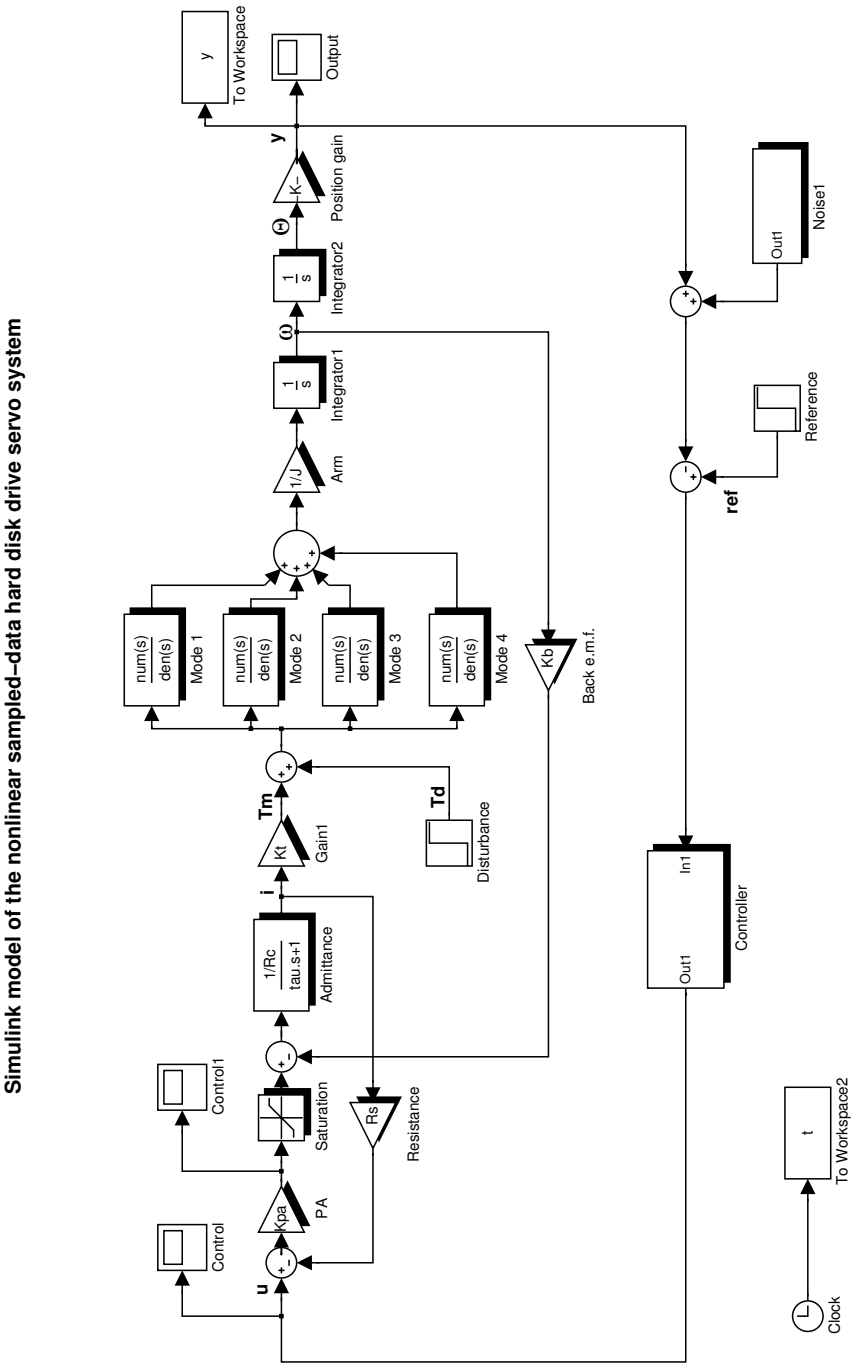

Fig. 10.44. Simulation model of the nonlinear sampled data system

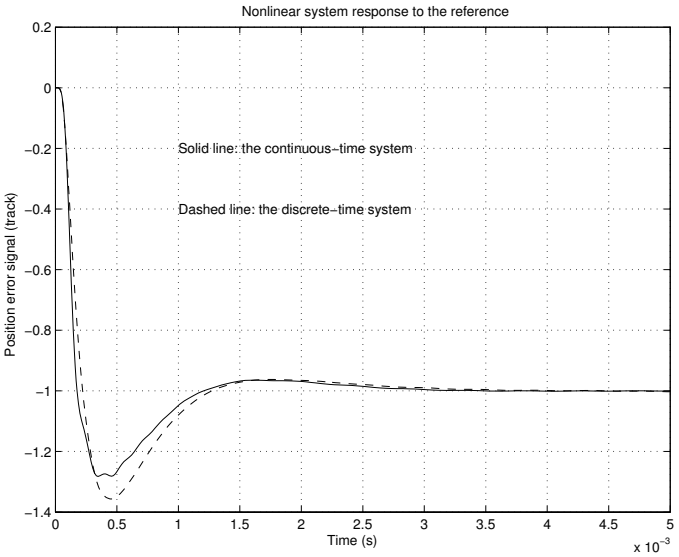

Fig. 10.45. Transient responses of the nonlinear systems

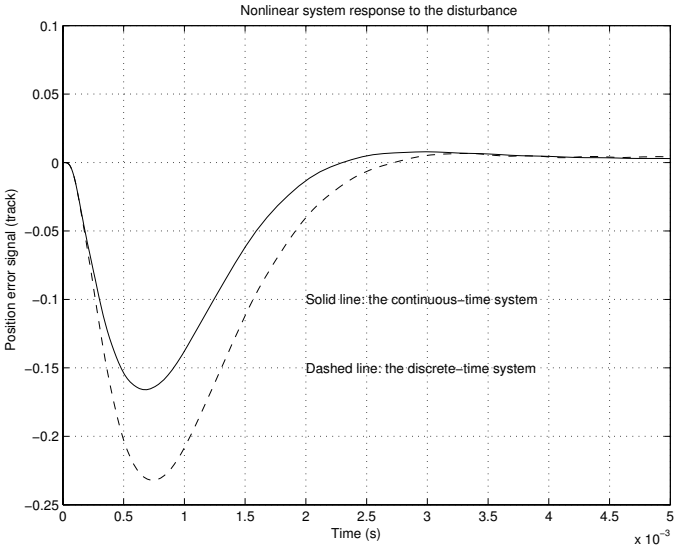

Fig. 10.46. Disturbance responses of the nonlinear systems

10.10 Conclusions

The experience gained in the design of the HDD servo controllers makes it possible to derive the following conclusions:

- The implementation of designed μ, $\mathcal{H}_\infty$ and $\mathcal{H}_\infty$ LSDP controllers in the HDD servo system gives satisfactory results with respect to robustness and performance. All three controllers ensure robust stability of the closed-loop system. The best robust performance is achieved by using the μ and $\mathcal{H}_\infty$ controllers. The implementation of the $\mathcal{H}_\infty$ LSDP controller gives the fastest transient response and the corresponding design is less complicated. This controller, however, leads to the worst performance in the low-frequency range, which results in a large steady-state error. In the given case the best trade-off between the robustness and transient response requirements is achieved by using the μ-controller that is, to some extent, due to the specially chosen weighting functions.
- The number of original uncertain parameters is very large (more than 25 in the given case). This complicates the derivation of the uncertainty model and produces heavy computation demands. This is why it is necessary to investigate the parameter importance with respect to the robustness and performance in order to reduce their number to an acceptable value. However, in the evaluation of the design, it is better to take into account all the possible uncertainties to ensure a satisfactory design in a real case.
- In the μ-synthesis, the order of the resultant controller depends on the order of the plant, of the weighting functions and of the scaling diagonal elements approximations. The designed controllers are usually of high orders, which complicates the implementation of the controller. Hence, an order reduction should usually be considered right after the controller design. Most controllers used in the HDD designs are of order between 8 and 15.
- Good disturbance attenuation requires sufficiently large closed-loop bandwidth. This may, however, lead to difficulties in achieving robust stability and robust performance in the presence of resonant modes. Some resonances whose frequencies are much higher than the closed-loop bandwidth and thus seem innocent may even actually destroy the robust stability of the system. In such cases, it is necessary to increase the damping of these modes by using techniques of passive/active damping.
- The presence of resonant modes may require sufficiently high sampling rates in the case of using a discrete-time controller.
- It is important to stress that better results, with respect to the transient response (overshoot and settling time), are difficult to obtain for the current plant parameters. If higher performance demands are required, it is necessary to change the HDD parameters, for instance to increase the VCM torque constant.

Notes and References

The history of the Hard Disk Drive control is presented in the fascinating papers of Abramovitch and Franklin [1, 2]. An excellent survey on similarities and contrasts in the magnetic and optical disk controls is given in [5]. In [77] one may find an attractive description of the HDD construction and functioning.

The book of Chen *et al.* [15] is the only book up to the moment that is entirely devoted to HDD servo systems and contains rich information related to the design of such systems. A tutorial on HDD control can be found in [106].

A detailed model of the HDD servo system, which has very much influenced the model used in this chapter, is presented in the book of Franklin *et al.* [39, Chapter 14]. Below 100 Hz the rotary actuator dynamics is affected by pivot bearing nonlinearity, which is known under the name "stick-slip" . It has a strong effect particularly in the case of small disk drives with lower actuator inertia. Analysis and simulation of this phenomenon are presented in [4, 156].

An important step in the design of HDD servo systems is the reliable estimation of the various disturbances and noises acting on the system. Methods for such estimations are described in [3, 27, 61].

The harmonic compensation used to reduce RRO is considered in [16, 74].

The track-seeking and track-following modes require different control algorithms. Track-seeking algorithms are described in [39, 123]. The switching of control mode from track-seeking to track-following should be smooth so that the residual vibration of the read/write head suspension is minimal. There are several control algorithms that work for both track-seeking and following, see for instance [70, 63]. Such algorithms utilise two-degree-of-freedom (2DOF) controllers in which case the track seeking is accomplished by using a feedforward controller along with a reference trajectory.

Apart from the track seeking and track following the HDD also contains a spindle velocity control loop. The purpose of this loop is to control the air flow over the disk in order to guarantee the appropriate flying height of the read/write head. This is a low-frequency control loop and its design does not represent a serious difficulty.

Further expansion of the closed-loop bandwith of the HDD control system may be achieved by using the so-called dual-stage servos that consist of a low-bandwidth coarse actuator (the usual VCM) and a high bandwidth fine actuator. The fine actuator has a small stroke and may be implemented as a *piezoelectric transducer(PZT)* [31]. The design of dual-stage servos is considered in [22, 66, 76].

Other important aspects of the analysis and design of HDD servo systems are presented in [50, 69, 83, 99, 164], to name a few.

11

Robust Control of a Distillation Column

In this chapter we present the design of a robust control system for a high-purity distillation column. The original nonlinear model of the column is of high order and it includes parametric gain and time-delay uncertainty. A low-order linearised distillation column model is used in the design of a two-degree-of freedom (2DOF) $\mathcal{H}_\infty$ loop-shaping controller and a μ-controller. Both controllers ensure robust stability of the closed-loop system and fulfillment of a mixture of time-domain and frequency-domain specifications. A reduced order μ-controller is then found that preserves the robust stability and robust performance of the closed-loop system. The simulation of the closed-loop system with the nonlinear distillation column model shows very good performance for different reference and disturbance signals as well as for different values of the uncertain parameters.

11.1 Introduction

Distillation is an important process in the separation and purification of chemicals. The process exploits the difference at boiling points of multicomponent liquids. The control of distillation columns is difficult, because the distillation process is highly nonlinear and the corresponding linearised models are often ill-conditioned around the operating point.

The aim of the design, presented in this chapter, is to find a controller that achieves robust stability and robust performance of the closed-loop control system of a high-purity distillation column. The original nonlinear model of the column is of 82nd order and it includes uncertainties in the form of parametric gains and time delay. The uncertainty model is considered in the form of an input multiplicative complex uncertainty. In our design exercises, we found that it is difficult to achieve the desired performance of the closed-loop system using one-degree-of-freedom controllers. Hence, we turned to the $\mathcal{H}_\infty$ two-degree-of-freedom loop-shaping design procedure and μ-synthesis/analysis method. The

designs are based on a 6th-order linearised distillation column model. Both designed controllers ensure robust stability of the closed-loop system and achieve a mixed set of time-domain and frequency-domain specifications. We present several time-domain and frequency-domain characteristics of the corresponding closed-loop systems that makes possible the comparison of controllers efficiency. An 11th-order reduced-order μ-controller is found that preserves the stability and performance of the closed-loop system in the presence of uncertainties. The simulation of the closed-loop system with this μ-controller and with the nonlinear distillation column model is conducted in Simulink® and shows very good performance for different reference and disturbance signals as well as for different values of the uncertain parameters.

11.2 Dynamic Model of the Distillation Column

A typical two-product distillation column is shown in Figure 11.1. The objective of the distillation column is to split the feed F, which is a mixture of a light and a heavy component with composition z_F, into a distillate product D with composition y_D, which contains most of the light component, and a bottom product B with composition z_B, which contains most of the heavy component. For this aim, the column contains a series of trays that are located along its height. The liquid in the columns flows through the trays from top to bottom, while the vapour in the column rises from bottom to top. The constant contact between the vapour and liquid leads to increasing concentration of the more-volatile component in the vapour, while simultaneously increasing concentration of the less volatile component in the liquid. The operation of the column requires that some of the bottom product is reboiled at a rate V to ensure the continuity of the vapor flow and some of the distillate is refluxed to the top tray at a rate L to ensure the continuity of the liquid flow.

The notations used in the derivation of the column model are summarised in Table 11.1 and the column data are given in Table 11.2.

The index i denotes the stages numbered from the bottom ($i = 1$) to the top ($i = N_{\text{tot}}$) of the column. Index B denotes the bottom product and D the distillate product. A particular high-purity distillation column with 40 stages (39 trays and a reboiler) plus a total condensor is considered.

The nonlinear model equations are:

1. Total material balance on stage i

$$\mathrm{d}M_i/\mathrm{d}t = L_{i+1} - L_i + V_{i-1} - V_i$$

2. Material balance for the light component on each stage i

$$\mathrm{d}(M_i x_i)/\mathrm{d}t = L_{i+1}x_{i+1} + V_{i-1}y_{i-1} - L_i x_i - V_i y_i$$

This equation leads to the following expression for the derivative of the liquid mole fraction

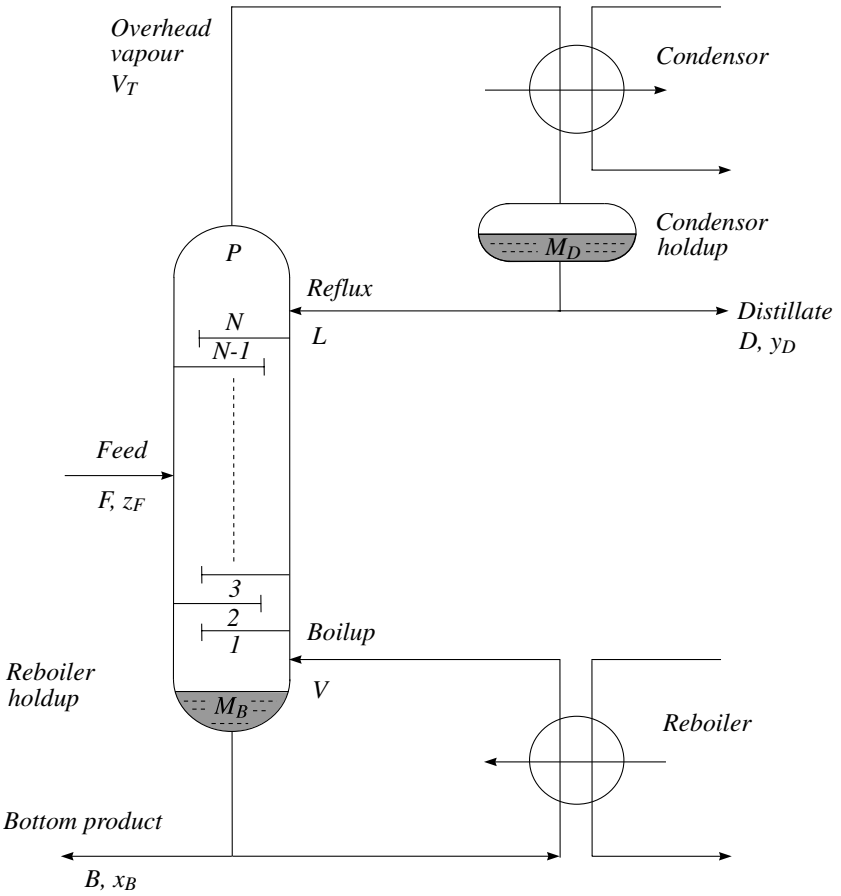

Fig. 11.1. The distillation column system

$$\mathrm{d}x_i/\mathrm{d}t = (\mathrm{d}(M_i x_i)/\mathrm{d}t - x_i(\mathrm{d}M_i/\mathrm{d}t))/M_i$$

3. Algebraic equations
   The vapour composition y_i is related to the liquid composition x_i on the same stage through the algebraic vapour-liquid equilibrium

$$y_i = \alpha x_i/(1 + (\alpha - 1)x_i)$$

   From the assumption of constant molar flows and no vapour dynamics, one obtains the following expression for the vapour flows

$$V_i = V_{i-1}$$

   The liquid flows depend on the liquid holdup on the stage above and the vapor flow as follows

Table 11.1. Column nomenclature

Symbol	Description
F	Feed rate [kmol/min]
z_F	feed composition [mole fraction]
q_F	fraction of liquid in feed
D and B	distillate (top) and bottom product flowrate [kmol/min]
y_D and x_B	distillate and bottom product composition (usually of light component) [mole fraction]
L	reflux flow [kmol/min]
V	boilup flow [kmol/min]
N	number of stages (including reboiler)
$N_{\text{tot}} = N + 1$	total number of stages (including condensor)
i	stage number (1 – bottom, N_F – feed stage, N_T – total condensor)
L_i and V_i	liquid and vapour flow from stage i [kmol/min]
x_i and y_i	liquid and vapour composition of light component on stage i
M_i	liquid holdup on stage i [kmol] (M_B – reboiler, M_D – condensor holdup)
α	relative volatility between light and heavy component
τ_L	time constant for liquid flow dynamics on each stage [min]

Table 11.2. Column data

N	N_{tot}	N_F	F	z_F	q_F	D
40	41	21	1	0.5	1	0.5
B	L	V	y_D	x_B	M_i	τ_L
0.5	2.706 29	3.206 29	0.99	0.01	0.5	0.063

$$L_i = L0_i + (M_i - M0_i)/\tau_L + \lambda(V_{i-1} - V0_{i-1})$$

where $L0_i$ [kmol/min] and $M0_i$ [kmol] are the nominal values for the liquid flow and holdup on stage i and $V0_i$ is the nominal boilup flow. If the vapour flow into the stage effects the holdup then the parameter λ is different from zero. For the column under investigation $\lambda = 0$.

The above equations apply at all stages except in the top (condensor), feed stage and bottom (reboiler).

1. For the feed stage, $i = N_F$ (it is assumed that the feed is mixed directly into the liquid at this stage)

$$\mathrm{d}M_i/\mathrm{d}t = L_{i+1} - L_i + V_{i-1} - V_i + F$$

$$\mathrm{d}(M_i x_i)/\mathrm{d}t = L_{i+1}x_{i+1} + V_{i-1}y_{i-1} - L_i x_i - V_i y_i + F z_F$$

2. For the total condensor, $i = N_{\text{tot}} (M_{N_{\text{tot}}} = M_D, L_{N_{\text{tot}}} = L_T)$

$$\mathrm{d}M_i/\mathrm{d}t = V_{i-1} - L_i - D$$

$$\mathrm{d}(M_i x_i)/\mathrm{d}t = V_{i-1} - L_i x_i - D x_i$$

3. For the reboiler, $i = 1 (M_i = M_B, V_i = V_B = V)$

$$\mathrm{d}(M_i x_i)/\mathrm{d}t = L_{i+1} x_{i+1} - V_i y_i - B x_i$$

As a result, we obtain a nonlinear model of the distillation column of 82nd order. There are two states per tray, one representing the liquid composition and the other representing the liquid holdup. The model has four manipulated inputs (L_T, V_B, D and B) and three disturbances (F, z_F and q_F).

In order to find a linear model of the distillation column it is necessary to have a steady-state operating point around which the column dynamics is to be linearised. However, the model contains two integrators, because the condensor and reboiler levels are not under control. To stabilise the column, we make use of the so called *LV-configuration of the distillation column* where we use D to control M_D and B to control M_B. This is done by two proportional controllers with both gains equal to 10.

The nonlinear model is linearised at the operating point given in Table 11.2 (the values of F, L, V, D, B, y_D, x_B and z_F). These steady-state values correspond to an initial state where all liquid compositions are equal to 0.5 and the tray holdups are also equal to 0.5 [kmol]. The steady-state vector is obtained for $t = 5000$ min by numerical integration of the nonlinear model equations of the LV-configuration given in the M-file `cola_lv.m`. The linearisation is carried out by implementing the M-file `cola_lin` that makes use of the equations given in the file `cola_lv_lin.m`. The 82nd-order, linear model is stored in the variable $G_4 u$ and has four inputs (the latter two are actually disturbances)

$$[L_T \;\; V_B \;\; F \;\; z_F]$$

and two outputs

$$[y_D \;\; x_B]$$

Before reducing the model order, the model $G_4 u$ is scaled in order to make all inputs/disturbances and all outputs at about the same magnitude. This is done by dividing each variable by its maximum change, *i.e.*

$$u = U/U_{\max};\; y = Y/Y_{\max}$$

where $U,\; Y$ are the input and output of the model $G_4 u$ in original units, $U_{\max},\; Y_{\max}$ are the corresponding maximum values allowed, and $u,\; y$ are the scaled variables. The scaling is achieved by using the input scaling matrix

$$S_i = \begin{bmatrix} 1 & 0 & 0 & 0 \\ 0 & 1 & 0 & 0 \\ 0 & 0 & 0.2 & 0 \\ 0 & 0 & 0 & 0.1 \end{bmatrix}$$

and output scaling matrix

$$S_o = \begin{bmatrix} 100 & 0 \\ 0 & 100 \end{bmatrix}$$

The scaled model is then found as $G_4 = SoG_4uS_i$.

The final stage in selecting the column model is the order reduction of the scaled model G_4. This is done by using the commands `sysbal` and `hankmr`. As a result, we obtain a 6th-order model saved in the variable G.

All commands for finding the 6th-order linear model of the distillation column are contained in the file `mod_col.m`. The frequency responses of the singular values of G are compared with the singular values of the 82nd order linearised model G_4 in Figure 11.2. It is seen that the behaviour of both models is close until the frequency 2 rad/min.

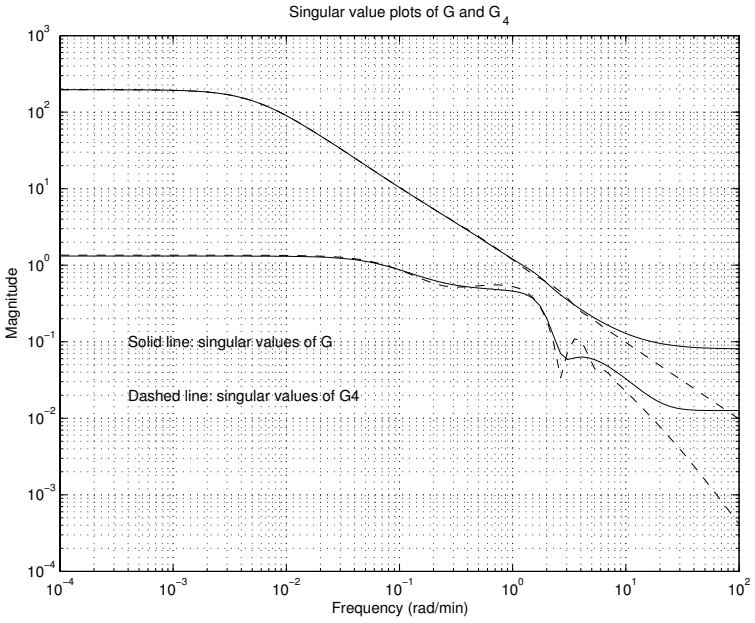

Fig. 11.2. Singular values of G and G_4

11.3 Uncertainty Modelling

The uncertainties considered in the distillation column control systems are a gain uncertainty of $\pm 20\%$ and a time delay of up to 1 min in each input channel. Thus, the uncertainty may be represented by the transfer matrix

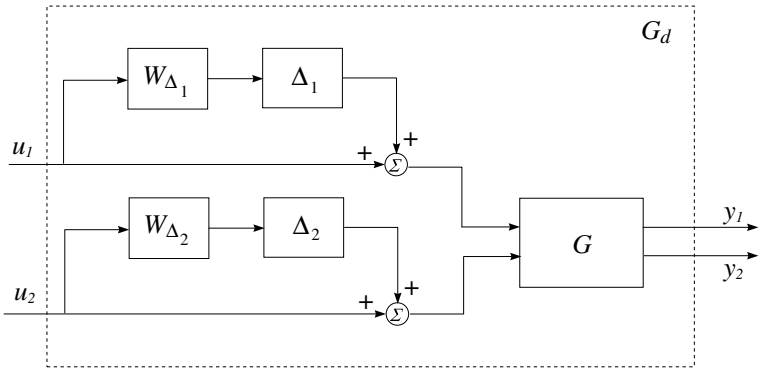

Fig. 11.3. Distillation column with input multiplicative uncertainty

$$W_u = \begin{bmatrix} k_1 \mathrm{e}^{-\Theta_1 s} & 0 \\ 0 & k_2 \mathrm{e}^{-\Theta_2 s} \end{bmatrix}$$

where $k_i \in [0.8 \;\; 1.2]$; $\Theta_i \in [0.0 \;\; 1.0]$; $i = 1, 2$. It is convenient to represent this uncertainty by an input multiplicative uncertainty, as shown in Figure 11.3, with

$$\Delta = \begin{bmatrix} \Delta_1 & 0 \\ 0 & \Delta_2 \end{bmatrix}$$

where $|\Delta_1| \leq 1, \; |\Delta_2| \leq 1$. The uncertainty weighting function

$$W_\Delta = \begin{bmatrix} W_{\Delta_1} & 0 \\ 0 & W_{\Delta_2} \end{bmatrix}$$

is determined in the following way.

Denote by $\overline{W}_{u_i} = 1$ the nominal transfer function in the ith channel for $k_i = 1$ and $\Theta_i = 0$; $i = 1, 2$.

According to Figure 11.3 we have that

$$W_{u_i} = (1 + W_{\Delta_i} \Delta_i) \overline{W}_{u_i}, \;\; i = 1, 2$$

Taking into account that $|\Delta_i| \leq 1$ it follows that the relative uncertainty should satisfy

$$\frac{\left| W_{u_i}(j\omega) - \overline{W}_{u_i}(j\omega) \right|}{\left| \overline{W}_{u_i}(j\omega) \right|} \leq \left| W_{\Delta_i}(j\omega) \right|, \; i = 1, 2$$

where $W_{u_i}(j\omega) = k_i \mathrm{e}^{j\omega\Theta_i} = k_i(\cos(\omega\Theta_i) + j \sin(\omega\Theta_i))$. In this way, to choose the uncertainty weight W_{Δ_i} is equivalent to determining an upper bound of the frequency response of the relative uncertainty

$$\frac{\left| W_{u_i}(j\omega) - \overline{W}_{u_i}(j\omega) \right|}{\left| \overline{W}_{u_i}(j\omega) \right|} = \sqrt{(k_i \cos(\omega\Theta_i) - 1)^2 + (k_i \sin(\omega\Theta_i))^2}.$$

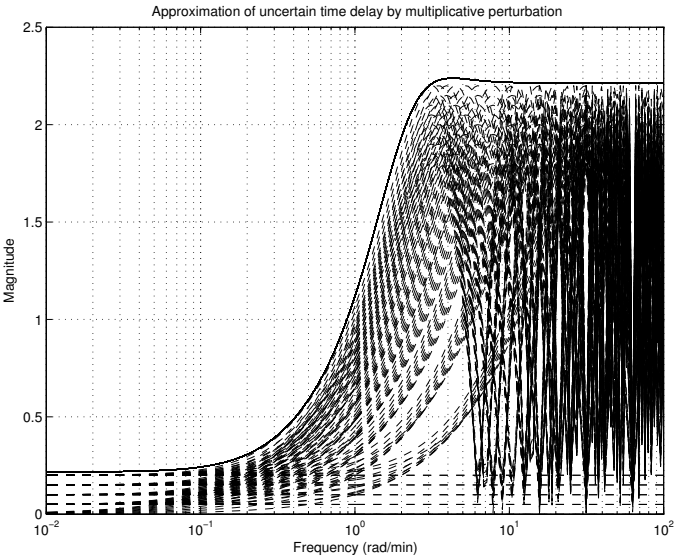

Fig. 11.4. Approximation of the uncertain time delay

The frequency responses of the relative uncertainty

$$\frac{\left|W_{u_i}(j\omega) - \overline{W}_{u_i}(j\omega)\right|}{\left|\overline{W}_{u_i}(j\omega)\right|}$$

are computed by the file `unc_col.m` and shown in Figure 11.4. These responses are then approximated by 3rd-order transfer functions using the file `wfit.m`. As a result, one obtains

$$W_{\Delta_i} = \frac{2.2138s^3 + 15.9537s^2 + 27.6702s + 4.9050}{1.0000s^3 + 8.3412s^2 + 21.2393s + 22.6705},\ i = 1, 2$$

11.4 Closed-loop System-performance Specifications

The aim of the distillation column control-system design is to determine a controller that meets robust stability and robust performance specifications for the LV configuration. Since these specifications are difficult to satisfy with a one-degree-of-freedom controller, we present the design of two-degree-of-freedom controllers that ensure robust stability and robust performance of the closed-loop system. In the given case, the robust stability means guaranteed closed-loop stability for all $0.8 \leq k_1,\ k_2 \leq 1.2$ and $0 \leq \Theta_1,\ \Theta_2 \leq 1$ min. The time-domain specifications are given in terms of step-response requirements, which must be met for all values of $k_1,\ k_2, \Theta_1$ and Θ_2. Specifically, for a unit

step command to the first input channel at $t = 0$, the scaled plant outputs y_1 (tracking) and y_2 (interaction) should satisfy:

- $y_1(t) \geq 0.9$ for all $t \geq 30$ min;
- $y_1(t) \leq 1.1$ for all t;
- $0.99 \leq y_1(\infty) \leq 1.01$;
- $y_2(t) \leq 0.5$ for all t;
- $-0.01 \leq y_2(\infty) \leq 0.01$.

Correspondingly, similar requirements should be met for a unit step command at the second input channel.

In addition, the following frequency-domain specification should be met:

- $\overline{\sigma}(\hat{K}_y\hat{S})(j\omega) < 316$, for each ω, where $\hat{K}_y$ denotes the feedback part of the unscaled controller. (Here and latter, a variable with a hat refers to the case of unscaled plant.) This specification is included mainly to avoid saturation of the plant inputs.
- $\overline{\sigma}(\hat{G}\hat{K}_y)(j\omega) < 1$, for $\omega \geq 150$; or $\overline{\sigma}(\hat{K}_y\hat{S})(j\omega) \leq 1$, for $\omega \geq 150$.

In the above, $\overline{\sigma}$ denotes the largest singular value, and $\hat{S} = (I + \hat{G}\hat{K}_y) < 1$ is the sensitivity function for $\hat{G}$.

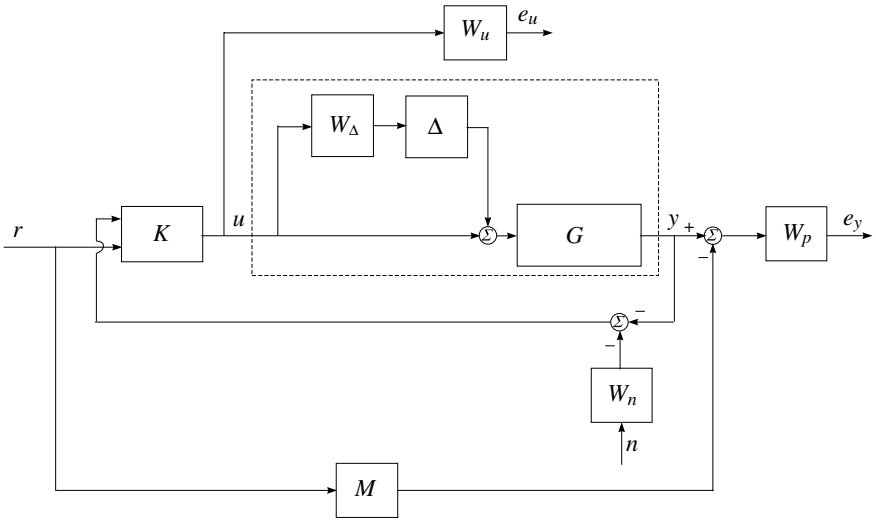

Fig. 11.5. Closed-loop interconnection structure of the distillation column system

The block diagram of the closed-loop system incorporating the design requirements consideration represented by weights is shown in Figure 11.5. The plant enclosed by the dashed rectangle consists of the nominal scaled model G plus the input multiplicative uncertainty. The controller K implements a

feedback from outputs y_D and x_B and a feedforward from the reference signal r. The measurement of the distillate and bottom products composition is corrupted by the noise n. The desired dynamics of the closed-loop system is sought by implementation of a suitably chosen model M. The model M represents the desired dynamic behaviour of the closed-loop system from the reference signal to the outputs. The usage of a model of the desired dynamics allows us to take easily into account the design specifications.

The transfer function matrix of the model M is selected as

$$M = \begin{bmatrix} \frac{1}{Ts^2+2\xi Ts+1} & 0 \\ 0 & \frac{1}{Ts^2+2\xi Ts+1} \end{bmatrix}$$

The coefficients of the transfer functions ($T = 6,\ \ \xi = 0.8$) in both channels of the model are chosen such as to ensure an overdamped response with a settling time of about 30 min. The off-diagonal elements of the transfer matrix are set as zeros in order to minimise the interaction between the channels.

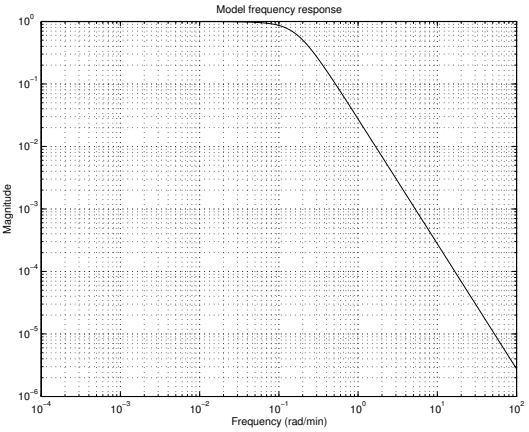

Fig. 11.6. Model frequency response

The frequency response of the model M is shown in Figure 11.6.

Let the scaled, two-degree-of-freedom controller be partitioned as

$$K(s) = [K_y(s)\ K_r(s)]$$

where K_y is the feedback part of the controller and K_r is the prefilter part. It is easy to show that

$$\begin{bmatrix} e_p \\ e_u \end{bmatrix} = \begin{bmatrix} W_p(S\tilde{G}K_r - M) & -W_pTW_n \\ W_u(I + K_y\tilde{G})^{-1}K_r & -W_uK_ySW_n \end{bmatrix} \begin{bmatrix} r \\ n \end{bmatrix}$$

where $S = (I+\tilde{G}K_y)^{-1}$ is the sensitivity function for the scaled plant, $T = (I+\tilde{G}K_y)^{-1}\tilde{G}K_y$ is the complementary sensitivity function and $\tilde{G} = G(I+W_\Delta \Delta)$ is the uncertain, scaled plant model.

The performance objective is to satisfy

$$\left\| \begin{bmatrix} W_p(S\tilde{G}K_r - M) & -W_p T W_n \\ W_u(I + K_y\tilde{G})^{-1}K_r & -W_u K_y S W_n \end{bmatrix} \right\|_\infty < 1 \tag{11.1}$$

for each uncertain $\tilde{G}$.

The performance and control action weighting functions are chosen as

$$W_p = \begin{bmatrix} 0.55\frac{9.5s+3}{9.5s+10^{-4}} & 0.3 \\ 0.3 & 0.55\frac{9.5s+3}{9.5s+10^{-4}} \end{bmatrix}, \quad W_u = \begin{bmatrix} 0.87\frac{s+1}{0.01s+1} & 0 \\ 0 & 0.87\frac{s+1}{0.01s+1} \end{bmatrix}$$

The implementation of the performance weighting function W_p aims to ensure closeness of the system dynamics to the model over the low-frequency range. Note that this function contains nonzero off-diagonal elements that make it easier to meet the time-domain specifications. A small constant equal to 10^{-4} is added in the denominator in each channel to make the design problem regular.

The usage of the control weighting function W_u allows us to limit the magnitude of control actions over the specified frequency range ($\omega \geq 150$).

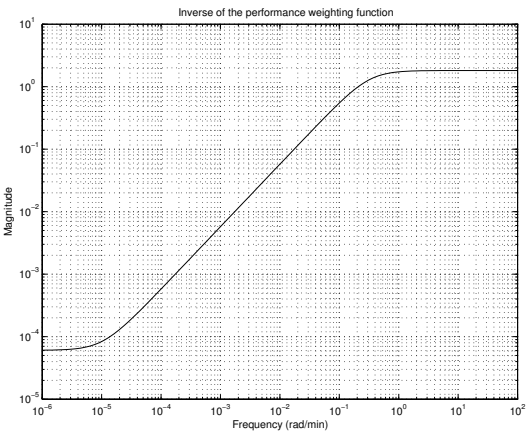

Fig. 11.7. Inverse of performance weighting function

The magnitude plot of the inverse of the performance weighting function W_p is shown in Figure 11.7 and the magnitude plot of the control weighting function is shown in Figure 11.8.

The noise shaping filter

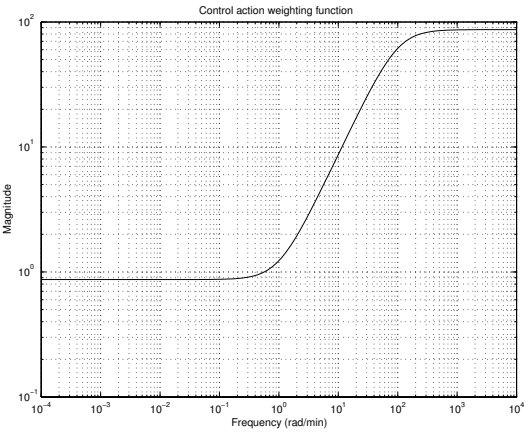

Fig. 11.8. Control-action weighting function

$$W_n = \begin{bmatrix} 10^{-2}\frac{s}{s+1} & 0 \\ 0 & 10^{-2}\frac{s}{s+1} \end{bmatrix}$$

is determined according to the spectral contents of the sensor noises accompanying the measurement of the distillate and bottom product composition.

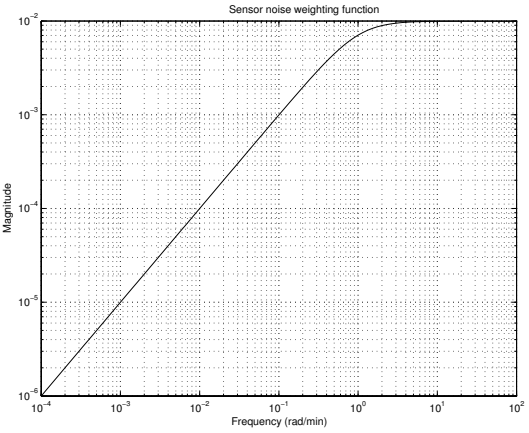

Fig. 11.9. Noise weighting function

The magnitude plot of the noise shaping filter is shown in Figure 11.9.

The model transfer function, the performance and control weighting functions as well as the noise shaping filter are all set in the file `wts_col.m`.

11.5 Open-loop and Closed-loop System Interconnections

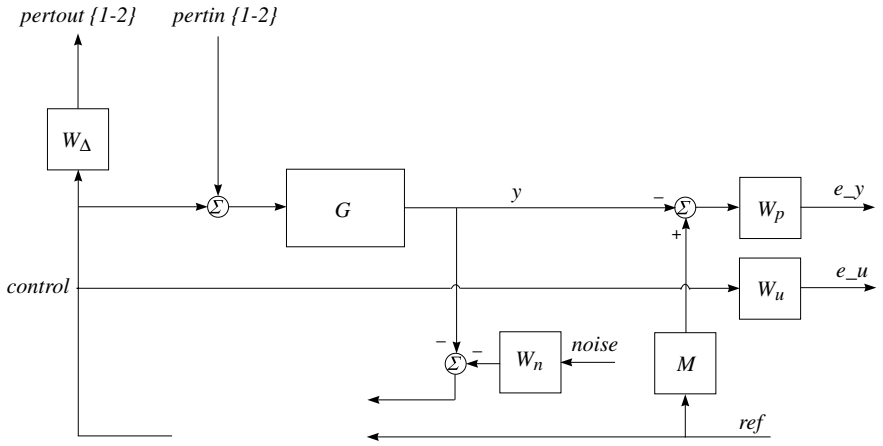

Fig. 11.10. Open-loop interconnection structure of the distillation column system

The open-loop system interconnection is obtained by the M-file `olp_col`. The internal structure of the eight-input, ten-output open-loop system, which is saved as the variable `sys_ic`, is shown in Figure 11.10. The inputs and outputs of the uncertainties are saved as the variables `pertin` and `pertout`, the references and the noises – as the variables `ref` and `noise`, respectively, and the controls – as the variable `control`.

All variables have two elements (*i.e.* 2-dimensional vectors).

The schematic diagram showing the specific input/output ordering for the variable `sys_ic` is given in Figure 11.11.

The block-diagram used in the simulation of the closed-loop system is shown in Figure 11.12. The corresponding closed-loop system interconnection, which is saved as the variable `sim_ic`, is obtained by the M-file `sim_col.m`.

The schematic diagram showing the specific input/output ordering for the variable `sim_ic` is shown in Figure 11.13.

11.6 Controller Design

Successful design of the distillation column control system may be obtained by using the $\mathcal{H}_\infty$ loop-shaping design procedure (LSDP) and the μ-synthesis. Note that in the case of LSDP we do not use the performance specifications implemented in the case of μ-synthesis. Instead of these specifications we use a prefilter W_1 and a postfilter W_2 in order to shape appropriately the open-loop transfer function W_1GW_2.

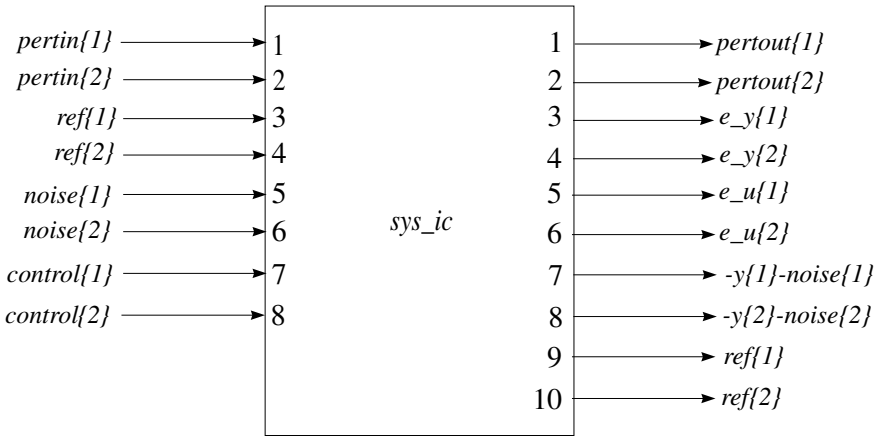

Fig. 11.11. Schematic diagram of the open-loop interconnection

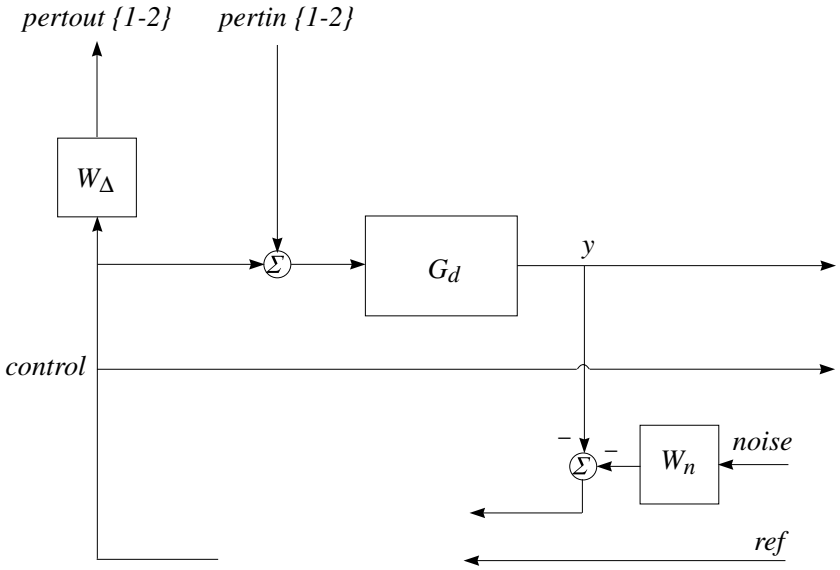

Fig. 11.12. Closed-loop interconnection structure of the distillation column system

11.6.1 Loop-shaping Design

In the present case, we choose a prefilter with transfer function

$$W_1 = \begin{bmatrix} 1.7\frac{1.1s+1}{10s} & 0 \\ 0 & 1.7\frac{1.1s+1}{10s} \end{bmatrix}$$

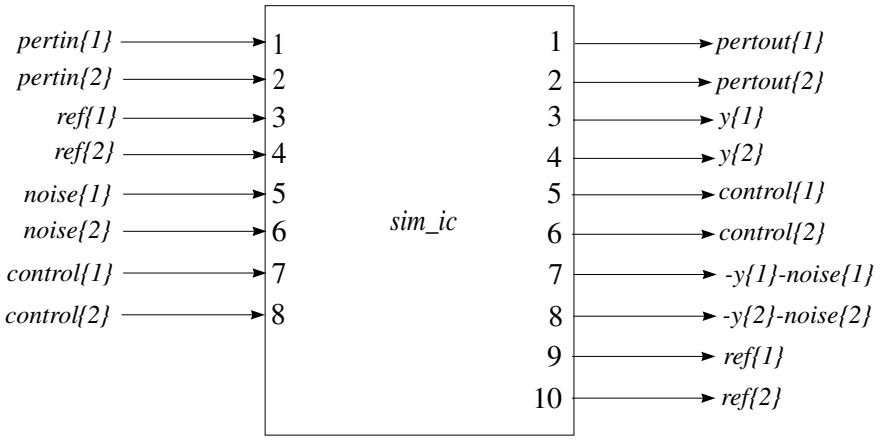

Fig. 11.13. Schematic diagram of the closed-loop interconnection

The choice of the gain equal to 1.7 is done to ensure a sufficiently small steady-state error. Larger gain leads to smaller steady-state errors but worse transient response.

The postfilter is taken simply as $W_2 = I_2$.

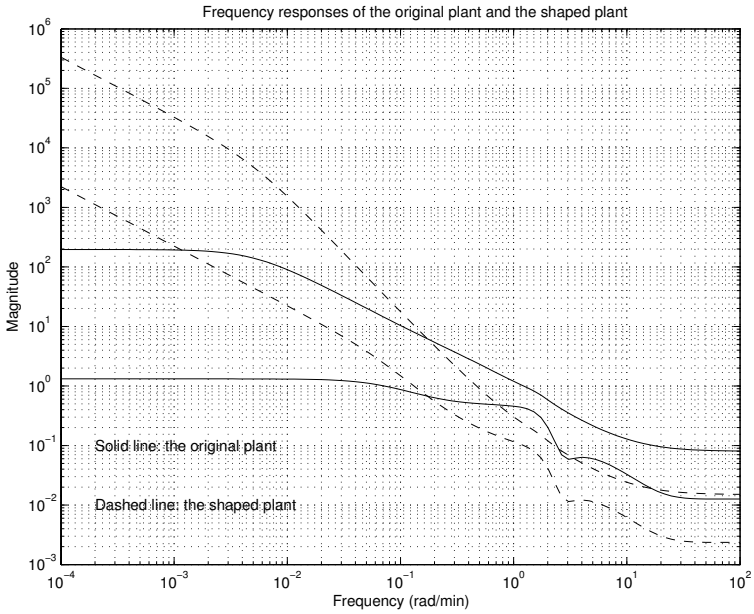

Fig. 11.14. Singular values of the original system and shaped system

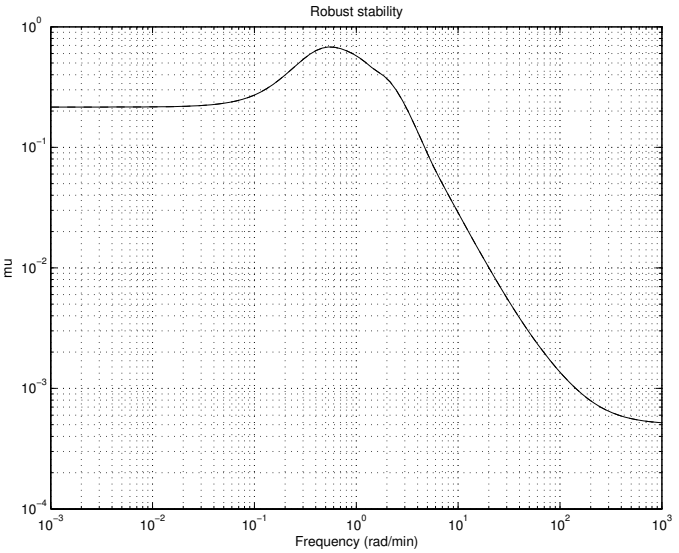

Fig. 11.15. Robust stability for loop-shaping controller

The singular value plots of the original and shaped systems are shown in Figure 11.14. The design of the two-degree-of-freedom LSDP controller is done by using the M-file `lsh_col.m` that implements the function `ncfsyn`. The controller obtained is of order 10.

The robust stability analysis of the closed-loop system is done by the file `mu_col` the frequency response plot of the structured value μ shown in Figure 11.15. According to this plot the closed-loop system preserves stability for all perturbations with norm less than 1/0.6814. As usual, the requirements for nominal performance and robust performance are not fulfilled with this controller.

The closed-loop frequency responses are obtained by using the file `frs_col.m`.

The singular value plot of the unscaled closed-loop system transfer function is shown in Figure 11.16. Both low-frequency gains are equal to 1 that ensures zero steady-state errors in both channels.

The singular value plots of the transfer function matrix with respect to the noises (Figure 11.17) show that the noises are attenuated by at least a factor of 10^4 times at the system output.

The singular-value plots of the transfer function matrices $\hat{G}\hat{K}_y$ and $\hat{K}_y\hat{S}$ are shown in Figures 11.18 and 11.19, respectively. The maximum of the largest singular value of $\hat{G}\hat{K}_y$ is less than 1 for $\omega \geq 150$ and the maximum of the largest singular value of $\hat{K}_y\hat{S}$ is less than 200 so that the corresponding frequency-domain specification is met.

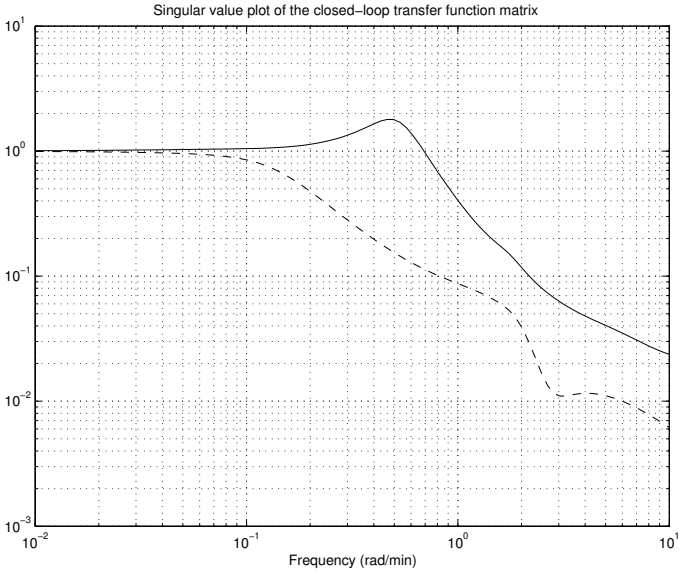

Fig. 11.16. Frequency response of the closed-loop system with loop-shaping controller

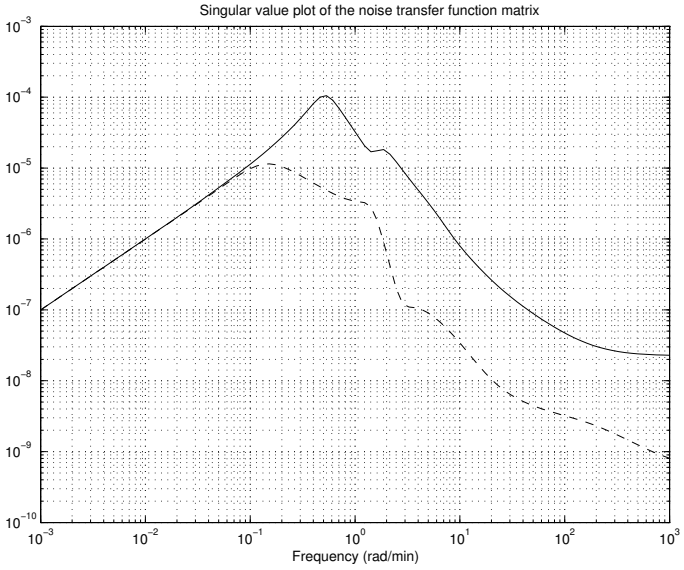

Fig. 11.17. Frequency response to the noises

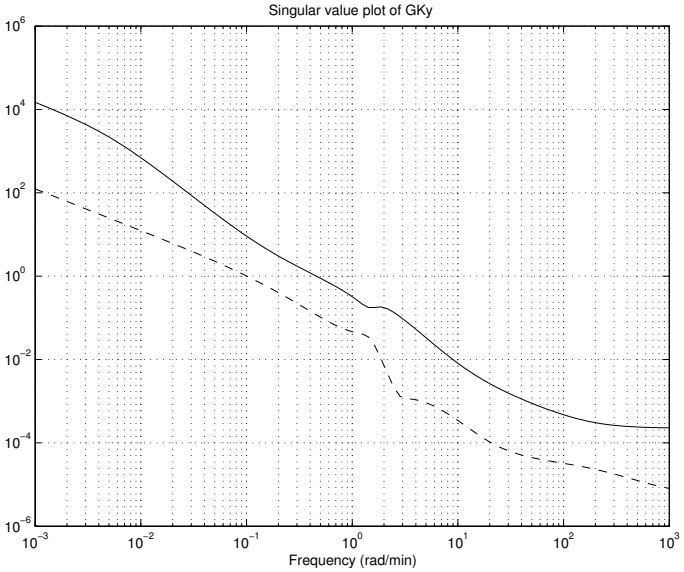

Fig. 11.18. Singular-value plot of $\hat{G}\hat{K}_y$

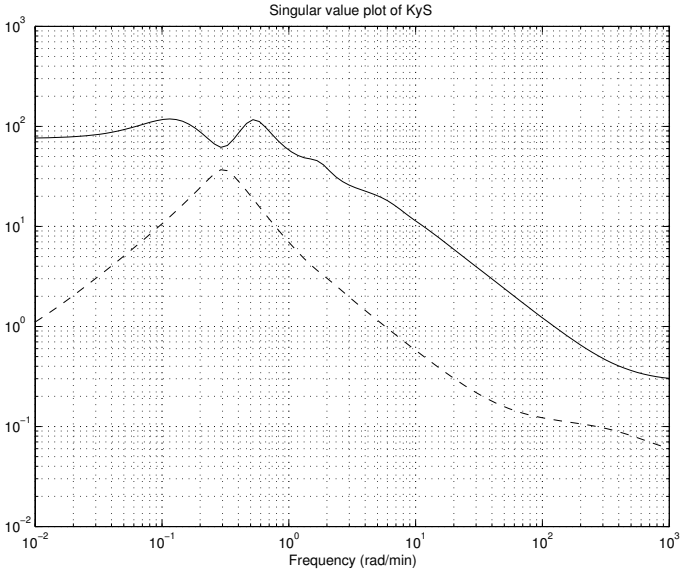

Fig. 11.19. Singular-value plot of $\hat{K}_y\hat{S}$

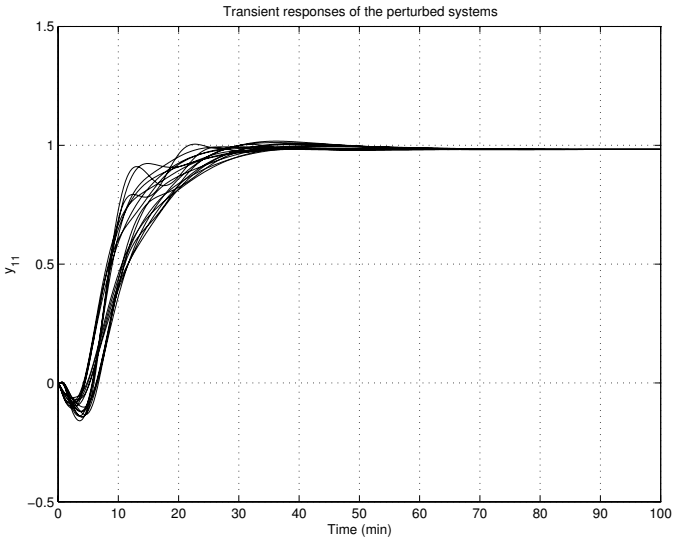

Fig. 11.20. Perturbed transient response y_{11} for loop-shaping controller

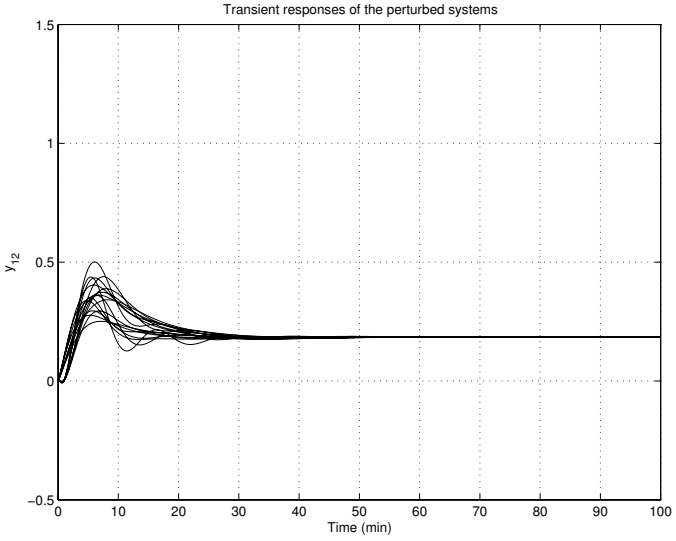

Fig. 11.21. Perturbed transient response y_{12} for loop-shaping controller

In Figures 11.20 – 11.23 we show the transient responses of the scaled closed-loop system obtained by the file `prtcol.m` for different values of the

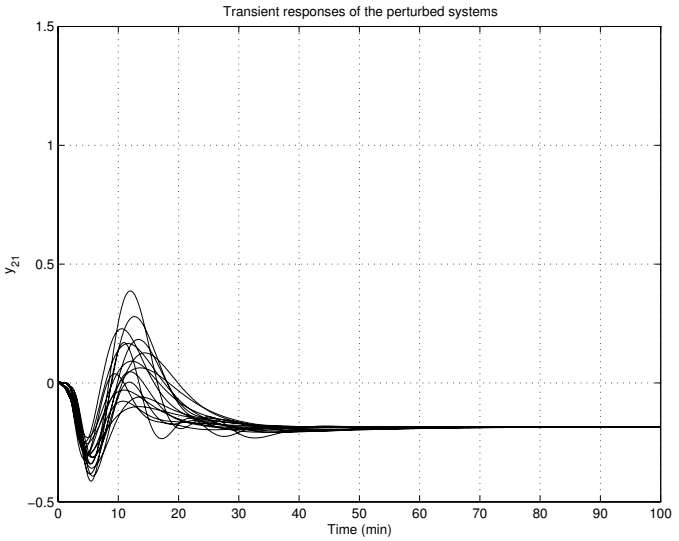

Fig. 11.22. Perturbed transient response y_{21} for loop-shaping controller

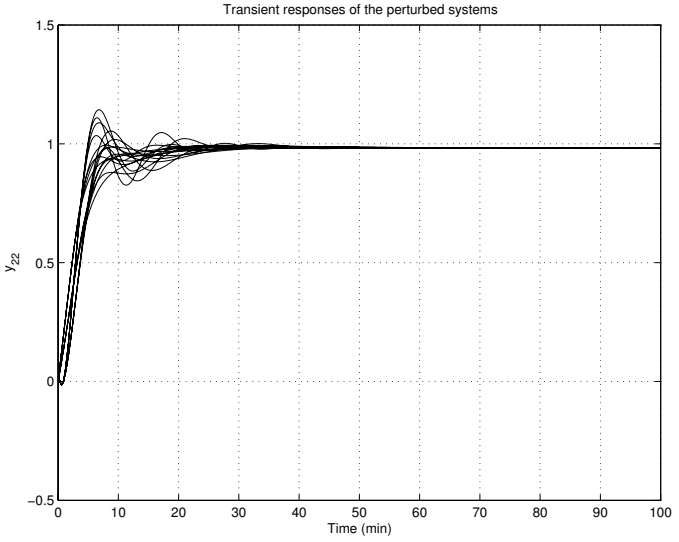

Fig. 11.23. Perturbed transient response y_{22} for loop-shaping controller

uncertain gain and time delay. The time-domain specification is met and the closed-loop system transient response has a small settling time.

The control action in the closed-loop system for the same variations of the uncertain parameters is shown in Figures 11.24 – 11.27.

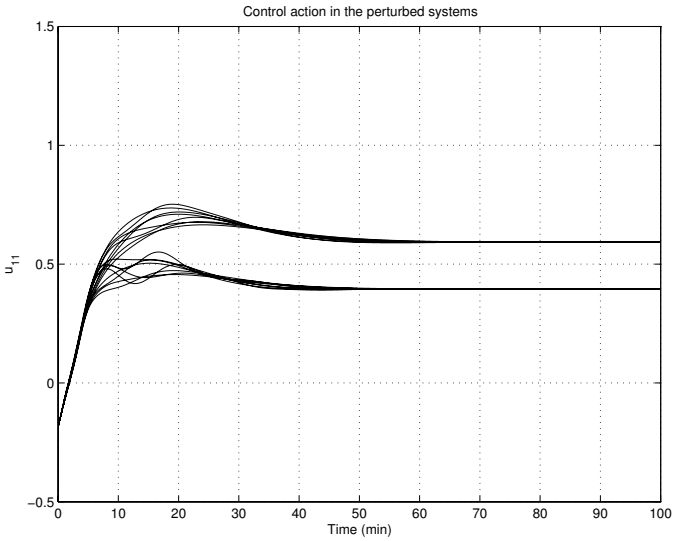

Fig. 11.24. Perturbed control action u_{11} for loop-shaping controller

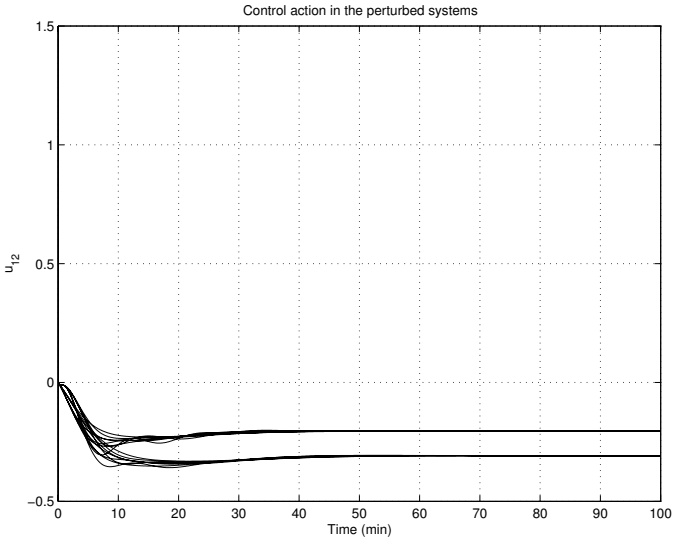

Fig. 11.25. Perturbed control action u_{12} for loop-shaping controller

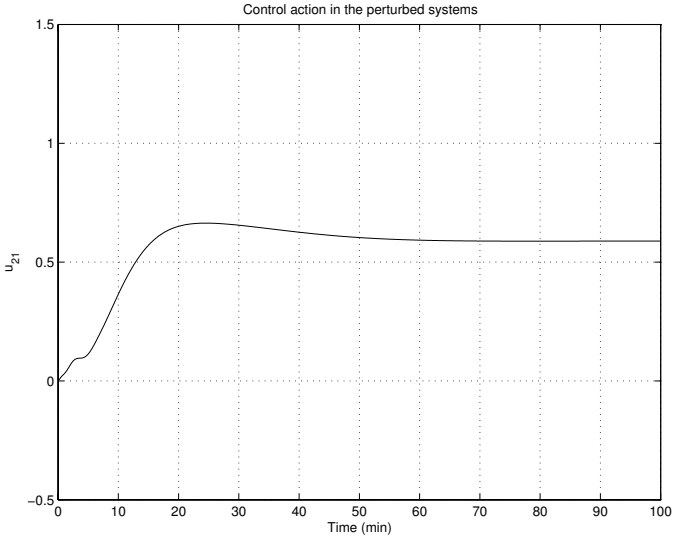
Control action in the perturbed systems
1.5
1
0.5
0
−0.5
u_{21}
0
10
20
30
40
50
60
70
80
90
100
Time (min)

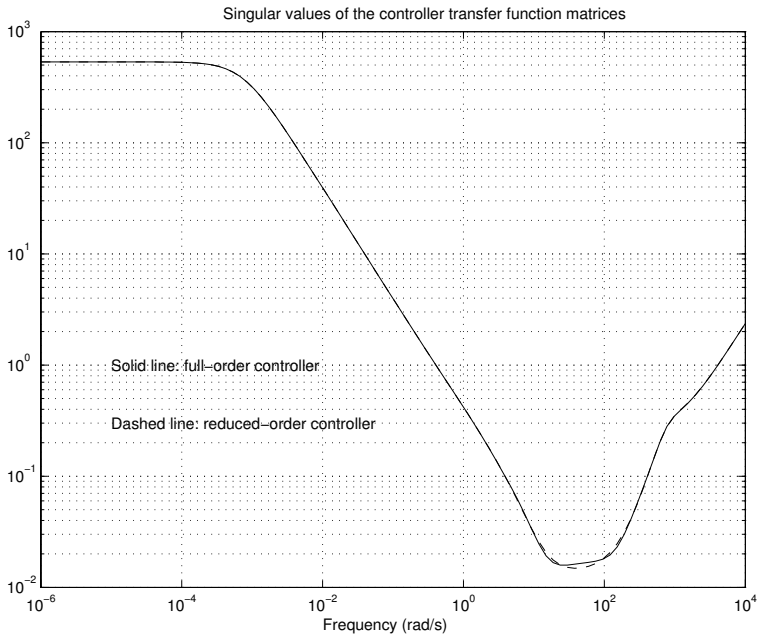

Fig. 12.39. Singular values of the full-order controller and reduced-order controller

chosen equal to 250 Hz that corresponds to a sampling period T_s of 0.004 s. For this frequency we derive a discretised model of the open-loop system by using the function `samhld`. The controller may be synthesised by the aid either of $\mathcal{H}_\infty$ optimisation (by using the function `dhinfsyn`), or μ-synthesis (by using the function `dkit`). In the following, we consider the μ-synthesis of a discrete-time controller that is obtained by implementing the files `dms_rock.m` and `ddk_rock.m`.

As in the μ-synthesis of the continuous-time controller, the synthesis is conducted for the full-order vehicle model. Hence, the uncertainty structure under consideration is of the form

```
BLK_DK = [-1 1;-1 1;-1 1;-1 1;-1 1;-1 1;-1 1;3 2]
```

In the discrete-time case, the frequency range is on the unit circle and chosen as the interval $[0, \pi]$. To set up 100 frequencies, the following line is used

```
OMEGA_DK = [pi/100:pi/100:pi];
```

For the discrete-time design it is necessary to include the command line

```
DISCRETE_DK = 1;
```

The design follows the usual route, by calling the function `dkit`. In Table 12.5 the results of the discrete time D-K iterations are listed.

Table 12.5. Results of the D-K iterations

Iteration	Controller order	Maximum value of μ
1	14	2.101
2	22	0.600
3	28	0.730

The discrete-time controller K_D obtained is of 28th order. Note that better robustness is achieved with the controller obtained at the 2nd step. This controller, however, does not ensure the desired closed-loop dynamics.

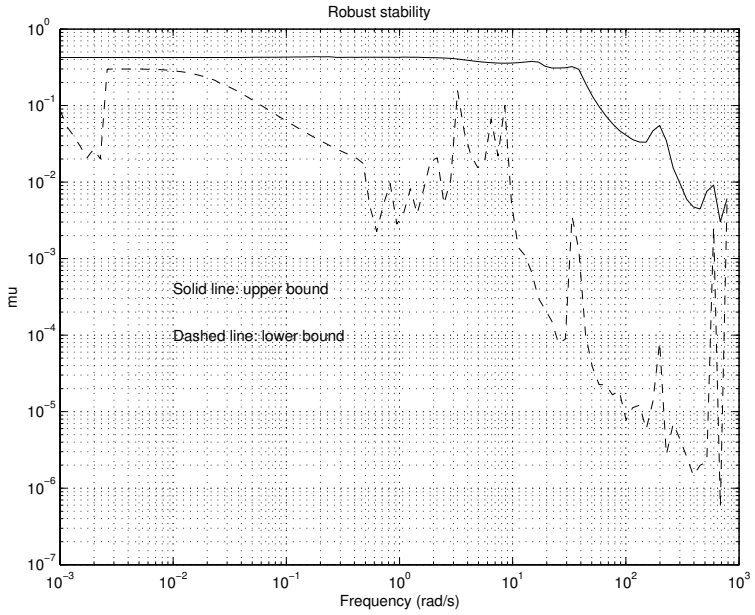

Fig. 12.40. Robust stability of the closed-loop system with K_D

Robust stability and robust performance of the closed-loop system with K_D are shown in Figures 12.40 and 12.41, respectively, in which the μ values over frequency range are calculated by the file `dmu_rock.m`. It is seen that the discrete-time closed-loop system achieves both robust stability and robust performance, just as in the continuous-time case with K_{mu}.

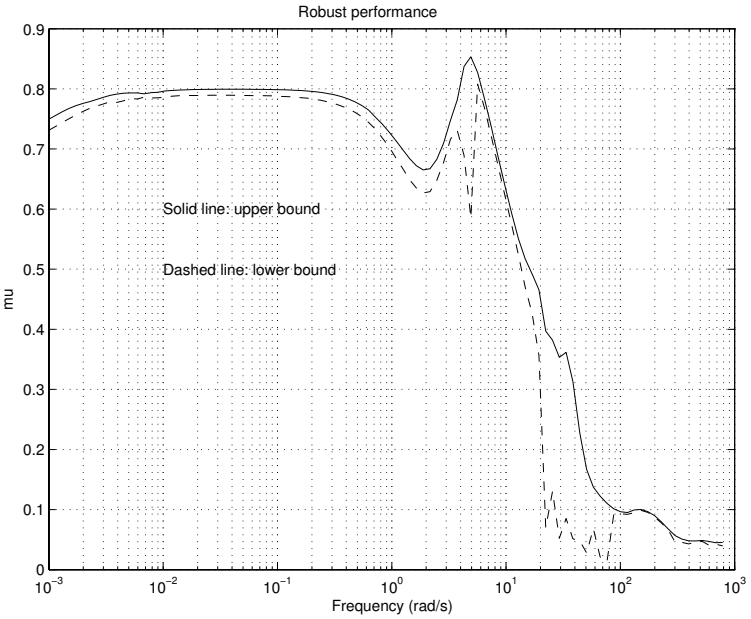

Fig. 12.41. Robust performance of the closed-loop system with K_D

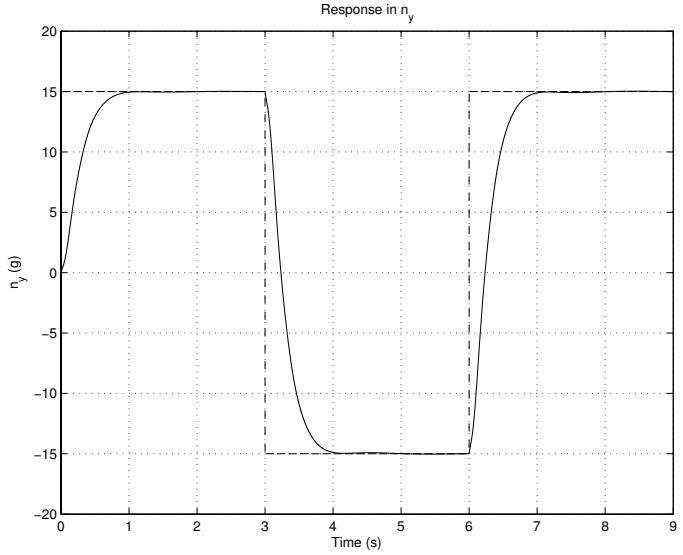

Fig. 12.42. Transient response for K_D, $t = 15$ s

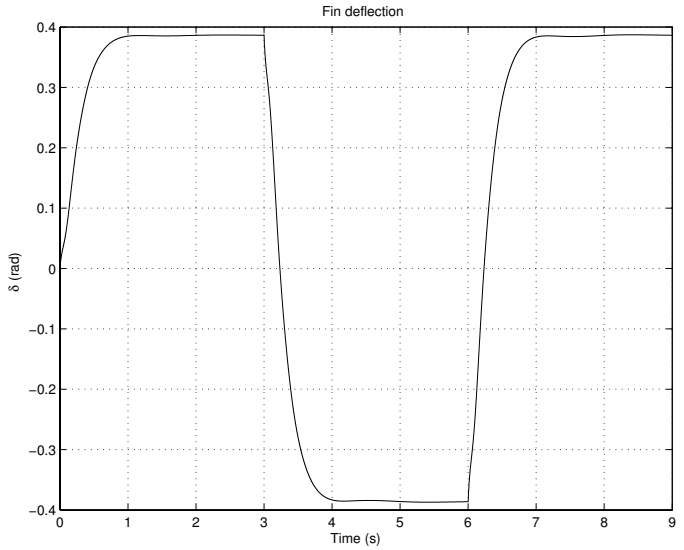

Fig. 12.43. Control action in the closed loop system for K_D, $t = 15$ s

In Figures 12.42 and 12.43 we show the transient response of the closed loop system with respect to the reference signal, and the corresponding control action, respectively. These two figures are generated by the file `dcl_rock.m` that utilises the function `sdtrsp`.

The results displayed above show that the achieved behaviour of the sampled data, closed-loop system are close to those in the continuous-time case, with each corresponding μ-controller.

12.7 Simulation of the Nonlinear System

The dynamics of the nonlinear, time-varying rocket model differs from that of the linear, time-invariant model used in the analysis and design described in the previous sections. Also, for large reference signals there is a strong interconnection between the longitudinal and lateral motions that may affect the stability and performance of the whole system. It is therefore important to study the dynamic behaviour of the closed loop, nonlinear, time-varying system with the designed controller that regulates the six-degree-of-freedom rocket motion.

The closed-loop rocket stabilisation system of the nonlinear, time-varying plant is simulated by using the Simulink® models `c_rock.mdl` (for the continuous-time system with an analogue controller) as well as `d_rock.mdl` (for the sampled data system with a digital controller). Both systems involve

two identical controllers for the longitudinal and lateral motion. The sampled-data system also contains 16-bit analogue-to-digital and digital-to-analogue converters. (The outputs of the digital-to-analogue converters are scaled to give the reference input of the servo-actuators.) Both models allow us to simulate the closed-loop system for different reference, disturbance and noise signals. The roll motion is stabilised by a separate gyro with simple lead-lag compensator. (A robust roll controller is also possible to implement.)

In Figure 12.44 we show the Simulink® model `d_rock.mdl` of the nonlinear, sampled-data, closed-loop system.

Before carrying out simulation it is necessary to assign the model parameters by using the M-file `init_c_rock.m` (in the continuous-time case) or the the M-file `init_d_rock.m` (in the discrete-time case).

Before the perturbation motion begins to affect (*i.e.* before the time instance t_0), only the nonlinear equations of the unperturbed (program) motion are solved. (This ensures that the parameters of the linearised model at t_0 are the same as those used in the controller design.) After t_0, the equations of the perturbed motions are solved by using the S-function `s_rock.m`. The initial conditions for the perturbed motion are assigned in the file `inc_rock.m` that is invoked by `s_rock.m`. During the time interval $[0, t_0]$, the equations of the unperturbed motion are solved in the file `inc_rock.m` by using the function `sol_rock.m`. The values of the pitch angle θ for the program motion are assigned in the file `theta_rock.m`.

The simulation of the perturbed motion, which involves the controller action, is based on the nonlinear differential and algebraic equations (12.1)–(12.5).

In Figures 12.45 and 12.46 we show the transient response of the nonlinear sampled-data system with respect to the normal accelerations n_y and n_z, respectively, for a reference step change of $15g$ occurring at $t_0 = 15$ s in each channel. In the simulation we used the discrete-time controller designed for the same moment of the time in the previous section. It is seen that the behaviour of n_z is very close to the behaviour of the corresponding variable shown in Figure 12.42. The small difference in the responses of n_y and n_z is due to the influence of the Earth's gravity on the pitch angle.

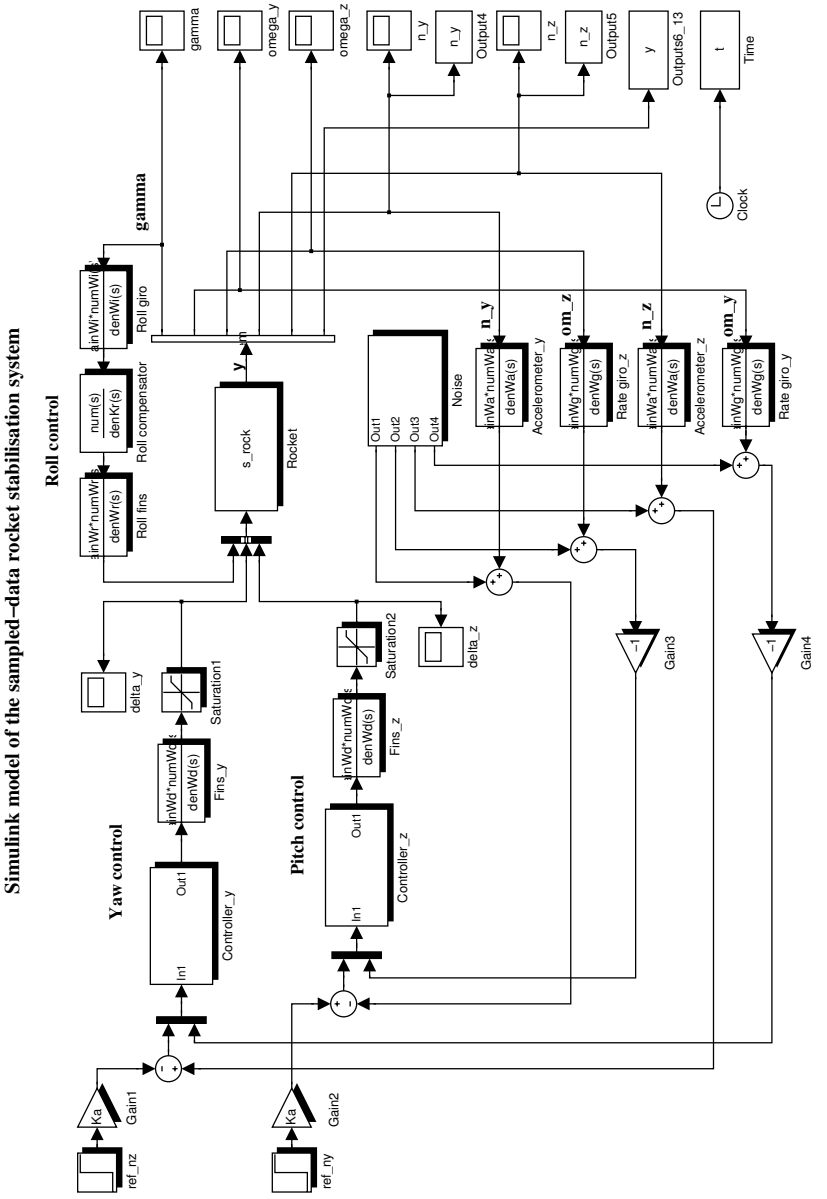

Fig. 12.44. Simulation model of the nonlinear sampled data system

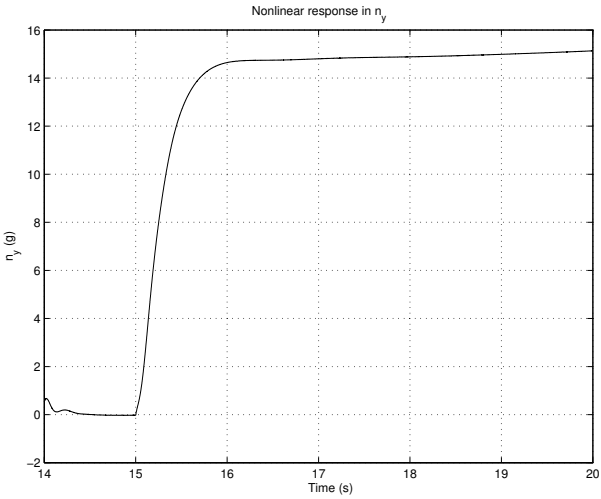

Fig. 12.45. Transient responses in n_y of the nonlinear sampled-data system

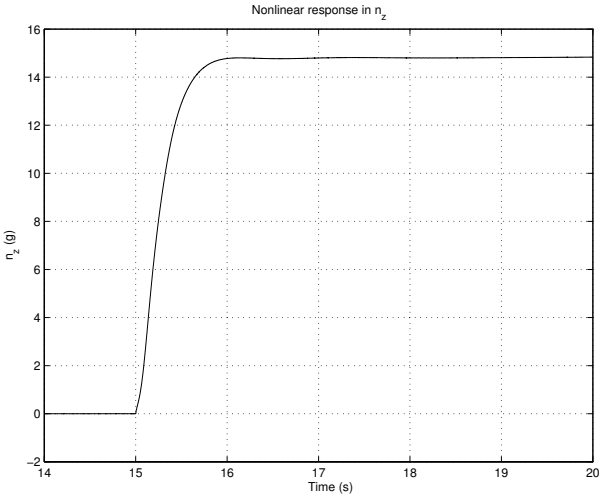

Fig. 12.46. Transient responses in n_z of the nonlinear sampled-data system

12.8 Conclusions

From the results/experiences obtained, the design of a robust stabilisation system for a winged, supersonic rocket may be summarised as the following.

- The linearised equations of the rocket should be arranged in a proper way in order to avoid the appearance of an additional integrator in the uncertainty model. The inclusion of this integrator leads to violation of the conditions for $\mathcal{H}_\infty$ design.
- Both $\mathcal{H}_\infty$ optimisation and μ-synthesis approaches may be used to design controllers that, for a specified moment of flight dynamics, achieve robust stability of the rocket stabilisation system in the presence of disturbances and sensor noises. However, the $\mathcal{H}_\infty$ controller can not ensure robust performance in the given case. The μ-controller achieves both robust stability and robust performance of the closed-loop system.
- The μ-controller obtained may be used successfully for different altitudes and Mach numbers. However, in order to control the rocket efficiently through the whole flight envelope it may be necessary to implement several controllers designed for different flight conditions.
- A digital controller has been successfully designed for a discrete-time model of the open-loop system. The corresponding sampled data, closed-loop system achieves robust stability and robust performance at almost the same as the continuous-time one.
- The μ-synthesis in the discrete-time case shows that achieving a smaller value of μ may lead to the deterioration of the system dynamics, *i.e.* better robustness may be achieved at the price of poorer dynamics. This is why a value of μ slightly less than 1 may be a good trade-off between the requirements for the robustness and dynamic performance.
- The simulation of the nonlinear, time-varying closed-loop system shows that for a sufficiently large interval of time, the dynamics behaviour is close to that of the time-invariant system which has fixed model parameters.

Notes and References

The design of rocket and spacecraft flight-control systems is considered in depth in many books, see for example [11, 12, 54, 172]. The design of robust flight-control systems is presented in [7, 36]. Ensuring good performance of the closed-loop system for the whole range of the flight operating conditions by a fixed controller is rarely possible and, in general, it is necessary to change the controller parameters as the rocket model varies. For this aim, it is possible to use some technique of *gain scheduling*: see the survey papers [84, 131]. The classical approach for gain scheduling is to design several time-invariant controllers for different points in the operational region and then interpolate their parameters for the intermediate values, see, for instance, [130, 118, 13].

This approach has several disadvantages, for instance it is difficult to guarantee robust stability and robust performance in the transition regions, *i.e.* between design points at which the controllers are designed. In this respect robust controllers are more suitable for gain scheduling since they ensure satisfactory performance at least in some neighbourhood around an operating point and thus fewer fixed controllers are needed. Another approach for gain scheduling is to derive a *linear, parameter-varying(LPV)* model of the rocket and then design an LPV controller that hopefully will achieve the desired performance for the whole range of operating conditions. Examples of using this approach may be found in [37, 143].

The elasticity of the rocket body may affect significantly the dynamics of the closed-loop system, see, for instance, [11, 91].

13

Robust Control of a Flexible-Link Manipulator

In this chapter we discuss the robust control system design of a flexible-link manipulator that moves in the horizontal plane.

Lightweight manipulators possess many advantages over the traditional bulky manipulators. The most important benefits include high payload-to-arm weight ratio, faster motion, safer operation, improved mobility, low cost, longer reach and better energy efficiency, *etc.* However, the reduction of weight leads to the increase of the link elasticity that significantly complicates the control of the manipulator. The difficulty in control is caused by the fact that the link model is a distributed parameter plant. In this case, several elastic modes are required to achieve sufficiently high accuracy. Also, the plant has several uncertain parameters (payload mass, hub and structural damping factors, *etc.*) that influence significantly the system performance. The inherent, nonminimum phase behaviour of the flexible manipulator is another obstacle to achieving simultaneously a high-level performance as well as good robustness.

The aim of the present case study is to design a control system for a single-link flexible manipulator. A two-mode dynamic model of the manipulator is first obtained by using the Lagrangian-assumed modes method. This is followed by the modelling of uncertainties involved in the manipulator. The uncertainties include the real parametric uncertainties in the payload mass as well as in the hub and structural damping factors. These parameters are the basic uncertainty source in the dynamic behaviours of the flexible-link manipulators. The μ-synthesis method is then applied to design a robust, noncollocated controller on the feedback signals of joint angle and tip acceleration. In the design, in order to obtain a feasible solution, a simplified uncertainty description is considered in the D-K iterations. Appropriate weighting functions are chosen in the design to ensure robust stability and robust performance. It is shown in this chapter that good robust performance has been achieved in the design. The closed-loop system exhibits excellent tip-motion performance for a wide range of payload mass and the system efficiently suppresses the elastic vibrations during the fast motion of the manipulator tip. For the

sake of implementation and reliability in practice, a reduced-order controller is found that maintains the robust stability and robust performance of the closed-loop system. Finally, the advantages of the μ-controller over a conventional, collocated PD controller are demonstrated.

13.1 Dynamic Model of the Flexible Manipulator

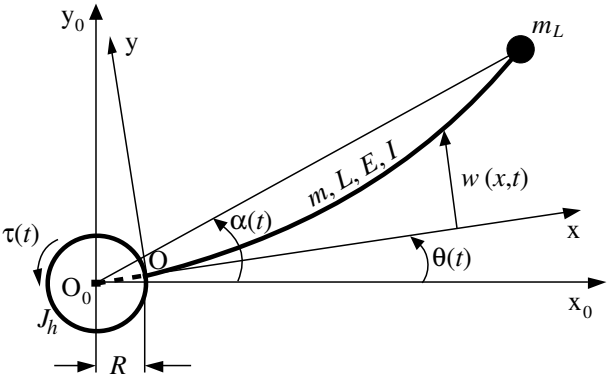

Fig. 13.1. Schematic diagram of the flexible-link manipulator

Figure 13.1 shows the schematic model used to derive the equations of motion for the flexible-link manipulator. The manipulator moves in the horizontal plane. Frame $x_0 - O_0 - y_0$ is the fixed-base frame. Frame $x - O - y$ is the local frame rotating with the hub. The x-axis coincides with the undeformed longitudinal axis of the link. The rotating inertia of the servomotor, the gear box, and the clamping hub are modelled as a single hub inertia J_h. The distance between the hub centre and the root of the link is denoted by R. The flexible link is assumed to be a homogeneous rod with a constant cross-sectional area. L is the length of the link, m is the mass per unit length of the link, I is the link cross-sectional moment of inertia and E is the Young's modulus of elasticity for the material of the link. The payload is modelled as a point mass m_L. The variables $\tau(t)$ and $\theta(t)$ are the driving torque and the joint angle, respectively. The elastic deflection of a point located at a distance x from O along the link is denoted by $w(x,t)$. It is assumed that the elastic deflections of the link lie in the horizontal plane, and are perpendicular to the x-axis and small in magnitude compared to the link length.

The motion equations of the flexible manipulator are to be derived by using the Lagrangian approach combined with the assumed-modes method [94]. The flexible link is modelled as an Euler–Bernoulli beam. The free vibration of the link is described by the partial differential equation [105]

$$EI\frac{\partial^4 w(x,t)}{\partial x^4} + m\frac{\partial^2 w(x,t)}{\partial t^2} = 0$$

with boundary conditions

$$w(0,t) = 0, \quad \frac{\partial w(0,t)}{\partial x} = 0$$

$$\frac{\partial^2 w(L,t)}{\partial x^2} = 0$$

$$\frac{\partial^3 w(L,t)}{\partial x^3} - \frac{m_L}{EI}\frac{\partial^2 w(L,t)}{\partial t^2} = 0$$

According to the assumed-modes method the elastic deflection can be expressed as

$$w(x,t) = \sum_{i=1}^{n} \varphi_i(x)\eta_i(t) \tag{13.1}$$

where $\eta_i(t)$ is the generalised coordinate of the ith mode, $\varphi_i(x)$ is the space eigenfunction of the ith mode, and n is the number of the modes that describe the link deflection. The mode angular frequencies $\omega_i,\ i = 1, ..., n$, of the flexible link are given by

$$\omega_i = \beta_i^2\sqrt{\frac{EI}{m}} \tag{13.2}$$

where $\beta_i,\ i = 1, ..., n$, are the first n positive roots of the transcendental equation

$$1 + \cosh(\beta L)\cos(\beta L) + \frac{m_L}{mL}(\beta L)\left(\sinh(\beta L)\cos(\beta L) - \cosh(\beta L)\sin(\beta L)\right) = 0 \tag{13.3}$$

The shape functions $\varphi_i(x),\ i = 1, ..., n$, satisfy the orthogonality condition

$$m\int_0^L \varphi_i(x)\varphi_j(x)dx + m_L\varphi_i(L)\varphi_j(L) = 0, \quad i \neq j$$

and can be written in the form

$$\varphi_i(x) = \lambda_i\left((\cosh(\beta_i x) - \cos(\beta_i x)) - \frac{\cosh(\beta_i L) + \cos(\beta_i L)}{\sinh(\beta_i L) + \sin(\beta_i L)}\left(\sinh(\beta_i x) - \sin(\beta_i x)\right)\right) \tag{13.4}$$

A normalisation of the shape functions convenient for the uncertainty modelling is accomplished by determining the coefficients $\lambda_i,\ i = 1, ..., n$, in (13.4) on the basis of the relation

$$m\int_0^L \varphi_i^2(x)dx + m_L\varphi_i^2(L) = 1$$

The joint angle θ and the deflection variables $\eta_i,\ i = 1, ..., n$, are used as generalised coordinates in the derivation of the equation of motion. As a result of applying the Lagrangian procedure, the following nonlinear dynamic model of the flexible manipulator is obtained

$$\begin{bmatrix} m_r(\eta) & m_{rf}^T \\ m_{rf} & I_n \end{bmatrix} \begin{bmatrix} \ddot{\theta} \\ \ddot{\eta} \end{bmatrix} + \begin{bmatrix} d_v & 0_n^T \\ 0_n & D_f \end{bmatrix} \begin{bmatrix} \dot{\theta} \\ \dot{\eta} \end{bmatrix} + \begin{bmatrix} 0 & 0_n^T \\ 0_n & C_f \end{bmatrix} \begin{bmatrix} \theta \\ \eta \end{bmatrix} + \begin{bmatrix} h_r(\dot{\theta}, \eta, \dot{\eta}) \\ h_f(\dot{\theta}, \eta) \end{bmatrix} = \begin{bmatrix} 1 \\ 0_n \end{bmatrix} \tau \tag{13.5}$$

where

$$\begin{aligned} \eta &= [\eta_1 \ ... \ \eta_n]^T \\ m_r(\eta) &= a_0 + \sum_{i=1}^{n} \eta_i^2 \\ a_0 &= J_a + \frac{1}{3} m \left((L+R)^3 - R^3 \right) + m_L (L+R)^2 \\ m_{rf} &= [a_1 \ ... \ a_n]^T \\ a_i &= m \int_0^L (x+R) \varphi_i(x) dx + m_L (L+R) \varphi_i(L) \\ C_f &= \text{diag}(\omega_1^2, \ ..., \ \omega_n^2) \\ D_f &= \text{diag}(d_{f1}, \ ..., \ d_{fn}) \\ h_r(\dot{\theta}, \eta, \dot{\eta}) &= \sum_{i=1}^{n} 2 \dot{\theta} \dot{\eta}_i \eta_i \\ h_f(\dot{\theta}, \eta) &= \left[-\dot{\theta}^2 \eta_1 \ ... \ -\dot{\theta}^2 \eta_n \right]^T \end{aligned} \tag{13.6}$$

I_n denotes the $n \times n$ identity matrix, 0_n is the n-dimensional null vector, and $d_v,\ d_{f1},\ ...,\ d_{fn}$ are damping coefficients. The terms $d_v \dot{\theta}$ and $D_f \dot{\eta}$ have been included to account for the viscous friction at the hub and for the structural damping of the flexible link, respectively.

The angle

$$\alpha = \theta + \arctan \frac{w(L,t)}{L+R} \tag{13.7}$$

is chosen as the coordinate that determines the position of the manipulator tip.

The following numerical values of the manipulator parameters are used: $L = 1$ m, $R = 0.4$ m, $J_h = 0.1$ kg m^2, $m = 0.54$ kg/m, flexural rigidity of the flexible link $EI = 18.4$ N m^2. The values of m and EI correspond to an aluminium link with $E = 6.9 \times 10^{10}$ N m^2, density $\rho = 2700$ kg/m^3 and a cross–section 0.004 m×0.05 m.

It is assumed that in performing a given motion the payload mass has a constant but unknown value in the range from 0.125 kg to 0.375 kg. It is also

assumed that the coefficients in the damping terms $d_v\dot{\theta}$ and $D_f\dot{\eta}$ are known inaccurately.

The first two natural frequencies of the flexible link, calculated for the average value of the payload according to (13.2) and (13.3), are $\omega_1 = 12.1$ rad/s and $\omega_2 = 99.2$ rad/s. Since the rest natural frequencies are very large ($\omega_3 = 302.5$ rad/s and so on), a two-mode model of the flexible manipulator is used in the controller design.

13.2 A Linear Model of the Uncertain System

In this section we first consider how to model the uncertainties of the flexible-link manipulator and then develop a complete, linear dynamic model of the system in the form of linear fractional transformation (LFT). As mentioned earlier, the uncertainties considered are related to the payload mass, hub damping coefficient and the damping levels of the first two modes. It is important to note that these parameters are the basic source of uncertainty dynamic behaviour of flexible-link manipulators.

In the modelling of uncertain damping levels of the flexible modes, we may set $d_{fi} = d_i\omega_i, i = 1, 2$ where ω_i are the first two natural frequencies and the damping factors $d_1,\ d_2$ are considered as uncertain parameters. The uncertain parameters $m_L,\ d_v,\ d_1,\ d_2$ may be represented as follows

$$m_L = \overline{m}_L(1 + p_m\delta_m),\ d_v = \overline{d}_v(1 + p_{d_v}\delta_{d_v})$$

$$d_1 = \overline{d}_1(1 + p_{d_1}\delta_{d_1}),\ d_2 = \overline{d}_2(1 + p_{d_2}\delta_{d_2})$$

where the uncertain variables $\delta_m, \delta_{d_v}, \delta_{d_1}, \delta_{d_2}$ are real and satisfy the normalised bound

$$-1 \le \delta_m, \delta_{d_v}, \delta_{d_1}, \delta_{d_2} \le 1$$

The nominal values and the maximum relative uncertainty bounds of those parameters are set as $\overline{m}_L = 0.25$ kg, $p_m = 0.5$, $\overline{d}_v = 0.15$ kg m^2/s, $p_{d_v} = 0.1$, $\overline{d}_1 = 0.03$ kg m^2, $p_{d_1} = 0.2$, $\overline{d}_2 = 0.1$ kg m^2, $p_{d_2} = 0.2$.

The plant input is the driving torque τ. The controlled variable is the tip position α and the measured variables are the joint angle θ and the tip acceleration $\ddot{\alpha}$.

To obtain a linear model of the manipulator the nonlinear terms $\sum_{i=1}^{n}\eta_i^2,\ h_r(\dot{\theta}, \eta, \dot{\eta})$ and $h_f(\dot{\theta}, \eta)$ in (13.5) are neglected due to the fact that their effects are relatively very small. Also, since $w(L, t) << L$, the function $\arctan(z)$ in (13.7) can be approximated by z. As a result, we may obtain the following equations

$$a_0\ddot{\theta} + d_v\dot{\theta} + a_1\ddot{\eta}_1 + a_2\ddot{\eta}_2 = \tau \tag{13.8}$$

$$\ddot{\eta}_i + d_i\omega_i\dot{\eta}_i + \omega_i^2\eta_i + a_i\ddot{\theta} = 0,\quad i = 1, 2 \tag{13.9}$$

$$\alpha = \theta + b_1\eta_1 + b_2\eta_2 \tag{13.10}$$

$$\ddot{\alpha} = \ddot{\theta} + b_1\ddot{\eta}_1 + b_2\ddot{\eta}_2 \tag{13.11}$$

where the following notation is used

$$b_i = \frac{\varphi_i(L)}{L+R}, \quad i = 1, 2 \tag{13.12}$$

The difficulty in modelling the uncertainty in this case study comes from the fact that the coefficients $a_0,\ a_1,\ a_2,\ \omega_1,\ \omega_2,\ b_1$ and b_2 in (13.8)–(13.11) are functions of the payload mass m_L. Among these coefficients, only a_0 explicitly depends on m_L in an affine form. The rest coefficients depend on m_L in a complicated, nonlinear and implicit manner as is seen from (13.2), (13.3), (13.4), (13.6), (13.12). Direct approximation of these coefficients by linear functions of the payload mass leads to a very inaccurate model and the uncertain parameter δ_m would be repeated 13 times. This difficulty is approached here by exploiting the relations between the coefficients as functions of the payload mass. The analysis of these functions shows that there exist sufficiently accurate linear dependencies between appropriately chosen coefficients that can be used to derive a simple and more accurate uncertainty model. The best-suited dependencies are chosen so as to reduce significantly the number of uncertain parameters in the final model achieving in the same time a high accuracy in the description of the uncertainty in the payload mass. This procedure is briefly described in the following.

Equations (13.8) and (13.9) can be rewritten in the form

$$a_0\ddot{\theta} + d_v\dot{\theta} = \tau - a_1\ddot{\eta}_1 - a_2\ddot{\eta}_2 \tag{13.13}$$

$$\frac{1}{\omega_1}\ddot{\eta}_1 + d_1\dot{\eta}_1 + \omega_1\eta_1 = -\frac{a_1}{\omega_1}\ddot{\theta} \tag{13.14}$$

$$\frac{1}{\omega_2}\ddot{\eta}_2 + d_2\dot{\eta}_2 + \omega_2\eta_2 = -\frac{a_2}{\omega_2}\ddot{\theta} \tag{13.15}$$

The coefficients $a_1/\omega_1,\ a_2/\omega_2$ that appear in (13.14) and (13.15) may be expressed as linear functions of a_0, which is in turn a function of m_L, by using the following approximate relationships

$$\frac{a_1}{\omega_1} \approx k_1 a_0 + k_2 \tag{13.16}$$

$$\frac{a_2}{\omega_2} \approx k_3 a_0 + k_4 \tag{13.17}$$

where $k_1,\ k_2,\ k_3$ and k_4 are constants to be determined appropriately. The numerically calculated values of a_1/ω_1 and a_2/ω_2 are shown, as functions of m_L, in Figure 13.2. By using the least square method, linear approximations are obtained (Figure 13.2). The coefficients of the linear approximations are $k_1 = 0.12905,\ k_2 = -0.017706,\ k_3 = 5.5600 \times 10^{-4}$ and $k_4 = 6.8034 \times 10^{-4}$ (all numbers are given to five significant digits).

Accordingly for the variables $(a_i/\omega_i)\ddot{\theta},\ i = 1, 2$, we have

$$\frac{a_1}{\omega_1}\ddot{\theta} \approx (k_1 a_0 + k_2)\ddot{\theta} \tag{13.18}$$

$$\frac{a_2}{\omega_2}\ddot{\theta} \approx (k_3 a_0 + k_4)\ddot{\theta} \tag{13.19}$$

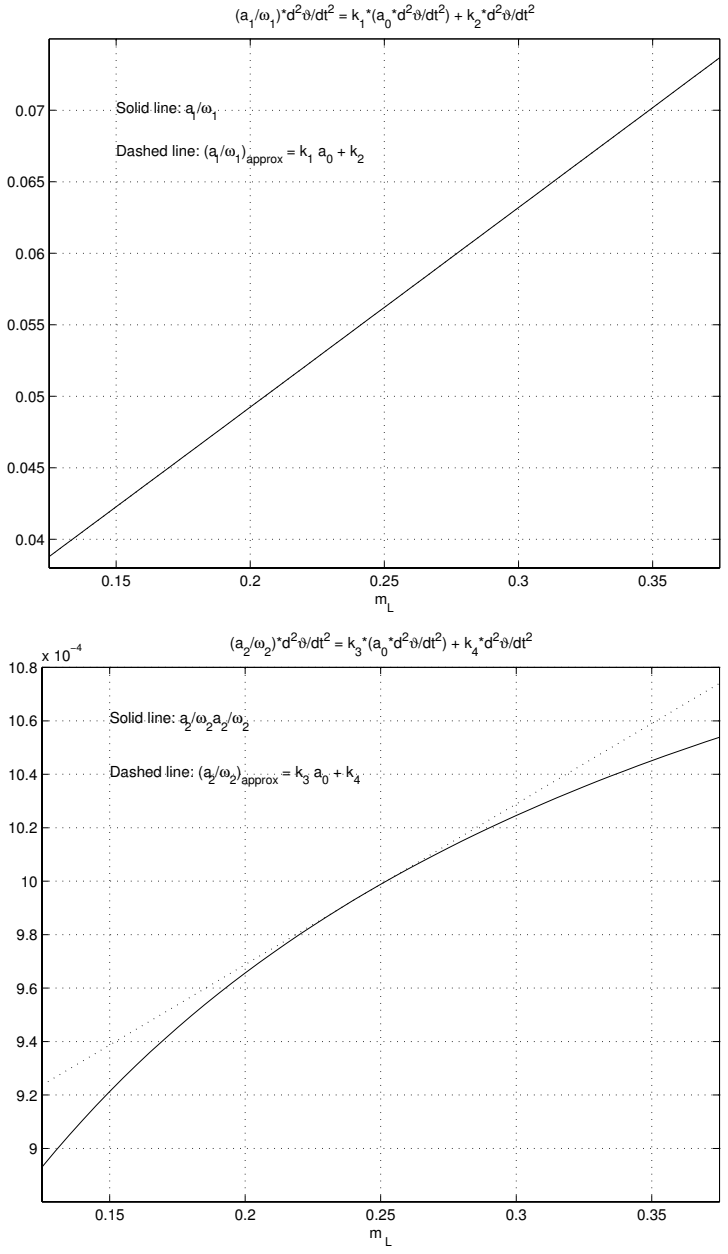

Fig. 13.2. Approximation of a_1/ω_1 (above) and a_2/ω_2 (below) in the expressions for $(a_i/\omega_i)\ddot{\theta}_i,\ i = 1, 2$

Using (13.18) and (13.19), the variables $(a_i/\omega_i)\ddot{\theta}$, $i = 1, 2$, are determined from the variables $a_0\ddot{\theta}$ and $\ddot{\theta}$, and (13.13) can be depicted in a block diagram as in Figure 13.3.

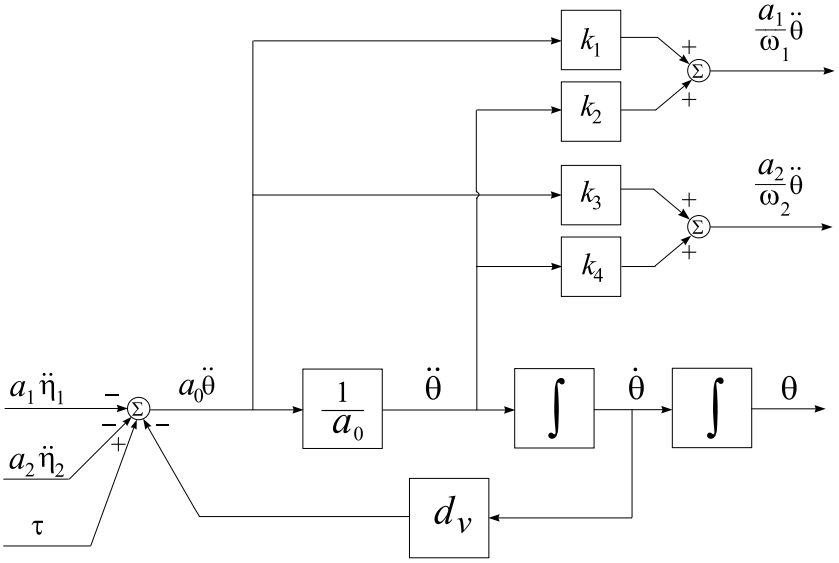

Fig. 13.3. Block diagram of the joint angle equation

In a similar way, the quantities $a_i\ddot{\eta}_i$, appearing in (13.13), can be calculated from $(1/\omega_i)\ddot{\eta}_i$ and $\ddot{\eta}_i$ on the basis of

$$a_1 \approx k_5 \frac{1}{\omega_1} + k_6$$

$$a_2 \approx k_{11} \frac{1}{\omega_2} + k_{12}$$

The actual, calculated values and the approximation quantities of a_1 and a_2, as functions of m_L, are shown in Figure 13.4, where $k_5 = 7.2587$, $k_6 = 0.077825$, $k_{11} = 10.165$ and $k_{12} = -0.0033967$.

Again, the block diagrams showing the determination of $a_1\ddot{\eta}_1$ and $a_2\ddot{\eta}_2$ from the variables $\ddot{\eta}_1$ and $\ddot{\eta}_2$ are shown in Figures 13.5 and 13.6, respectively.

The coefficients ω_1 and ω_2 can be expressed in terms of b_1 and b_2, respectively, according to

$$\omega_1 = k_9 b_1 + k_{10}$$

$$\omega_2 = k_{15} b_2 + k_{16}$$

Figure 13.7 plots the actual and approximate quantities of ω_1 and ω_2, as functions of m_L, with $k_9 = 7.7970$, $k_{10} = -0.089136$, $k_{15} = -13.355$ and $k_{16} = 89.500$.

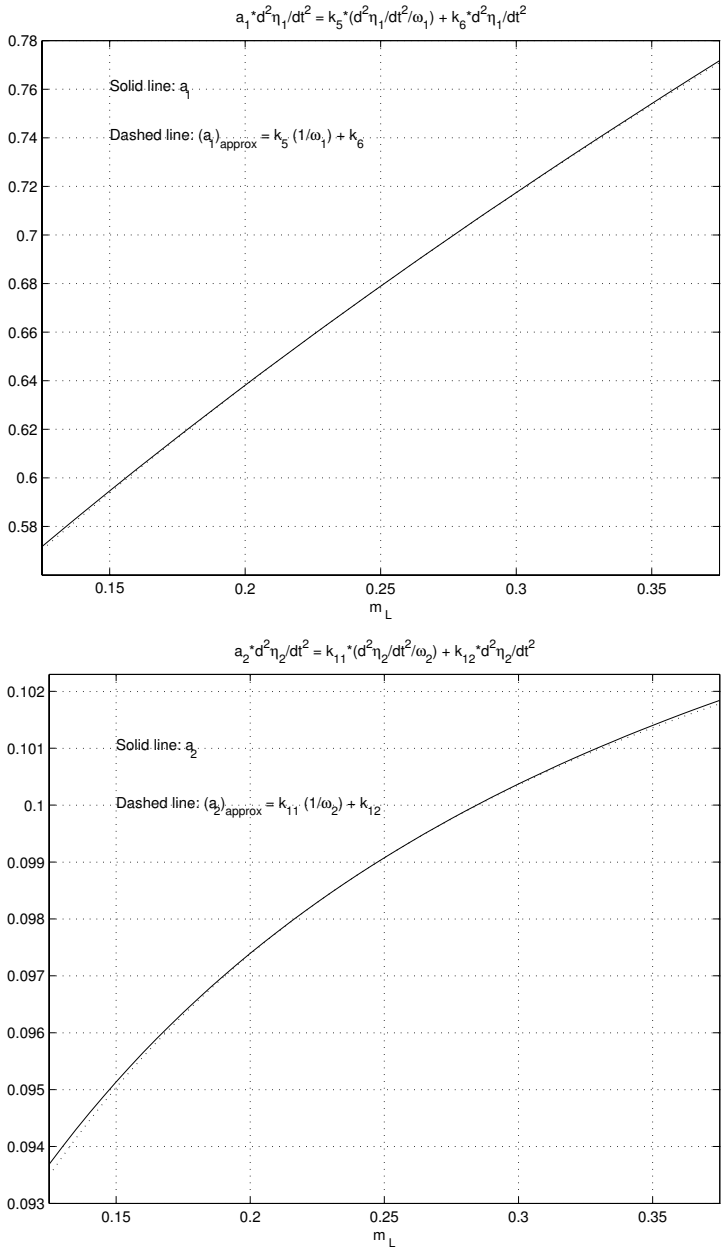

Fig. 13.4. Approximation of a_1 (above) and a_2 (below) in the expressions for $a_i\ddot{\eta}_i,\ i = 1, 2$

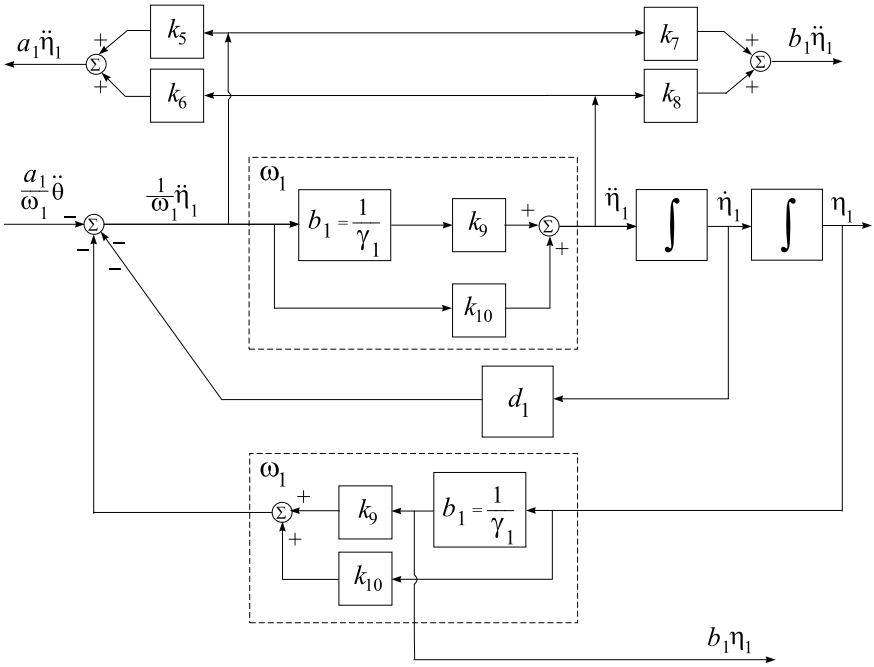

Fig. 13.5. Block diagram of the first elastic mode

In this way we obtain an uncertainty model corresponding to (13.8) and (13.9). In this model only the coefficients a_0^{-1}, ω_1 and ω_2 depend on the payload mass, while the coefficients ω_1 and ω_2 are repeated twice.

The part of the uncertainty model corresponding to (13.10) and (13.11) can be derived without introducing new uncertainty parameters. The terms $b_i\ddot{\eta}_i$, $i = 1, 2$, are expressed by $(1/\omega_i)\ddot{\eta}_i$ and $\ddot{\eta}_i$ using the relationships

$$b_1 \approx k_7 \frac{1}{\omega_1} + k_8$$

$$b_2 \approx k_{13} \frac{1}{\omega_1} + k_{14}$$

Similarly, Figure 13.8 plots the calculated and approximate quantities of b_1 and b_2, as functions of m_L, with $k_7 = -18.980$, $k_8 = 3.1319$, $k_{13} = 7.4054$ and $k_{14} = -8.1915$.

The block diagrams showing the variables $b_1\ddot{\eta}_1$ and $b_2\ddot{\eta}_2$, based on the variables $\ddot{\eta}_1$ and $\ddot{\eta}_2$, are already included in Figures 13.5 and 13.6, respectively.

In the expressions for ω_1, ω_2 and $b_1\eta_1$, $b_2\eta_2$, the coefficients b_1 and b_2 can be represented as LFTs in the real uncertain parameter δ_m by using the following approximate relationships

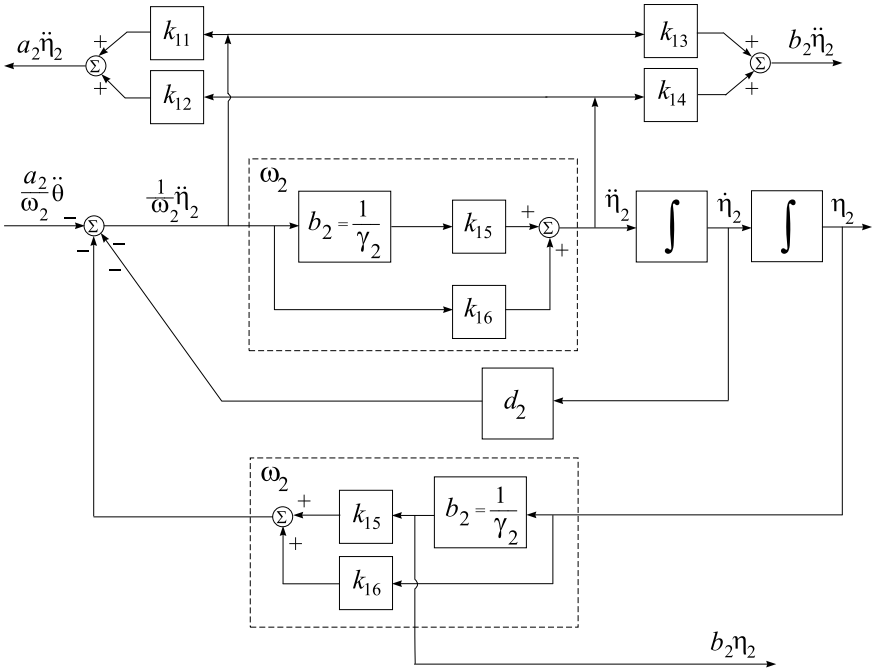

Fig. 13.6. Block diagram of the second elastic mode

$$b_1 \approx \frac{1}{\gamma_1}$$

$$b_2 \approx \frac{1}{\gamma_2}$$

where γ_1 and γ_2 depend affinely on m_L and can be written as

$$\gamma_1 = \overline{\gamma}_1(1 + p_{\gamma_1}\delta_m)$$

$$\gamma_2 = \overline{\gamma}_2(1 + p_{\gamma_2}\delta_m)$$

The calculated and approximate quantities of b_1 and b_2 as functions of m_L are shown in Figure 13.9 for $\overline{\gamma}_1 = 0.64095$, $p_{\gamma_1} = 0.16414$, $\overline{\gamma}_2 = -1.3780$ and $p_{\gamma_2} = 0.36534$.

The constants $k_1, ..., k_{16}, \overline{\gamma}_1, p_{\gamma_1}, \overline{\gamma}_2$ and p_{γ_2} are all determined by least squares approximations in such a way that for the nominal payload mass the corresponding relationships are satisfied perfectly (interpolation conditions). Hence for the nominal payload the manipulator model is accurate. In the approximations, the worst relative error for each relationship is always obtained at the case $m_L = 0.125$ kg, and the largest relative error among all these is less than than 3.4% . These constants are found by using the file `par_flm`.

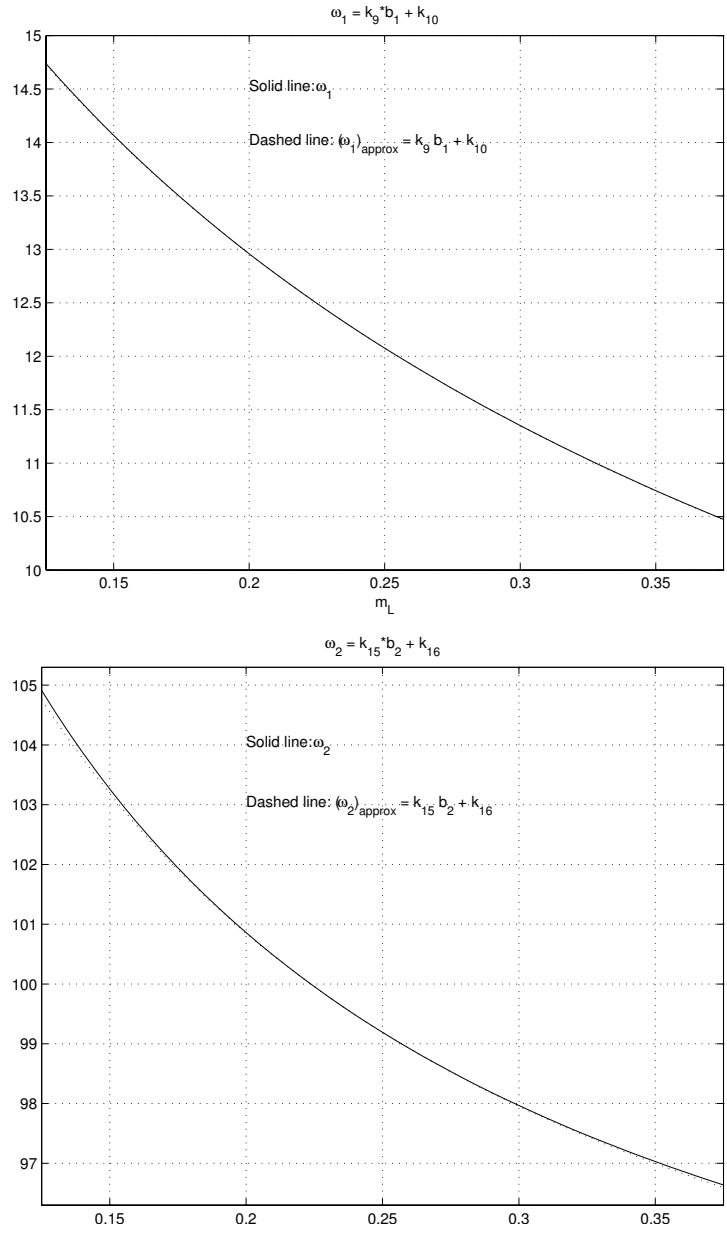

Fig. 13.7. Approximation of ω_1 (above) and ω_2 (below)

Once appropriate approximations of the coefficients have been obtained it is possible to develop the uncertainty models corresponding to (13.13)–(13.15). This is done by using the file `mod_flm`.

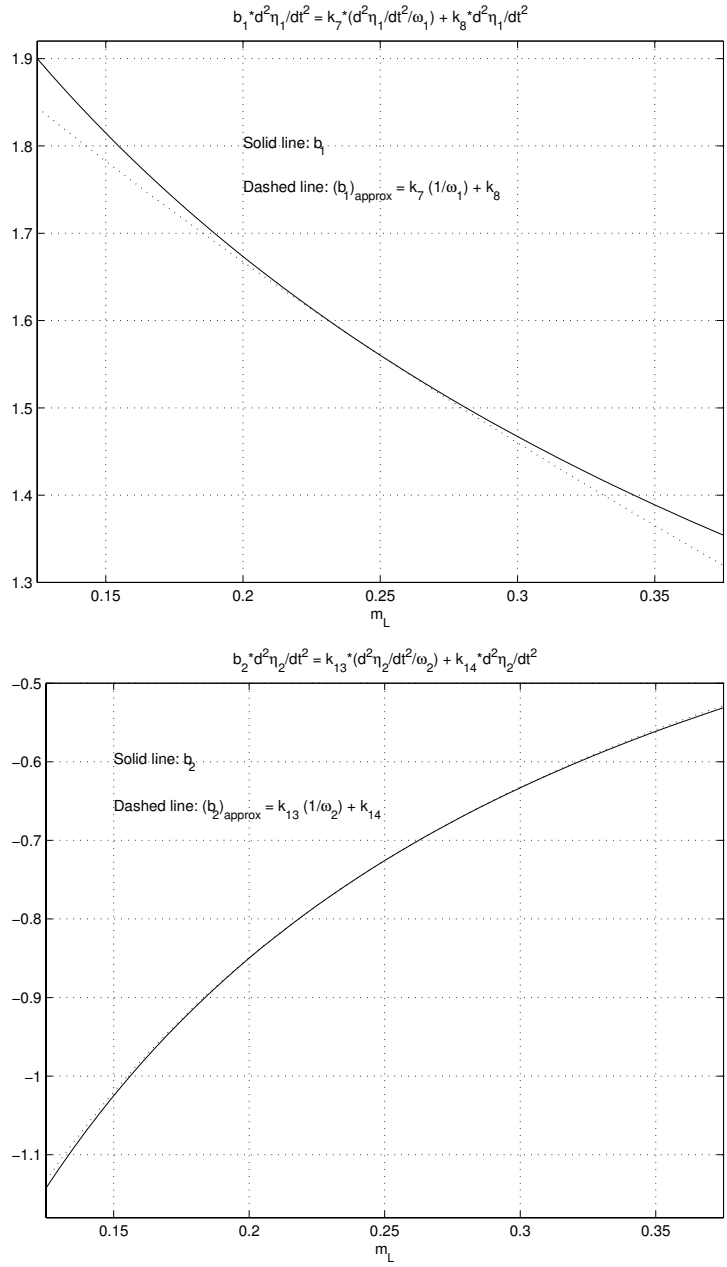

Fig. 13.8. Approximation of b_1 (above) and b_2 (below) in the expressions for $b_i\ddot{\eta}_i,\ i = 1, 2$

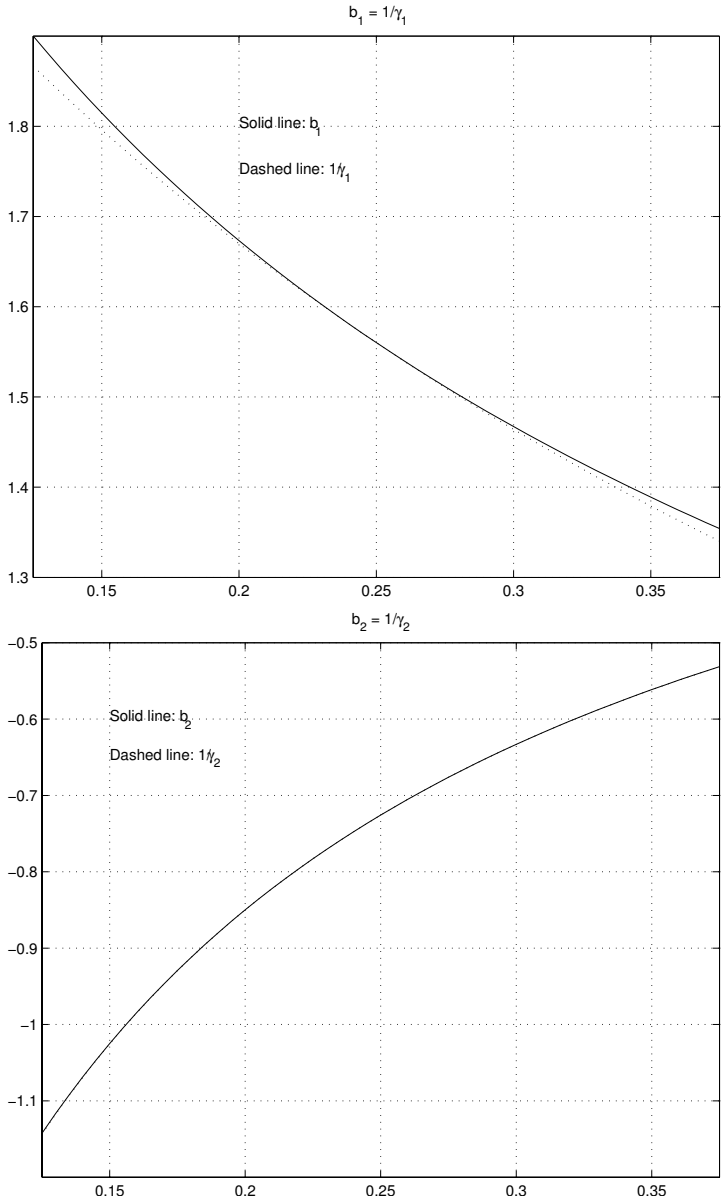

Fig. 13.9. Approximation of b_1 (above) and b_2 (below) in the expressions for ω_i and $b_i\eta_i,\ i = 1, 2$

In Figure 13.10 we show the block diagram of the joint angle with uncertain parameters derived from the block diagram shown in Figure 13.2.

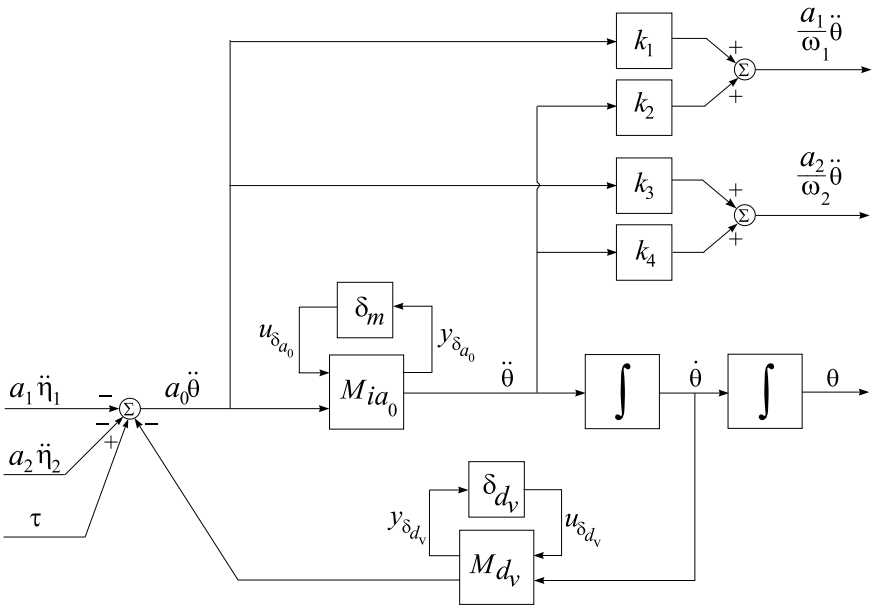

Fig. 13.10. Block diagram of the joint angle with uncertain parameters

The corresponding interconnection is obtained by using the function `sysic`. A schematic diagram of the input/output ordering for this interconnection is shown in Figure 13.11.

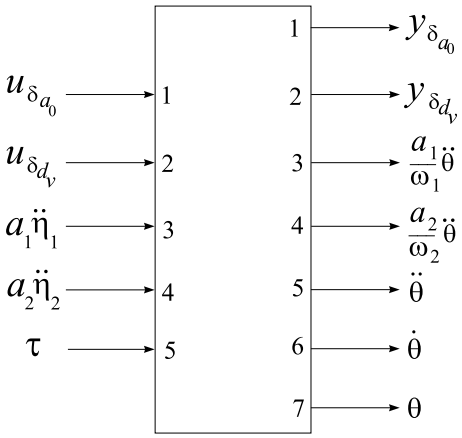

Fig. 13.11. Schematic diagram of the joint angle connection

The uncertainty model of the first elastic mode is given in Figure 13.12 and a schematic diagram of the corresponding interconnection is shown in Figure 13.13.

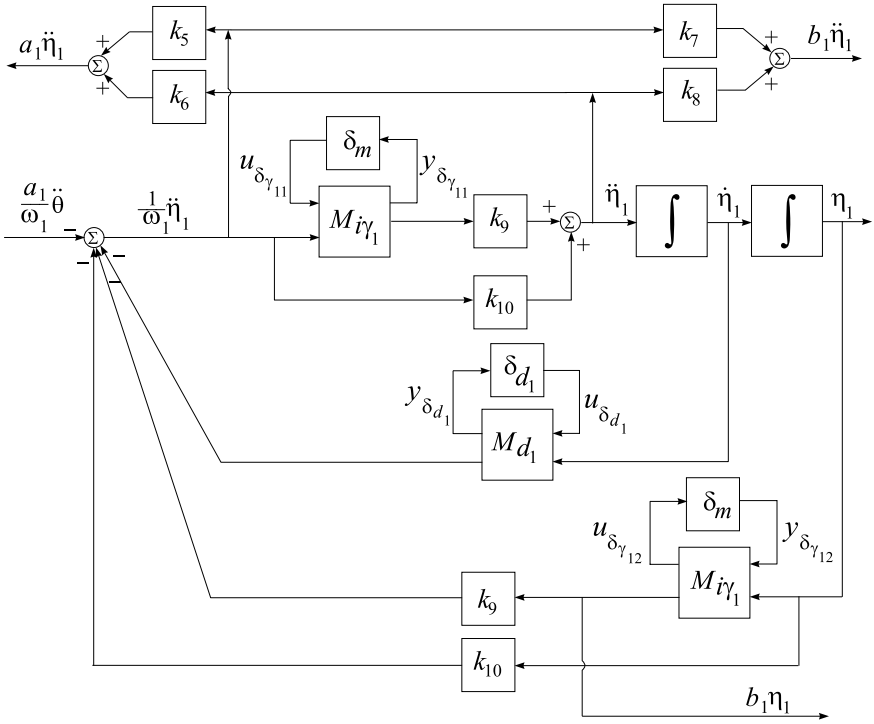

Fig. 13.12. First elastic mode with uncertain parameters

The uncertainty model of the second elastic mode (Figure 13.14) is obtained in a similar way and a schematic diagram of the input/output ordering is shown in Figure 13.15.

A schematic diagram for the output equations interconnection is shown in Figure 13.16.

Finally, the uncertainty model of the flexible link manipulator is obtained by connecting the models shown in Figures 13.10, 13.12 and 13.14. A schematic diagram of the input/output ordering of the corresponding interconnection is shown in Figure 13.17. This model has 9 inputs and 20 outputs.

Based on the above modelling, an LFT model of the flexible-link manipulator with diagonal uncertainty matrix

$$\Delta = \mathrm{diag}(\delta_m I_5, \delta_v, \delta_{d_1}, \delta_{d_2}) \tag{13.20}$$

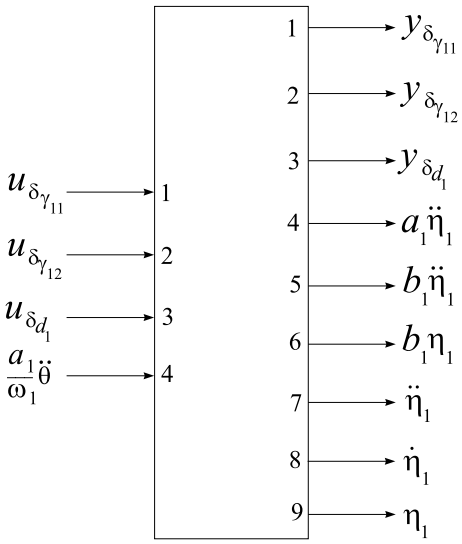

Fig. 13.13. Schematic diagram of the first elastic mode interconnection

can be readily obtained. Note that in this modelling of uncertainties the uncertain parameter δ_m appears repeatedly five times.

The accuracy of such a derived model may be verified by the comparison of the Bode plots of the exact and approximate models of the manipulator. Figure 13.18 shows the Bode plots for the case $m_L = 0.125$ kg. The plots are obtained from the corresponding transfer functions of the input τ and output θ. The Bode plot of the exact model is computed on the basis of (13.8) and (13.9), using the exact values of the coefficients. The Bode plot of the "approximate" model is calculated based on the derived uncertainty model. It can be seen that the match between those two models is very good. Similar closeness of the corresponding plots holds for transfer functions of other plant outputs from the input τ.

It has been found in this case study that if the approximation of the coefficients in (13.8)–(13.11) as functions of the payload mass is conducted directly with linear dependencies, then the model obtained would be very inaccurate. And, in that case, the uncertain parameter δ_m would repeat itself 13 times in the uncertainty model.

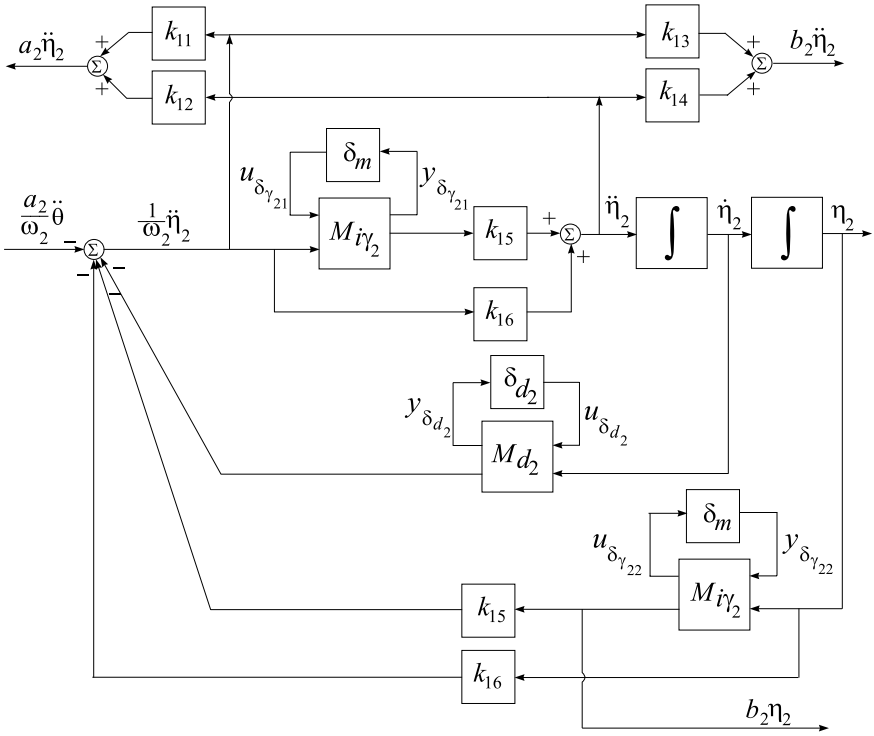

Fig. 13.14. Second elastic mode with uncertain parameters

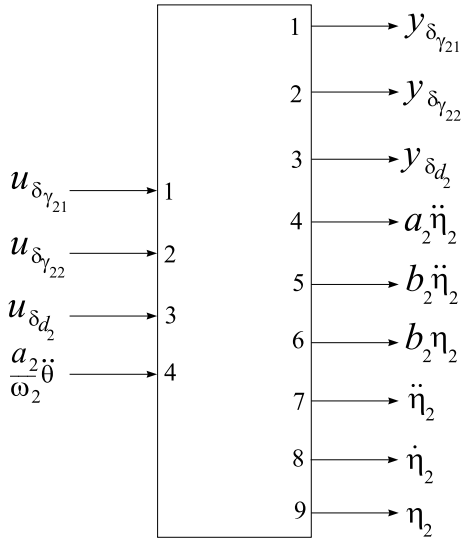

Fig. 13.15. Schematic diagram of the second elastic mode interconnection

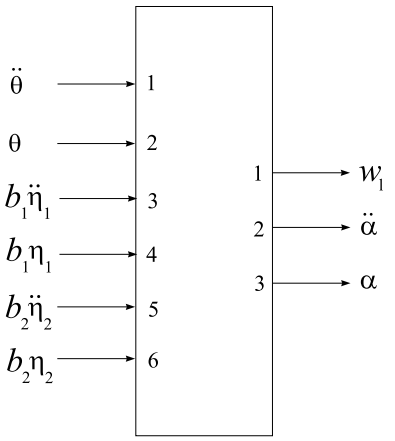

Fig. 13.16. Schematic diagram of the output equations interconnection

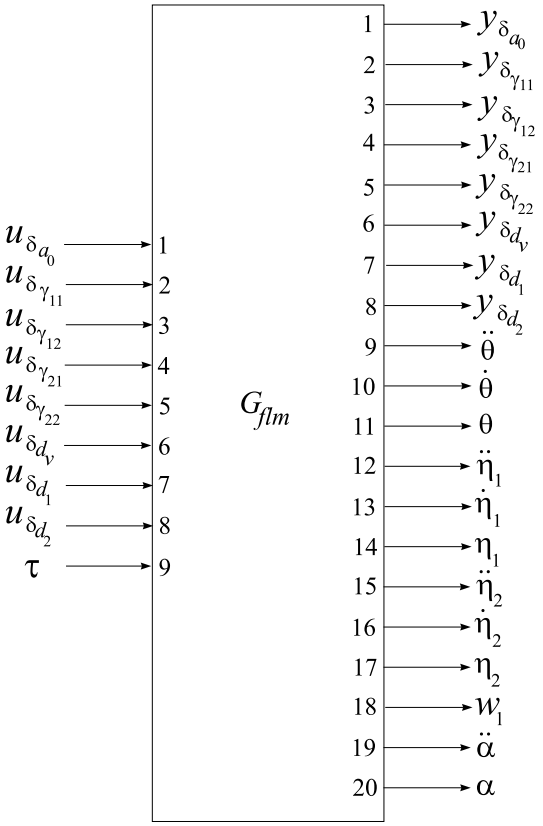

Fig. 13.17. Schematic diagram of the flexible-link manipulator interconnection

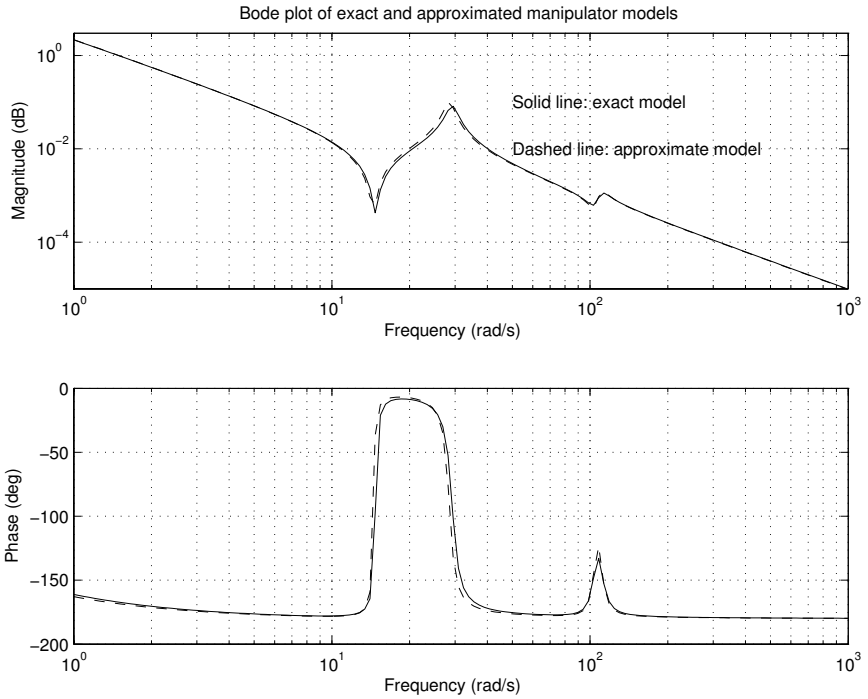

Fig. 13.18. Bode plots of exact and approximated manipulator models for $m_L = 0.125$ kg

13.3 System-performance Specifications

In this flexible-link manipulator control-system design exercise, the purpose is to find a controller that suppresses efficiently the elastic vibrations of the flexible link in fast motions and moves the tip to a desired position in the presence of uncertainties in the payload mass, hub and structural damping factors. Since the uncertainties considered are real and structured, the most appropriate robust control design method to be applied in the present case is the μ-synthesis.

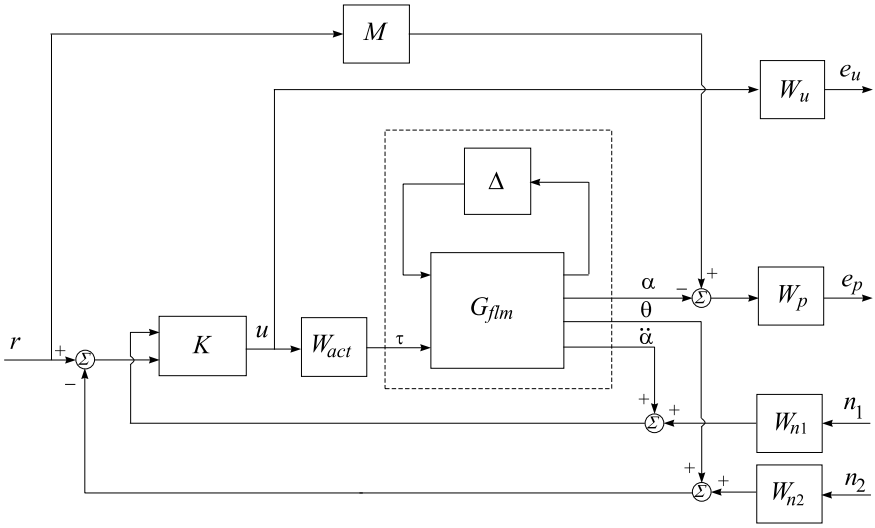

Fig. 13.19. Closed-loop interconnection structure of the flexible-link manipulator system

The block diagram of the closed-loop system incorporating the design requirements is shown in Figure 13.19. The controller K works on the feedback signals of the tip acceleration $\ddot{\alpha}$ and the joint angle θ. The inclusion of the tip acceleration in the control scheme aims to achieve better tip-motion performance and leads to a noncollocated controller structure. Furthermore, in the given design case, we select a suitable dynamic model and target the dynamics of the designed closed-loop system to be close to that model. The use of such a model to represent the desired dynamics allows us to take into account the requirements on system performance more easily and directly. In other words, such a model (named M in Figure 13.19) prescribes the desired dynamic behaviour of the closed-loop system from the reference signal to the tip position. In Figure 13.19 the plant G, enclosed by the dashed rectangle, is in the form of upper LFT, $G = F_U(G_{flm}, \Delta)$, with the nominal model G_{flm}

and the parametric uncertainty matrix Δ (in (13.20)). The internal, current control loop of the servo drive W_{act} is modelled as a first-order lag with the time constant 0.003 s.

Let the 3×1 transfer matrix G be partitioned as

$$G(s) = \begin{bmatrix} G_{\alpha\tau}(s) \\ G_{\theta\tau}(s) \\ G_{\ddot{\alpha}\tau}(s) \end{bmatrix}$$

where $G_{\alpha\tau}$, $G_{\theta\tau}$, $G_{\ddot{\alpha}\tau}$ are the transfer functions from the control torque τ to the outputs α, θ and $\ddot{\alpha}$, respectively, and let the controller

$$K(s) = [K_1(s)\ K_2(s)]$$

It can be shown by direct manipulations that

$$\begin{bmatrix} e_p \\ e_u \end{bmatrix} = \Phi \begin{bmatrix} r \\ n_1 \\ n_2 \end{bmatrix}$$

where

$$\Phi = \begin{bmatrix} W_p(SG_{\alpha\tau}W_{act}K_2 - M) & W_pSG_{\alpha\tau}W_{act}K_1W_{n_1} & -W_pSG_{\alpha\tau}W_{act}K_2W_{n_2} \\ W_uSK_2 & W_uSK_1W_{n_1} & -W_uSK_2W_{n_2} \end{bmatrix}$$

and

$$S = \frac{1}{1 - G_{\ddot{\alpha}\tau}W_{act}K_1 + G_{\theta\tau}W_{act}K_2}$$

The design objective for the controller K is thus to be set as

$$\|\Phi\|_\infty < 1 \tag{13.21}$$

for all perturbed $\begin{bmatrix} G_{\alpha\tau}(s) \\ G_{\theta\tau}(s) \\ G_{\ddot{\alpha}\tau}(s) \end{bmatrix} = F_U(G_{flm}, \Delta)$.

It is clear that, with appropriately chosen weighting functions, a controller K satisfying the above (13.21) makes the closed-loop system robustly stable, robustly achieving good matching to the dynamic model M (in terms of e_p), and with restricted control effort (in terms of e_u).

The model transfer function to be matched is taken in this design as

$$M = \frac{625}{s^2 + 50s + 625}$$

The coefficients of this transfer function are chosen to ensure overdamped response with a settling time of about 0.19 s. The performance weighting functions are chosen as

$$W_p = \frac{s^2 + 25s + 150}{s^2 + 22s + 0.15}, \quad W_u = 10^{-5}\frac{5s + 1}{0.05s + 1}$$

The criterion for the performance weighting function W_p aims to ensure the closeness of the system dynamics to that of the model M over the low-frequency range. The use of the control weighting function W_u allows us to bound the magnitude of the control action in the frequency range containing the natural frequencies of the flexible link. The magnitude plots of the inverses of the performance and control weighting functions are shown in Figure 13.20.

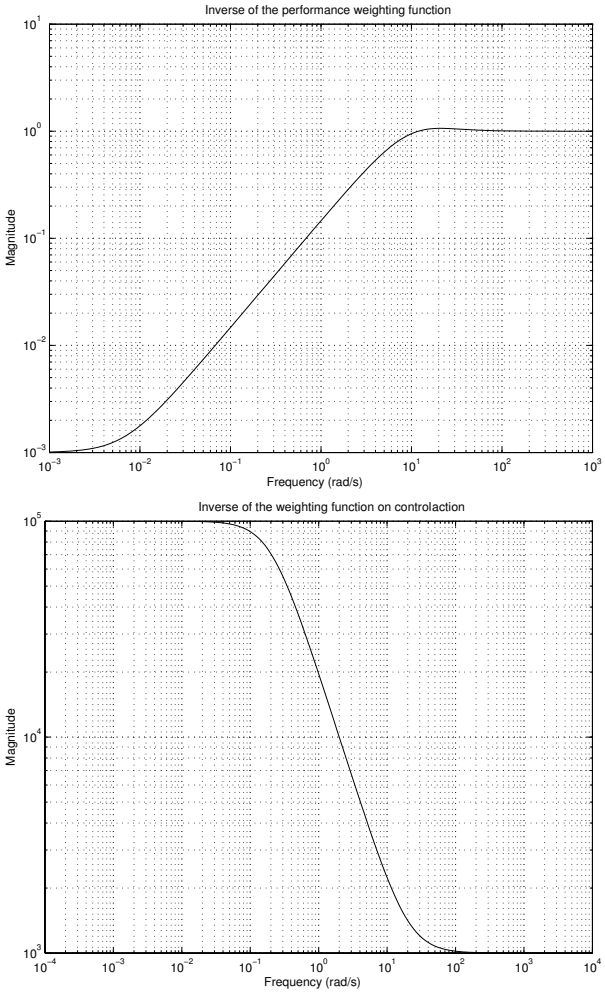

Fig. 13.20. Inverses of performance weighting function (above) and control weighting function (below)

The noise shaping filters

$$W_{n_1} = 2 \times 10^{-5} \frac{s+1}{0.01s+1}, \quad W_{n_2} = 10^{-7} \frac{0.5s+1}{0.005s+1}$$

are determined according to the spectral contents of the sensor noises n_1 and n_2 at the measurements of the tip acceleration and joint angle signals, respectively. The magnitude plots of the noise shaping filters are shown in Figure 13.21.

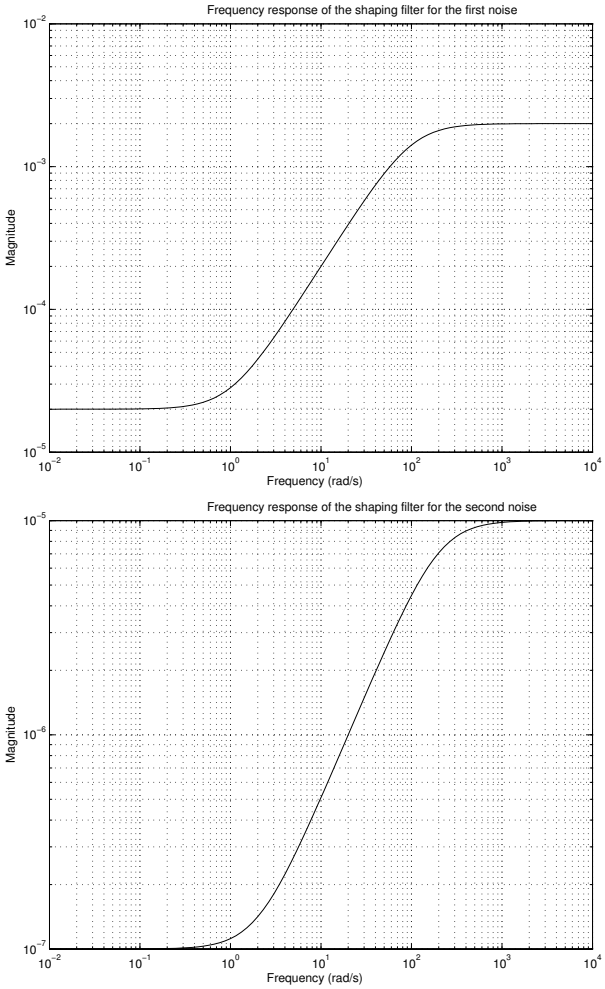

Fig. 13.21. Noise weighting functions

The model transfer function, the performance and control weighting functions as well as the noise shaping filters are assigned in the file `wts_flm.m`.

13.4 System Interconnections

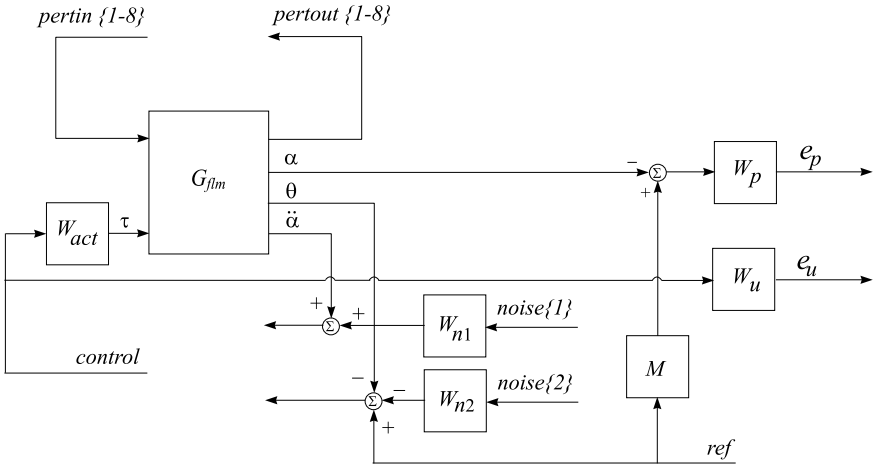

Fig. 13.22. Open-loop interconnection structure of the flexible-link manipulator system

The open-loop interconnection is obtained by the M-file `olp_flm`. The internal structure of the 12-input/12-output open-loop system, which is saved in the variable `sys_ic`, is shown in Figure 13.22. The inputs and outputs of the uncertainties are saved in the variables `pertin` and `pertout`, the reference and the noises saved in the variables `ref`, `noise1` and `noise2`, and the control signal in the variable `control`.

Both variables `pertin` and `pertout` have eight elements, while the rest variables are scalars.

A schematic diagram of the specific input/output ordering for the variable `sys_ic` is shown in Figure 13.23.

The block-diagram used in the simulation of the closed-loop system is shown in Figure 13.24. The corresponding closed-loop interconnection, which is saved in the variable `sim_ic`, is obtained by the M-file `sim_flm`.

A schematic diagram of the specific input/output ordering for the variable `sim_ic` is shown in Figure 13.25.

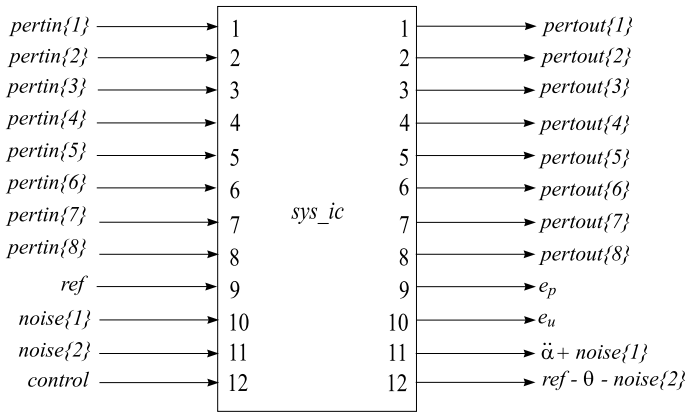

Fig. 13.23. Schematic diagram of the open-loop interconnection

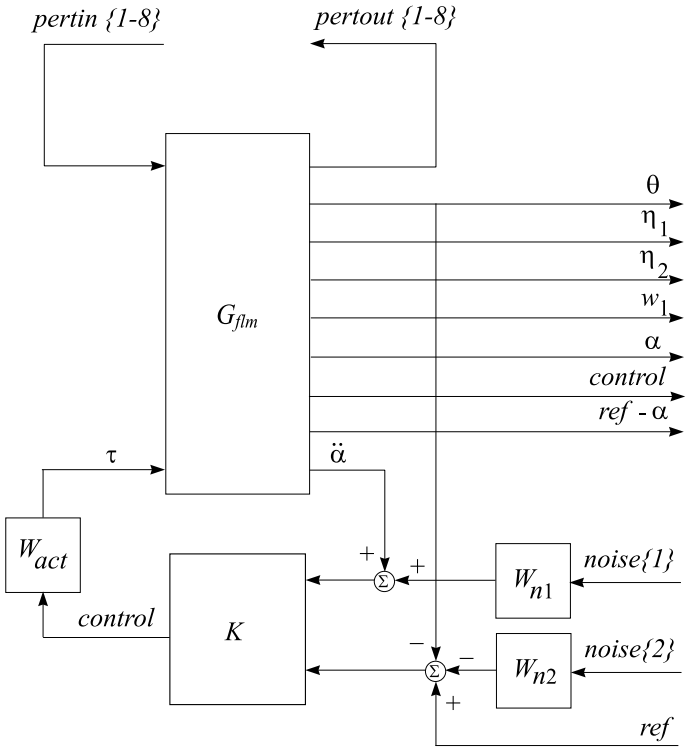

Fig. 13.24. Closed-loop interconnection structure of the flexible-link manipulator system

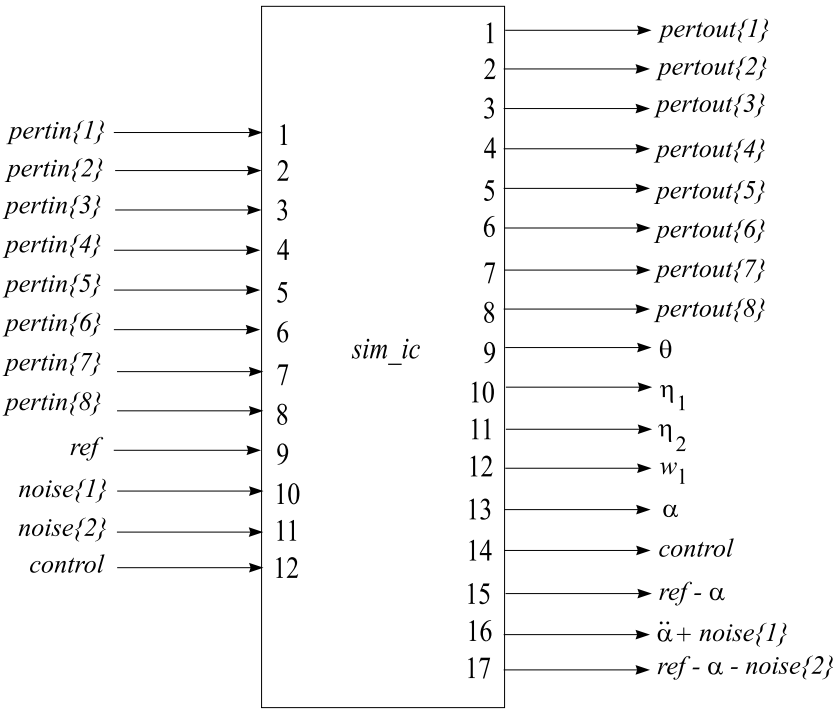

Fig. 13.25. Schematic diagram of the closed-loop interconnection

13.5 Controller Design and Analysis

Let us denote by $P(s)$ the transfer function matrix of the twelve-input, twelve-output open-loop system consisting of the flexible-link manipulator model and the actuator and weighting functions (Figure 13.22). Define a block structure of uncertainty Δ_P as

$$\Delta_P := \left\{ \begin{bmatrix} \Delta & 0 \\ 0 & \Delta_F \end{bmatrix} : \Delta \in \mathcal{R}^{8\times 8},\ \Delta_F \in \mathcal{C}^{3\times 2} \right\}$$

The first part of this matrix corresponds to the uncertain block Δ that is used in the modelling of the uncertainties in the flexible manipulator. The second block Δ_F is a fictitious uncertainty 3×2 block and is introduced to represent the robust performance objective in the framework of the μ-approach. The inputs to the block Δ_F are the weighted error signals e_p and e_u and the outputs from Δ_F are the exogenous signals r, n_1 and n_2 (inputs to the manipulator closed-loop system).

As discussed in previous sections, in order to meet the design objectives a stabilising controller $K = [K_1(s)\ K_2(s)]$ is to be found such that, at each frequency $\omega \in [0, \infty]$, the structured singular value satisfies the condition

$$\mu_{\Delta_P}[F_L(P,K)(j\omega)] < 1$$

The fulfillment of the above condition guarantees the robust performance of the closed-loop system, *i.e.*

$$\|\Phi\|_\infty < 1 \tag{13.22}$$

In the computation of a μ-controller, there is, however, a numerical problem. That is, with the inclusion of the multiple 5×5 real uncertainty block (corresponding to δ_m) the D-K iteration algorithm does not converge. In particular, it is difficult to obtain the approximation of a 5×5 scaling function matrix in the D-step. Hence, in our computation that multiple 5×5 real uncertainty block was removed in the uncertainty matrix during the D-K iteration. It should be stressed that the robust stability and robust performance analysis of the closed-loop system of the designed controller, which will be presented next, is tested with regard to the whole uncertainty structure, *i.e.* with the inclusion of that multiple 5×5 real uncertainty block.

The μ-synthesis is carried out by using the M-file `ms_flm.m`. The uncertainty structure and other parameters used in the D-K iteration are set in the auxiliary file `dk_flm.m`.

The progress of the D-K iteration is shown in Table 13.1.

Table 13.1. Results of the μ-synthesis

Iteration	Controller order	Maximum value of μ
1	14	1.564
2	18	1.078
3	22	0.618
4	28	0.484

In the design exercise, an appropriate controller is obtained after the fourth D-K iteration. The controller is stable and has an order of 28.

The magnitude and phase plots of the μ-controller are shown in Figure 13.26.

It can be seen from Table 13.1 that after the fourth iteration the maximum value of μ is equal to 0.484. Note that this, however, does not necessarily mean that the robust performance has been achieved since we neglected the multiple 5×5 real uncertainty block in the computation. Hence, additional robust performance analysis is needed as below.

The μ-analysis of the closed-loop system is conducted by the file `mu_flm` that takes into account all uncertainty blocks discussed in Section 13.2.

The frequency response plot of the structured singular value for verification of robust stability is shown in Figure 13.27. The maximum value of μ is 0.444 that means that the stability of the system is preserved under perturbations that satisfy $\|\Delta\|_\infty < \frac{1}{0.444}$.

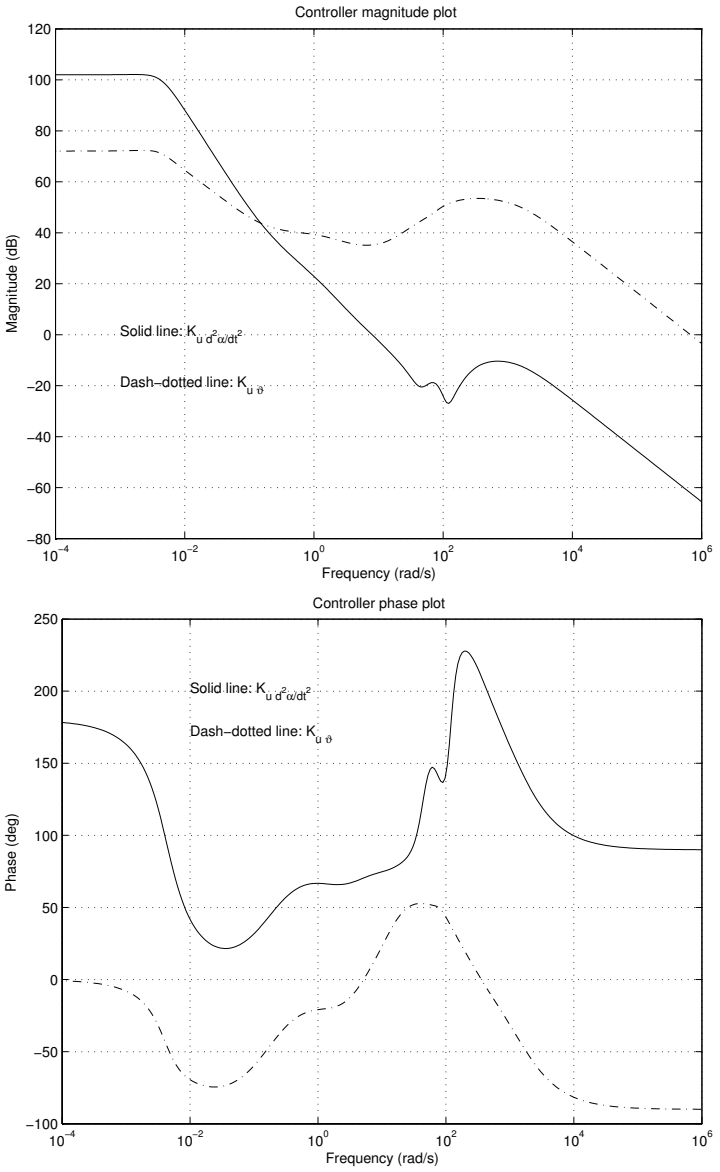

Fig. 13.26. Controller magnitude (above) and phase (below) plots

The frequency response of μ for the robust performance analysis is shown in Figure 13.28. The closed-loop system achieves robust performance since the maximum value of μ is equal to 0.806.

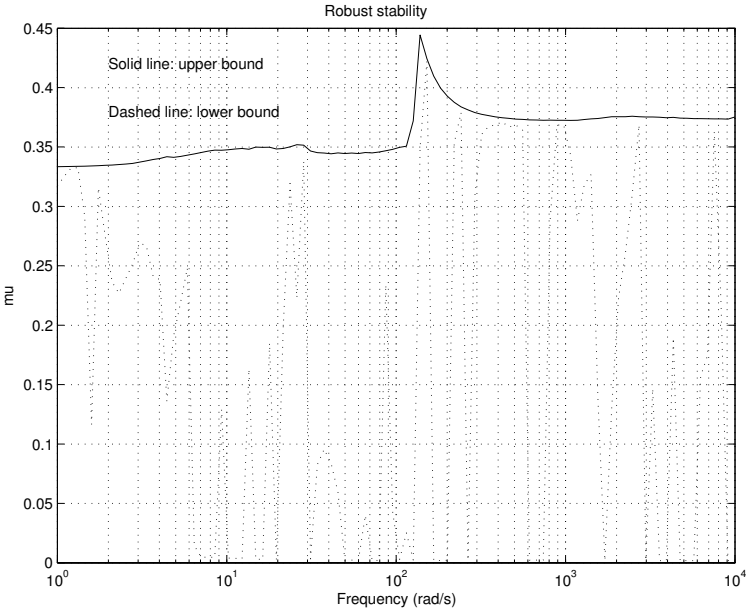

Fig. 13.27. Robust stability for μ-controller

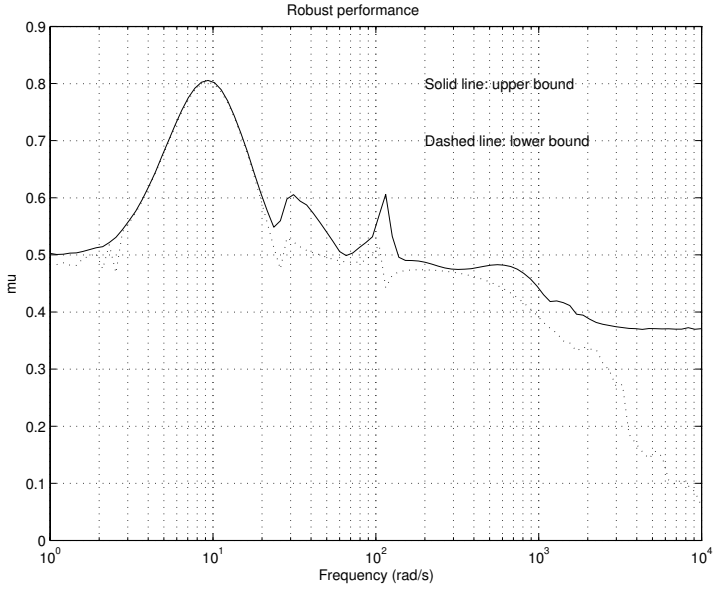

Fig. 13.28. Robust performance for μ-controller

Consider now the closed-loop transient responses that are computed by using the M-file `clp_pend`.

The reference trajectory for the manipulator tip movement in the simulation is chosen in the form

$$r = \begin{cases} at - (a/\psi)\sin(\psi t) + r_0, & 0 \le t \le t_m \\ r(t_m), & t_m < t \le t_f \end{cases}$$

This trajectory allows the tip to be moved smoothly from an arbitrary initial position r_0 to a desired final position $r(t_m) = at_m$, with an appropriate ψ.

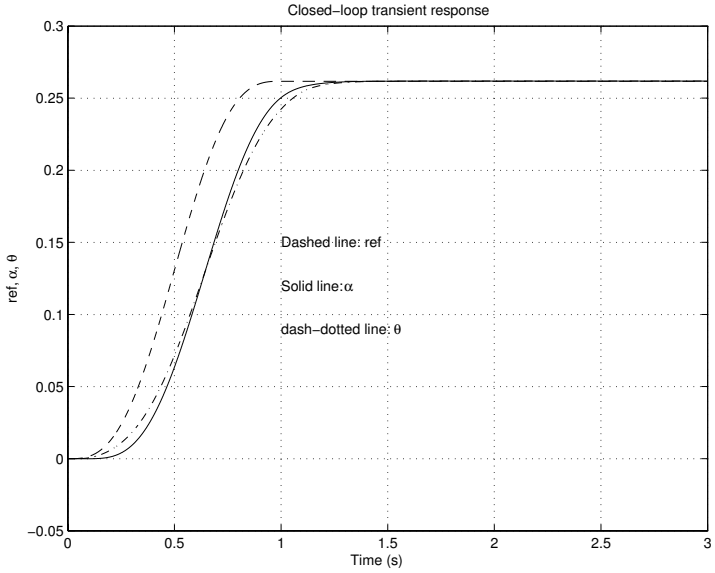

Fig. 13.29. Closed-loop transient response for μ-controller

In Figure 13.29 we show the transient response of the tip position α along with the joint angle θ and the reference r.

The transient response of the tip deflection $w(L,t)$ is shown in Figure 13.30.

The control action generated by the designed μ-controller is shown in Figure 13.31.

The closed-loop frequency responses are obtained by the M-file `frs_flm.m`.

The Bode plot of the closed-loop system is shown in Figure 13.32. The closed-loop bandwidth is about 10 rad/s. Note that a good match in magnitude between the closed-loop system and the dynamic model M is achieved for frequencies up to 70 rad/s.

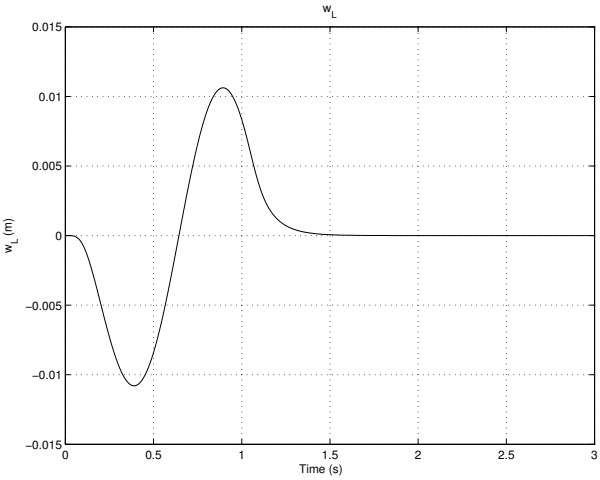

Fig. 13.30. Tip-deflection transient response for μ-controller

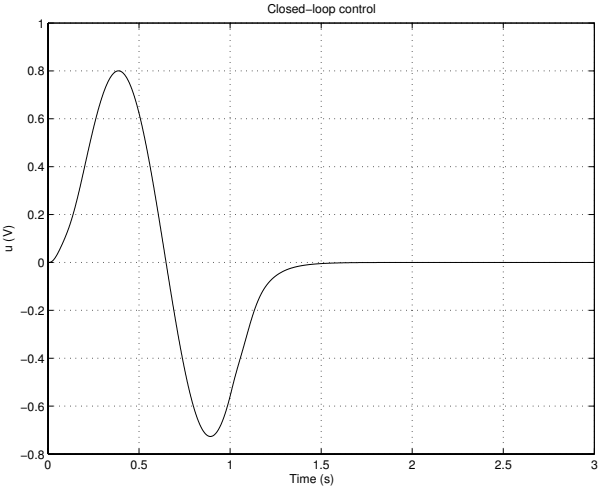

Fig. 13.31. Control action for μ-controller

The Bode plots of the tip-deflection transfer function are shown in Figure 13.33. The maximum amplitude of the tip deflection is observed for the input signal with frequency 40 rad/s.

Finally, in Figure 13.34 we show the magnitude plots with respect to the first and second noise. It is seen from the figure that the noise in measuring the joint angle has a negligible effect on the system output.

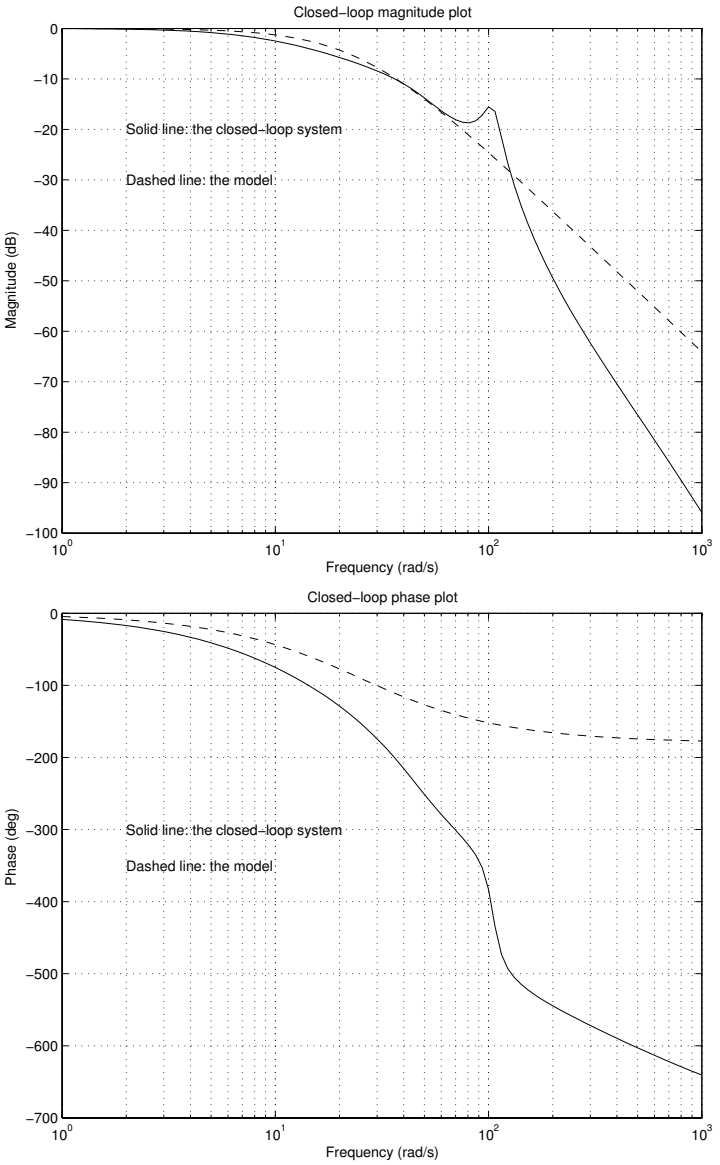

Fig. 13.32. Closed-loop magnitude (above) and phase (below) plots

We consider now the order reduction of the designed controller. As indicated in Table 13.1, the order of the μ-controller is 28. It would be good for implementation if the order could be reduced while essentially keeping the achieved performance. For this aim, we use the M-file `red_flm.m`. Af-

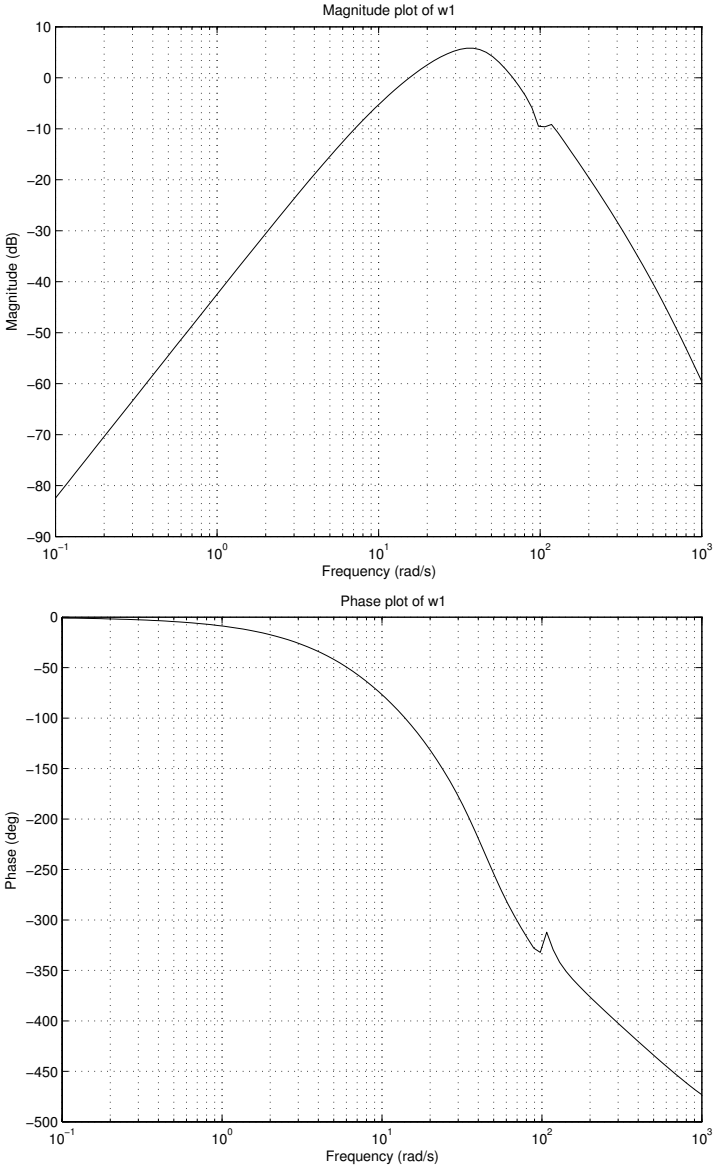

Fig. 13.33. Magnitude (above) and phase (below) plots for the tip deflection

ter the balanced realisation transformation of the controller and by neglecting the small Hankel singular values, the order of the controller can be reduced to 11 without losing too much performance. In Figure 13.35 we compare the frequency responses of the maximum singular values of the full-order

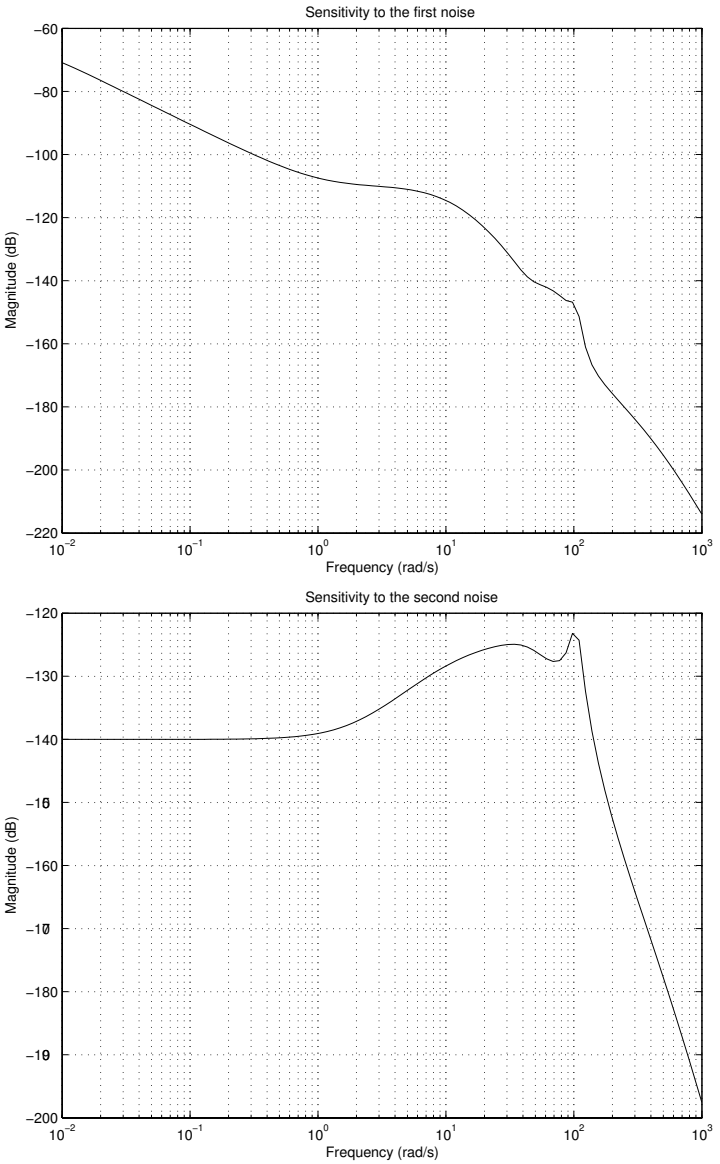

Fig. 13.34. Magnitude plots for the first and second noise

and reduced-order controllers. The frequency responses of both full-order and reduced-order controllers practically coincide. The transient responses of the closed-loop system with full-order and with reduced-order controller are also practically indistinguishable. (Figures are not included here.)

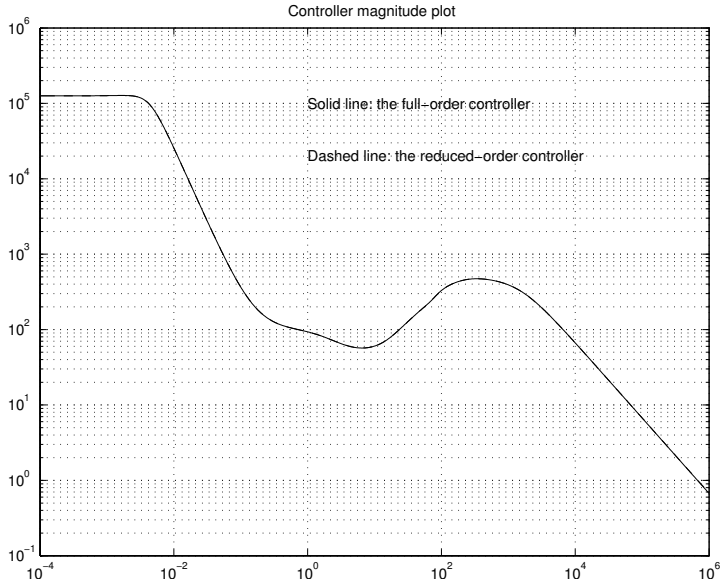

Fig. 13.35. Frequency responses of the full-order and reduced-order controllers

It is interesting to compare the results obtained with the μ-controller with those from the conventional collocated PD controller in the form of

$$u = k_P(r - \theta) - k_D\ddot{\theta}$$

The proportional and derivative coefficients are chosen as $k_P = 358$ N m/rad and $k_D = 28.5$ N m/(rad/s). The values of k_P and k_D are selected such that after neglecting the link flexibility the closed-loop transfer function coincides with the transfer function of the model. The results by using the μ-analysis method in this case (i.e. with the PD controller) are 0.447, 6.82 and 7.41 for the robust stability, nominal performance and robust performance, respectively. Therefore, the PD controller leads to poor nominal performance and poor robust performance, in comparison to the μ-controller designed. This can be seen by comparing Figures 13.36 and 13.37 with Figures 13.29 and 13.30, respectively.

It has to be noticed that good results in the design may also be obtained by using a collocated controller on the feedback from the joint angle θ and the velocity $\dot{\theta}$. The use of the tip acceleration $\ddot{\alpha}$, however, allows better results with respect to the robust performance to be obtained.

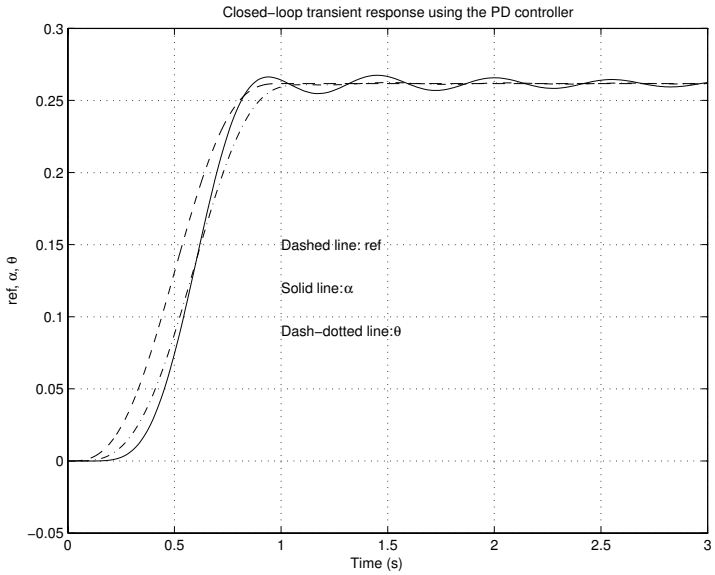

Fig. 13.36. Closed-loop transient response for the PD controller

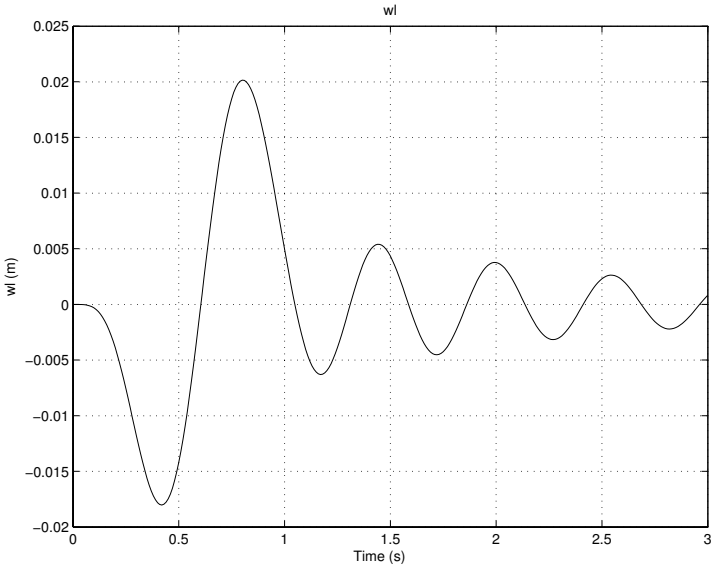

Fig. 13.37. Tip-deflection transient response for the PD controller

13.6 Nonlinear System Simulations

The performance of the μ-controller designed in the previous section is further investigated by simulations of the nonlinear closed-loop system with this controller. The simulation is carried out by the Simulink® model `nls_flm.mdl` using the nonlinear plant model (13.5). A number of simulations may be performed for several values of the payload mass and of the damping coefficients. The Simulink® model `nls_flm.mdl` is shown in Figure 13.38.

Before running the simulation, it is necessary to set the model parameters by using the M-file `init_flm.m`.

The time response of the tip position $\alpha(t)$, along with the joint angle θ and the reference r, for the case of the reduced-order μ-controller and nominal payload mass is given in Figure 13.39.

The tip deflection $w(L,t)$, for the nominal payload mass and the same reference signal, is shown in Figure 13.40. The values of the damping coefficients correspond to the case of light damping of the mechanical structure. In particular, the value of the hub damping coefficient d_r corresponds to a relative uncertainty of –20%. The damping coefficients d_{f_1} and d_{f_2} are taken so that the respective relative perturbations in d_1 and d_2 for the nominal payload are equal to –40%. The parameters of the reference signal used in the simulation ensure fast motion and are set as $a = 0.1\pi$ rad/s, $\psi = 2.5\pi$ s^{-1}, $r_0 = 0$ rad, $t_m = 0.8$ s and $t_f = 3$ s.

In the nonlinear system simulations, it is shown that the μ-controller efficiently suppresses the elastic vibrations during the fast motion of the manipulator tip. It thus justifies that the μ-synthesis is an appropriate robust design method in this exercise. It also confirms the validity of the uncertain model derived.

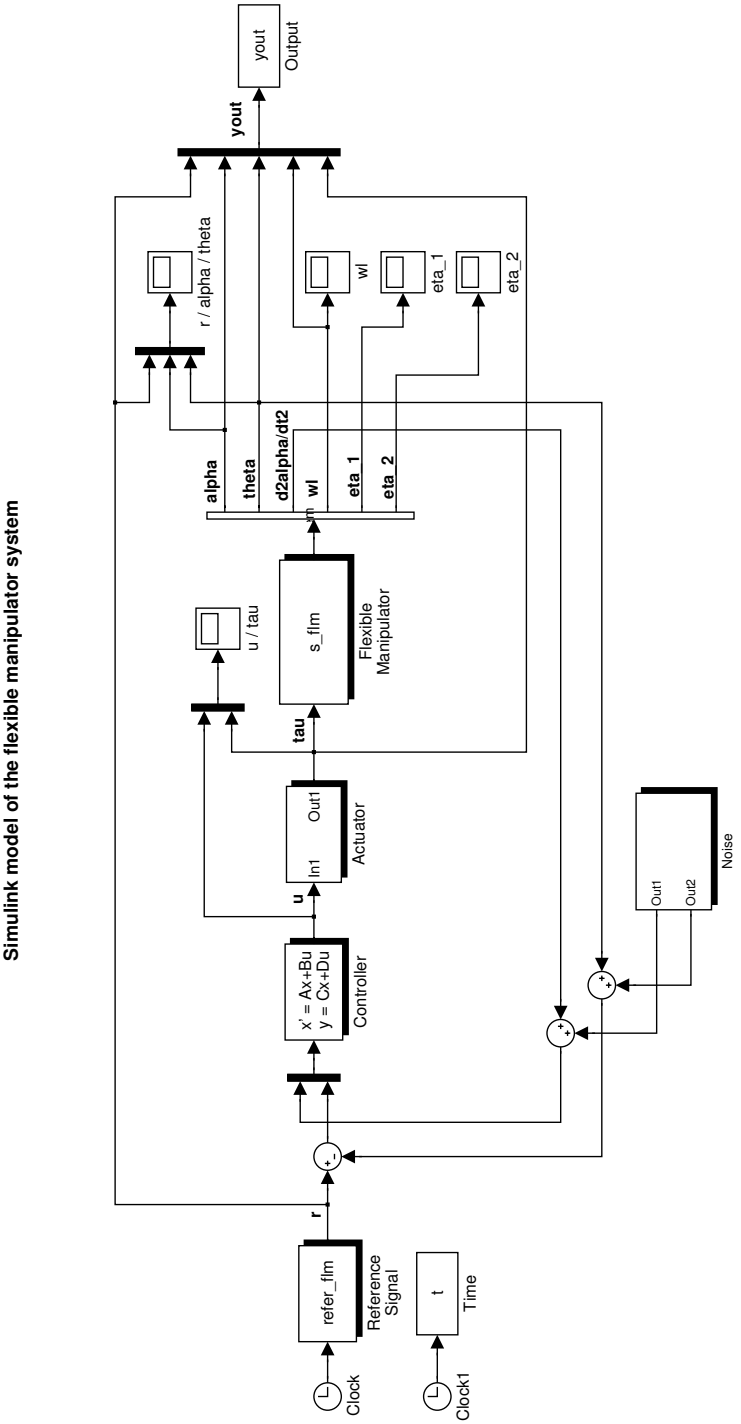

Fig. 13.38. Simulation model of the nonlinear system

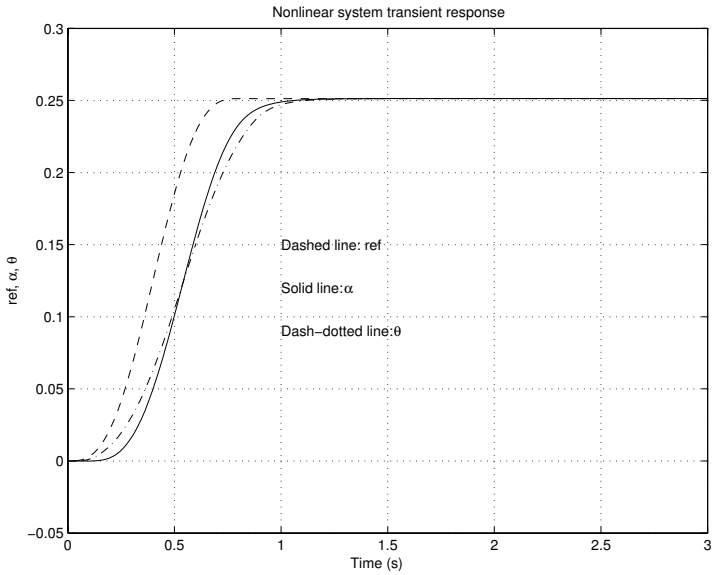

Fig. 13.39. Transient response of the nonlinear system

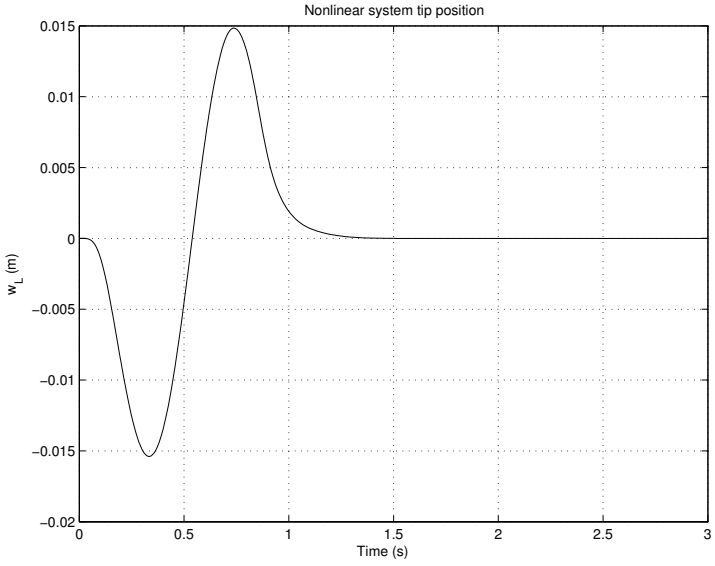

Fig. 13.40. Transient response of the nonlinear system $(w(L,t))$

13.7 Conclusions

A few conclusions may be drawn as the following, based on the analysis and design of the flexible manipulator control system:

- In applying linear robust control system design techniques for a nonlinear plant it is usually unavoidable to derive a complicated uncertainty model, because of the requirement of a sufficiently accurate linear approximation. That would, however, adversely affect the controller design and analysis. It is important, therefore, to simplify the model of uncertainty. Methods such as the numerical approximation used in this study can be considered.
- In contrast to many known models, the uncertainty model derived in this study for the flexible manipulator system contains real parametric uncertainties in a highly structured form. Such a model appeals naturally to the application of μ-synthesis and analysis method that greatly reduces the conservativeness in the controller design.
- A robust noncollocated controller on the feedback signals of joint angle and tip acceleration is designed in this study on the basis of the uncertainty model derived and by using the μ-synthesis. The μ-controller shows very good robust performance on the tip motion for a wide range of payload mass. The controller efficiently suppresses the elastic vibrations during the fast motion of the manipulator tip.
- The nonlinear system simulation results confirm the high performance of the controller designed and also verify the validity of the uncertain model used.
- It is also possible to investigate various noncollocated and collocated controller structures on different output feedback signals, with the uncertainty model and linearised plant derived in this study.

Notes and References

The control of flexible manipulators has been an area of intensive research in recent years. An efficient approach to improve the manipulator performance is to use a feedback from the manipulator tip position [44], tip acceleration [42] or base-strain [43]. The usage of such feedbacks leads to a noncollocated control scheme that may increase the closed-loop system sensitivity to modelling errors or to parameter uncertainties [125].

The necessity to achieve robustness of the manipulator control system in the presence of uncertainties makes it appropriate to apply the robust control design methods. In a few recent papers the authors develop different $\mathcal{H}_\infty$ controllers [45], [85], [146] and μ-synthesis controllers [73] for flexible-link manipulators. A common disadvantage in the previous robust designs for flexible manipulators is the use of unstructured uncertainty model that leads to potentially very conservative results.

References

1. D. Abramovitch and G. Franklin. A brief history of disk drive control. *IEEE Control Systems Magazine*, 22:28–42, 2002.
2. D. Abramovitch and G. Franklin. Disk drive control: The early years. In *Proceedings of the 15th IFAC Congress. Session T-Th-M12*, pages 1–12, Barcelona, Spain, July 2002. CD-ROM.
3. D. Abramovitch, T. Hurst, and D. Henze. An overview of the PES Pareto method for decomposing baseline noise sources in hard disk postion error signals. *IEEE Transactions on Magnetics*, 34:17–23, 1998.
4. D. Abramovitch, F. Wang, T. Hurst, and G. Franklin. Disk drive pivot nonlinearity modelling Part I: Frequency domain. In *Proceedings of the 1994 American Control Conference*, pages 2600–2603, Baltimore, MD, June 1994.
5. D.Y. Abramovitch. Magnetic and optical disk control: Parallels and contrasts. In *Proceedings of the 2001 American Control Conference*, pages 421–428, Arlington, VA, June 2001.
6. V.M. Adamjan, D.Z. Arov, and M.G. Krein. Analytic properties of Schmidt pairs for a Hankel operator and the generalized Schur-Takagi problem. *Mat. USSR Sbornik*, 15:31–73, 1971.
7. R.J. Adams, J.M Buffington, A.G. Sparks, and S.S. Banda. *Robust Multivariable Flight Control*. Springer-Verlag, New York, 1994.
8. U.M. Al-Saggaf and G.F. Franklin. An error bound for a discrete reduced order model of a linear multivariable system. *IEEE Transactions on Automatic Control*, AC-32:815–819, 1987.
9. G.J. Balas, J.C. Doyle, K. Glover, A. Packard, and R. Smith. *μ-Analysis and Synthesis Toolbox: User's Guide*. MUSYN Inc. and The Mathworks, Inc., 1995.
10. D.S. Bernstein and W.M. Haddad. LQG control with an $\mathcal{H}^\infty$ performance bound: A Riccati equation approach. *IEEE Transactions on Automatic Control*, AC-34:293–305, 1989.
11. J.H. Blakelock. *Automatic Control of Aircraft and Missiles*. Wiley, New York, 1991.
12. A.E. Bryson. *Control of Spacecraft and Aircraft*. Princeton University Press, Princeton, NJ, 1994.
13. H. Buschek. Design and flight test of a robust autopilot for the IRIS-T air-to-air missile. *Control Engineering Practice*, 11:551–558, 2003.

14. F.M. Callier and C.A. Desoer. *Linear System Theory*. Springer-Verlag, New York, 1991.
15. B.M. Chen, T.H. Lee, and V. Venkataramanan. *Hard Disk Drive Servo Systems*. Springer-Verlag, Berlin, 2002.
16. K.K. Chew and M. Tomizuka. Digital control of repetetive errors in disk drive systems. *IEEE Control Systems Magazine*, 10:16–20, 1990.
17. B.W. Choi, D.W. Gu, and I. Postlethwaite. Low-order $\mathcal{H}_\infty$ Sub-Optimal Controllers. *IEE Proceedings - Part D*, 141:243–248, 1994.
18. R.R.E. de Gaston and M.G. Safonov. Exact calculation of the multiloop stability margin. *IEEE Transactions on Automatic Control*, AC-33:156–171, 1988.
19. U.B. Desai and D. Pal. A transformation approach to stochastic model reduction. *IEEE Transactions on Automatic Control*, AC-29:1097–1100, 1984.
20. C.A. Desoer and W.S. Chan. The feedback interconnection of lumped linear time-invariant systems. *Journal of the Franklin Institute*, 300:335–351, 1975.
21. C.A. Desoer and M. Vidyasagar. *Feedback Systems: Input-Output Properties*. Academic Press, New York, 1975.
22. J. Ding, M. Tomizuka, and H. Numasato. Design and robustness analysis of dual stage servo system. In *Proceedings of the 2000 American Control Conference*, pages 2605–2609, Chicago, Illinois, June 2000.
23. J.C. Doyle. Analysis of feedback systems with structured uncertainties. *IEE Proceedings - Part D*, 129:242–250, 1982.
24. J.C. Doyle. Structured uncertainty in control system design. In *Proceedings of the 24 IEEE Conference on Decision and Control*, pages 260–265, December 1985.
25. J.C. Doyle. A review of μ: For case studies in robust control. In *Proceedings of 10th IFAC World Congress*, pages 395–402, Munich, Germany, July 1987.
26. J.C. Doyle, B.A. Francis, and A.R. Tannenbaum. *Feedback Control Theory*. Macmillan Publishing Co., New York, 1992.
27. C. Du, J. Zhang, and G. Guo. Vibration analysis and control design comparison of HDDs using fluid bearing and ball bearing spindles. In *Proceedings of the 2002 American Control Conference*, pages 1378–1383, Anchorage, AK, May 2002.
28. K.G. Eltohamy. Nonlinear optimal control of a triple inverted pendulum with single control input. *International Journal of Control*, 69:239–256, 1998.
29. D. Enns. *Model Reduction for Control Systems Design*. PhD thesis, Department of Aeronautics and Astronautics, Stanford University, Stanford, CA, 1984.
30. D. Enns. Model reduction with balanced realizations: An error bound and a frequency weighted generalization. In *Proceedings of the 23rd IEEE Conference on Decision and Control*, pages 127–132, Las Vegas, NV, 1984.
31. R.B. Evans, J.S. Griesbach, and W.C. Messner. Piezoelectric microactuator for dual stage control. *IEEE Transactions on Magnetics*, 35:977–982, 1999.
32. M.K.H. Fan and A.L. Tits. Characterization and efficient computation of the structured singular value. *IEEE Transactions on Automatic Control*, AC-31:734–743, 1986.
33. M.K.H. Fan, A.L. Tits, and J.C. Doyle. Robustness in the presence of mixed parametric uncertainty and unmodeled dynamics. *IEEE Transactions on Automatic Control*, AC-36:25–38, 1991.

34. K.V. Fernando and H. Nicholson. Singular perturbational model reduction of balanced systems. *IEEE Transactions on Automatic Control*, AC-27:466–468, 1982.
35. K.V. Fernando and H. Nicholson. Singular perturbational approximation for discrete-time systems. *IEEE Transactions on Automatic Control*, AC-28:240–242, 1983.
36. G. Ferreres. *A Practical Approach to Robustness Analysis with Aeronautical Applications*. Kluwer Academic/Plenum Publishers, New York, 1999.
37. I. Fialho, G.J. Balas, A.K. Packard, J. Renfrow, and C. Mullaney. Gain-scheduled lateral control of the F-14 aircrfat during powered approach landing. *Journal of Guidance, Control, and Dynamics*, 23:450–458, 2000.
38. B.A. Francis. *A Course in $\mathcal{H}^\infty$ Control Theory*, volume 88 of *Lecture Notes in Control and Information Sciences*. Springer-Verlag, 1987.
39. G.F. Franklin, J.D. Powell, and M.L. Workman. *Digital Control of Dynamic Systems*. Addison-Wesley, Menlo Park, CA, third edition, 1998.
40. K. Furuta, K. Kajiwara, and K. Kosuge. Digital control of a double inverted pendulum on an inclined rail. *International Journal of Control*, 32:907–924, 1980.
41. K. Furuta, T. Ochia, and N. Ono. Attitude control of a triple inverted pendulum. *International Journal of Control*, 39:1351–1365, 1984.
42. E. Garcia-Benitez, J. Walkins, and S. Yurkovich. Nonlinear control with acceleration feedback for a two-link flexible robot. *Control Engineering Practice*, 1:989–997, 1993.
43. S. Ge, T. Lee, and G. Zhu. Improving regulation of a single-link flexible manipulator with strain feedback. *IEEE Transactions on Robotics and Automation*, 14:179–185, 1998.
44. H. Geniele, R. Patel, and K. Khorasani. End-point control of a flexible-link manipulator: Theory and experiment. *IEEE Transactions on Control Systems Technology*, 5:559–570, 1997.
45. M. Ghanekar, D. Wang, and G. Heppler. Scaling laws for linear controllers of flexible link manipulators characterized by nondimensional groups. *IEEE Transactions on Robotics and Automation*, 13:117–127, 1997.
46. K. Glover. All optimal Hankel-norm approximations of linear multivariable systems and their l^∞-error bounds. *International Journal of Control*, 39:1115–1193, 1984.
47. K. Glover. Multiplicative approximation of linear multivariable systems with $\mathcal{L}_\infty$ error bounds. In *Proceedings of the 1986 American Control Conference*, pages 1705–1709, Minneapolis, MN, 1986.
48. K. Glover and J.C. Doyle. State-space formulae for all stabilizing controllers that satisfy an $\mathcal{H}^\infty$ norm bound and relations to risk sensitivity. *Systems & Control Letters*, 11:167–172, 1988.
49. K. Glover and E.A. Jonckheere. A comparison of two Hankel norm methods for approximating spectra. In C.I. Byrnes and A. Lindquist, editors, *Modelling, Identification and Robust Control*. North-Holland, Amsterdam, The Netherlands, 1986.
50. T.B. Goh, Z. Li, B.M. Chen, T.H. Lee, and T. Huang. Design and implementation of a hard disk drive servo system using robust and perfect tracking approach. In *Proceedings of the 38th IEEE Conference on Decision and Control*, pages 5247–5252, Phoenix, Arizona, December 1999.

51. M. Green. Balanced stochastic realizations. *Linear Algebra & its Applications*, 98:211–247, 1988.
52. M. Green. A relative error bound for balanced stochastic truncation. *IEEE Transactions on Automatic Control*, AC-33:961–965, 1988.
53. M. Green and D.J.N. Limebeer. *Linear Robust Control*. Prentice-Hall, Englewood Cliffs, NJ, 1995.
54. A.L. Greensite. *Analysis and Design of Space Vehicle Flight Control Systems*. Spartan, New York, 1970.
55. D.W. Gu, B.W. Choi, and I. Postlethwaite. Low-order stabilizing controllers. *IEEE Transactions on Automatic Control*, AC-38:1713–1717, 1993.
56. D.W. Gu, S.J. Goh, T. Fitzpatrick, I. Postlethwaite, and N. Measor. Application of an expert system for robust controller design. *Control'96*, 2:1004–1009, 1996.
57. D.W. Gu, P.Hr. Petkov, and M.M. Konstantinov. Direct Formulae for the $\mathcal{H}_\infty$ Sub-Optimal Central Controller. Technical Report 1998-7, Niconet Report, 1998. Available at http://www.win.tue.nl/niconet.
58. D.W. Gu, P.Hr. Petkov, and M.M. Konstantinov. Formulae for discrete $\mathcal{H}_\infty$ loop shaping design procedure controllers. In *Proceedings of the 15th IFAC World Congress, paper 276, Session T-Mo-M15*, Barcelona, Spain, July 2002. CD-ROM.
59. D.W. Gu, I. Postlethwaite, and M.C. Tsai. $\mathcal{H}_\infty$ super-optimal solutions. In C.T. Leondes, editor, *Advances in Control and Dynamic Systems*, volume 51, pages 183–246. Academic Press, San Diego, CA, 1992.
60. D.W. Gu, M.C. Tsai, and I. Postlethwaite. State-space formulae for discrete-time optimization. *International Journal of Control*, 49:1683–1723, 1989.
61. L. Guo, H.S. Lee, A. Hudson, and S.-H. Chen. A comprehensive time domain simulation tool for hard disk drive TPI prediction and mechanical/servo enhancement. *IEEE Transactions on Magnetics*, 35:879–884, 1999.
62. S. Hammarling. Numerical solution of the stable non-negative definite Lyapunov equation. *IMA Journal of Numerical Analysis*, 2:303–323, 1982.
63. S. Hara, T. Hara, L. Yi, and M. Tomizuka. Two degree-of-freedom controllers for hard disk drives with novel reference signal generation. In *Proceedings of the 1999 American Control Conference*, pages 4116–4121, San Diego, CA, June 1999.
64. J.W. Helton. Worst case analysis in the frequency domain: The $\mathcal{H}^\infty$ approach to control. *IEEE Transactions on Automatic Control*, AC-30:1154–1170, 1985.
65. J.W. Helton and O. Merino. *Classical Control Using $\mathcal{H}^\infty$ Methods*. Society for Industrial and Applied Mathematics, Philadelphia, PA, 1998.
66. D. Hernandez, S.-S. Park, R. Horowitz, and A.K. Packard. Dual stage track-following servo design for hard disk drives. In *Proceedings of the 1999 American Control Conference*, pages 4116–4121, San Diego, CA, June 1999.
67. D. Hoyle, R. Hyde, and D.J.N. Limebeer. An $\mathcal{H}^\infty$ approach to two-degree-of-freedom design. In *Proceedings of the 30th IEEE Conference on Decision and Control*, pages 1581–1585, Brighton, UK, December 1991.
68. C.S. Hsu, X. Yu, H.H. Yeh, and S.S. Banda. $\mathcal{H}_\infty$ compensator design with minimal order observer. In *Proceedings of the 1993 American Control Conference*, San Francisco, CA, June 1993.
69. Y. Huang, P. Mathur, and W.C. Messner. Robustness analysis on a high bandwidth disk drive servo system with an instrumented suspension. In *Proceedings*

of the 1999 American Control Conference, pages 3620–3624, San Diego, CA, June 1999.
70. J. Ishikawa, Y. Yanagita, and T. Hattori ans M. Hashimoto. Head positioning control for low sampling rate systems based on two degree-of-freedom control. *IEEE Transactions on Magnetics*, 32:1787–1792, 1996.
71. T. Iwasaki and R.E. Skelton. All low order $\mathcal{H}_\infty$ controllers with covariance upper bound. In *Proceedings of the 1993 American Control Conference*, San Francisco, CA, June 1993.
72. H. Kajiwara, P. Apkarian, and P. Gahinet. LPV techniques for control of an inverted pendulum. *IEEE Control Systems Magazine*, 19:44–54, 1999.
73. M. Karkoub, G. Balas, K. Tamma, and M. Donath. Robust control of flexible manipulators via μ-synthesis. *Control Engineering Practice*, 8:725–734, 2000.
74. C. Kempf, W. Messner, M. Tomizuka, and R. Horovitz. Comparison of four discrete-time repetetive control algorithms. *IEEE Control Systems Magazine*, 13:48–54, 1993.
75. S.W. Kim, B.D.O. Anderson, and A.G. Madievski. Error bound for transfer function order reduction using frequency weighted balanced truncation. *Systems & Control Letters*, 24:183–192, 1995.
76. M. Kobayashi, T. Yamaguchi, and R. Horowitz. Track-seeking controller design for dual-stage actuator in magnetic disk drives. In *Proceedings of the 2000 American Control Conference*, pages 2610–2614, Chicago, Illinois, June 2000.
77. C.M. Kozierok. *The PC Guide. The Reference Section on Hard Disk Drives.* January 2003. Available at http://www.PCGuide.com.
78. S. Kung. A new low-order approximation algorithm via singular value decomposition. In *Proceedings of the 18th IEEE Conference on Decision and Control*, Ft. Lauderdale, Florida, December 1979.
79. S. Kung and D.W. Lin. Optimal Hankel norm model reduction: Multivariable systems. *IEEE Transactions on Automatic Control*, AC-26:832–852, 1981.
80. P.J. Larcombe. On the generation and solution of the symbolic, open-loop charactersitic equation for a double inverted pendulum. *International Journal of Systems Science*, 24:2379–2390, 1993.
81. A.J. Laub. On computing balancing transformations. In *Proceedings of the Joint 1980 American Control Conference*, pages FA8–E, San Francisco, CA, August 1980.
82. A.J. Laub, M.T. Heath, C.C. Paige, and R.C. Ward. Computation of system balancing transformations and other applications of simultaneous diagonalization algorithms. *IEEE Transactions on Automatic Control*, AC-32:115–121, 1987.
83. H.S. Lee. Controller optimization for minimum position error signals of hard disk drives. In *Proceedings of the 2000 American Control Conference*, pages 3081–3085, Chicago, Illinois, June 2000.
84. D.J. Leith and W.E. Leithead. Survey of gain-scheduling analysis and design. *International Journal of Control Control*, 73:1001–1025, 2000.
85. Y. Li, B. Thang, Z. Shi, and Y. Lu. Experimental study for trajectory tracking of a two-link flexible manipulators. *International Journal of Systems Science*, 31:3–9, 2000.
86. D.J.N. Limebeer. The specification and purpose of a controller design study. In *Proceedings of the 30th IEEE Conference on Decision and Control*, pages 1579–1580, Brighton, UK, December 1991.

87. D.J.N. Limebeer, E.M. Kasenally, and J.D. Perkins. On the design of robust two degree of freedom controllers. *Automatica*, 29:157–168, 1993.
88. C.-A. Lin and T.-Y. Chiu. Model reduction via frequency weighted balanced realization. *CONTROL – Theory and Advanced Technology*, 8:341–351, 1992.
89. J.L. Lin. *Control System Design for Robust Stability and Robust Performance*. PhD thesis, Department of Engineering, University of Leicester, Leicester, UK, May 1992.
90. J.L. Lin, I. Postlethwaite, and D.W. Gu. μ-K iteration: a new algorithm for μ-synthesis. *Automatica*, 29:219–244, 1993.
91. R. Lind and M. Brenner. *Robust Aeroservoelastic Stability Analysis. Flight Test Applications*. Springer-Verlag, London, 1999. ISBN 1-85233-096-1.
92. A. Lindquist and G. Picci. On the stochastic realization problem. *SIAM Journal of Control and Optimization*, 17:365–389, 1979.
93. Yi Liu and B.D.O. Anderson. Singular perturbation of balanced systems. *International Journal of Control*, 50(4):1379–1405, 1989.
94. A. De Luca and B. Siciliano. Trajectory control of a non-linear one-link flexible arm. *International Journal of Control*, 50:1699–1715, 1989.
95. P. Lundström, S. Skogestad, and J.C. Doyle. Two-degree-of-freedom controller design for an ill-conditioned distillation process using μ-synthesis. *IEEE Transactions on Control Systems Technology*, 7:12–21, 1999.
96. J. Lunz. *Robust Multivariable Feedback Control*. Prentice Hall, London, 1989.
97. C.C. MacDuffee. *The Theory of Matrices*. Chelsea Publishing Co., New York, 1950.
98. J.M. Maciejowski. *Multivariable Feedback Design*. Addison-Wesley, Wokingham, England, 1989. ISBN 0-201-18243-2.
99. D.P. Magee. Optimal filtering to improve performance in hard disk drives: Simulation results. In *Proceedings of the 1999 American Control Conference*, pages 71–75, San Diego, CA, June 1999.
100. D. McFarlane and K. Glover. A loop shaping design procedure using $\mathcal{H}_\infty$ synthesis. *IEEE Transactions on Automatic Control*, AC-37:749–769, 1992.
101. D.C. McFarlane and K. Glover. *Robust Controller Design Using Normalized Coprime Factor Plant Descriptions*, volume 138 of *Lecture Notes in Control and Information Sciences*. Springer-Verlag, 1990.
102. G.A. Medrano-Cerda. Robust stabilization of a triple inverted pendulum-cart. *International Journal of Control*, 68:849–865, 1997.
103. G.A. Medrano-Cerda. Robust computer control of an inverted pendulum. *IEEE Control Systems Magazine*, 19:58–67, 1999.
104. Z. Meier, H. Farwig, and H. Unbehauen. Discrete computer control of a triple-inverted pendulum. *Optimal Control Applications & Methods*, 11:157–171, 1990.
105. L. Meirovitch. *Elements of Vibration Analysis*. McGraw-Hill, New York, 1986.
106. W. Messner and R. Ehrlich. A tutorial on controls for disk drives. In *Proceedings of the 2001 American Control Conference*, pages 408–420, Arlington, VA, June 2001.
107. D.G. Meyer. Fractional balanced reduction: Model reduction via fractional representation. *IEEE Transactions on Automatic Control*, AC-35(3):1341–1345, 1990.
108. B. C. Moore. Principle component analysis in linear systems: Controllability, observability, and model reduction. *IEEE Transactions on Automatic Control*, AC-26:17–31, 1981.

109. M. Morari and E. Zafiriou. *Robust Process Control*. Prentice-Hall, Englewood Cliffs, NJ, 1989.
110. S. Mori, H. Nishihara, and K. Furuta. Control of an unstable mechanical system. Control of pendulum. *International Journal of Control*, 23:673–692, 1976.
111. G. Murad. *Robust Multivariable Control of Industrial Production Processes: A Discrete-Time Multi-Objective Approach*. PhD thesis, Department of Engineering, University of Leicester, Leicester, UK, 1995.
112. G. Murad, D-W. Gu, and I. Postlethwaite. A Direct Model Reduction Approach for Discrete-Time Non-Minimal State-Space Systems. Internal Report 94-23, University of Leicester, Leicester, UK, September 1994.
113. G. Murad, D.-W. Gu, and I. Postlethwaite. Robust internal model control of a binary distillation column. In *IEEE International Conference on Industrial Technology*, pages 194–198, Shanghai, China, December 1996.
114. G. Murad, I. Postlethwaite, D.-W. Gu, and R. Samar. On the structure of an $\mathcal{H}^\infty$ two-degree-of-freedom internal model-based controller and its application to a glass tube production process. In *Proceedings of the Third European Control Conference*, pages 595–600, Rome, September 1995.
115. G. Murad, I. Postlethwaite, D.-W. Gu, and J.F. Whidborne. Robust control of a glass tube shaping process. In *Proceedings of the Second European Control Conference*, volume 4, pages 2350–2355, Gröningen, The Netherlands, June-July 1993.
116. Z. Nehari. On bounded bilinear forms. *Annals of Mathematics*, 65:153–162, 1957.
117. W.Y. Ng. *Interactive Multi-Objective Programming as a Framework for Computer-Aided Control System Design*. Lecture Notes in Control and Information Sciences. Springer-Verlag, 1989.
118. R.A. Nichols, R.T. Reichert, and W.J. Rugh. Gain scheduling for H_∞ controllers: A flight control example. *IEEE Trans. Control Systems Technology*, 1:69–53, 2001.
119. International Society Niconet. *SLICOT: Numerical Subroutine Library for Control and Systems Theory*. Available at http://www.win.tue.nl/niconet, 2001.
120. A. Packard and J.C. Doyle. The complex structured singular value. *Automatica, Special Issue on Robust Control*, 29:71–109, 1993.
121. A. Packard, M.K.H. Fan, and J.C. Doyle. A power method for the structured singular value. In *Proceedings of the 27th IEEE Conference on Decision and Control*, pages 2132–2137, Austin, Texas, December 1988.
122. A. Packard and P. Pandey. Continuity properties of the real/complex structured singular value. *IEEE Transactions on Automatic Control*, AC-38:415–428, 1993.
123. L.Y. Pao and G.F. Franklin. Time-optimal control of flexible structures. In *Proceedings of the 29th IEEE Conference on Decision and Control*, pages 2580–2581, Honolulu, HI, December 1990.
124. T. Pappas, A.J. Laub, and N.R. Sandell. On the numerical solution of the discrete-time algebraic Riccati equation. *IEEE Transactions on Automatic Control*, AC-25:631–641, 1980.
125. J. Park and H. Asada. Dynamic analysis of noncollocated flexible arms and design of torque transmission mechanisms. *ASME Journal of Dynamic Systems, Measurements and Control*, 116:201–207, 1994.

126. L. Pernebo and L.M. Silverman. Model reduction via balanced state space representations. *IEEE Transactions on Automatic Control*, AC-27:382–387, 1982.
127. I. Postlethwaite, J.L. Lin, and D.W. Gu. Robust control of a high purity distillation column using μ-K iteration. In *Proceedings of the 30th IEEE Conference on Decision and Control*, Brighton, UK, December 1991.
128. R.M. Redheffer. Remarks on the basis of network theory. *Journal of Mathematics and Physics*, 28:237–258, 1950.
129. R.M. Redheffer. On a certain linear fractional transformation. *Journal of Mathematics and Physics*, 39:269–286, 1960.
130. R.T. Reichert. Dynamic scheduling of modern-robust-control autopilot design for missiles. *IEEE Control Systems Magazine*, 12:35–42, 1992.
131. W.J. Rugh and J.S. Shamma. Research on gain scheduling. *Automatica*, 36:1401–1425, 2000.
132. M.G. Safonov. Stability margins of diagonally perturbed multivariable feedback systems. *IEE Proceedings - Part D*, 129:251–256, 1982.
133. M.G. Safonov and R.Y. Chiang. A Schur method for balanced-truncation model reduction. *IEEE Transactions on Automatic Control*, AC-34:729–733, 1989.
134. M.G. Safonov, R.Y. Chiang, and D.J.N. Limebeer. Hankel model reduction without balancing – A descriptor approach. In *Proceedings of the 26th IEEE Conference on Decision and Control*, Los Angeles, CA, December 1987.
135. M.G. Safonov, D.J.N. Limebeer, and R.Y. Chiang. Simplifying the $\mathcal{H}^\infty$ theory via loop-shifting, matrix-pencil and descriptor concepts. *International Journal of Control*, 50:2467–2488, 1989.
136. R. Samar, I. Postlethwaite, and D.-W. Gu. Model reduction with balanced realizations. *International Journal of Control*, 62:33–64, 1995.
137. R.S. Sánchez-Peña and M. Sznaier. *Robust Systems. Theory and Applications*. John Wiley & Sons, Inc., New York, 1998.
138. J. Sefton and K. Glover. Pole-zero cancellations in the general $\mathcal{H}_\infty$ problem with reference to a two block design. *Systems & Control Letters*, 14:295–306, 1990.
139. R.S. Sezginer and M.L. Overton. The largest singular value of $e^X A_o e^{-X}$ is convex on convex sets of commuting matrices. *IEEE Transactions on Automatic Control*, AC-35:229–230, 1990.
140. S. Skogestad. Dynamics and control of distillation columns. A tutorial introduction. *Trans. IChemE*, 75:1–36, 1997.
141. S. Skogestad, M. Morari, and J.C. Doyle. Robust control of ill-conditioned plants: High purity distillation. *IEEE Transactions on Automatic Control*, 33:1092–1105, 1988.
142. S. Skogestad and I. Postlethwaite. *Multivariable Feedback Control*. John Wiley and Sons Ltd, Chichester, UK, 1996.
143. M.S. Spillman. Robust longitudinal flight control design using linear parameter-varying feedback. *Journal of Guidance, Control, and Dynamics*, 23:101–108, 2000.
144. V. Sreeram, B.D.O. Anderson, and A.G. Madievski. New results on frequency weighted balanced reduction technique. In *Proceedings of the 1995 American Control Conference*, pages 4004–4009, Seattle, WA, June 1995.
145. A.A. Stoorvogel. *The $\mathcal{H}_\infty$ Control Problem: A State Space Approach*. Prentice Hall, Englewood Cliffs, NJ, 1992.

146. R. Sutton, G. Halikias, A. Plummer, and D. Wilson. Modelling and $\mathcal{H}_\infty$ control of a single-link flexible manipulator. *Proceedings of the Institution of Mechanical Engineers, Part I, Journal of Systems and Control Engineering*, 213:85–104, 1999.
147. K.S. Tang, K.F. Man, and D.-W. Gu. Structured Genetic Algorithm for Robust $\mathcal{H}_\infty$ Control Systems Design. *IEEE Transactions on Industrial Electronics*, 43(5):575–582, 1996.
148. M.S. Tombs and I. Postlethwaite. Truncated balanced realization of a stable non-minimal state space system. *International Journal of Control*, 46(4):1319–1330, 1987.
149. V.A. Tsacouridis and G.A. Medrano-Cerda. Discrete-time H_∞ control of a triple inverted pendulum with single control input. *IEE Proceedings-Control Theory Appl.*, 146:567–577, 1999.
150. G.-W. van der Linden and P.F. Lambrechts. H_∞ control of an experimental inverted pendulum with dry friction. *IEEE Control Systems Magazine*, 19:44–50, 1993.
151. A. Varga. Balancing free square-root algorithm for computing singular perturbation approximations. In *Proceedings of the 30th IEEE Conference on Decision and Control*, pages 1062–1065, Brighton, UK, December 1991.
152. A. Varga. On stochastic balancing related model reduction. In *Proceedings of the 39th IEEE Conference on Decision and Control*, pages 2385–2390, Sydney, Australia, December 2000.
153. M. Vidyasagar and H. Kimura. Robust controllers for uncertain linear multivariable systems. *Automatica*, 22:85–94, 1986.
154. M. Vidyasagar, H. Schneider, and B. Francis. Algebraic and topological aspects of feedback stabilization. *IEEE Transactions on Automatic Control*, AC-27:880–894, 1982.
155. D.J. Walker. Relationship between three discrete-time $\mathcal{H}_\infty$ algebraic Riccati equation solutions. *International Journal of Control*, 52:801–809, 1990.
156. F. Wang, T. Hurst, D. Abramovitch, and G. Franklin. Disk drive pivot nonlinearity modelling Part II: Time domain. In *Proceedings of the 1994 American Control Conference*, pages 2604–2607, Baltimore, MD, June 1994.
157. G. Wang, V. Sreeram, and W.Q. Liu. A new frequency-weighted balanced truncation method and an error bound. *IEEE Transactions on Automatic Control*, 44:1734–1737, 1999.
158. J.F. Whidborne, D.-W. Gu, and I. Postlethwaite. Algorithms for solving the method of inequalities – A comparative study. In *Proceedings of the 1995 American Control Conference*, June 1995.
159. J.F. Whidborne and G.P. Liu. *Critical Control Systems*. Research Studies Press Ltd, Taunton, Somerset, UK, 1993.
160. J.F. Whidborne, G. Murad, D.-W. Gu, and I. Postlethwaite. Robust control of an unknown plant – the IFAC 93 benchmark. *International Journal of Control*, 61:589–640, 1994.
161. J.F. Whidborne, I. Postlethwaite, and D.-W. Gu. Robust controller design using $\mathcal{H}^\infty$ loop-shaping and the method of inequalities. *IEEE Transactions on Control Systems Technology*, 2:455–461, 1994.
162. J.F. Whidborne, I. Postlethwaite, and D.-W. Gu. Multiobjective control system design – a mixed optimization approach. In R.P. Agarwal, editor, *Recent Trends in Optimization Theory and Applications*, volume 5 of *World Scientific Series in Applicable Analysis*, pages 467–482. World Scientific, 1995.

163. J.F. Whidborne, I. Postlethwaite, and D.-W. Gu. Robust control of a paper machine. *Control Engineering Practice*, 3:1475–1478, 1995.
164. M.T. White, M. Tomizuka, and C. Smith. Rejection of disk drive vibration and shock disturbances with a disturbance observer. In *Proceedings of the 1999 American Control Conference*, pages 4127–4131, San Diego, CA, June 1999.
165. W.N. White and R.C. Fales. Control of a double inverted pendulum with hydraulic actuation: A case study. In *Proceedings of the 1999 American Control Conference*, pages 495–499, San Diego, CA, June 1999.
166. M. Yamakita, T. Hoshino, and K. Furuta. Control practice using pendulum. In *Proceedings of the 1999 American Control Conference*, pages 490–494, San Diego, CA, June 1999.
167. D.C. Youla, H.A. Jabr, and J.J. Bongiorno. Modern Weiner-Hopf design of optimal controllers, Part ii: The multivariable case. *IEEE Transactions on Automatic Control*, AC-21:319–338, 1976.
168. D.C. Youla, H.A. Jabr, and C.N. Lu. Single-loop feedback stabilization of linear multivariable dynamical plants. *Automatica*, 10:159–173, 1974.
169. V. Zakian and U. Al-Naib. Design of dynamical and control systems by the method of inequalities. *IEE Proceedings - Control & Science*, 120:1421–1427, 1973.
170. G. Zames. Feedback and optimal sensitivity: Model reference transformations, multiplicative seminorms and approximate inverses. *IEEE Transactions on Automatic Control*, AC-26:301–320, 1981.
171. G. Zames and B.A. Francis. Feedback, minimax sensitivity, and optimal robustness. *IEEE Transactions on Automatic Control*, AC-28:585–600, 1983.
172. P. Zarchan. *Tactical and Strategic Missile Guidance*, volume 176 of *Progress in Astronautics and Aeronautics*. AIAA, Washington, DC, 3rd edition, 1998.
173. H.P. Zeiger and A.J. McEwen. Approximate linear realization of given dimension via Ho's algorithm. *IEEE Transactions on Automatic Control*, AC-19:153, 1974.
174. K. Zhou and J.C. Doyle. *Essentials of Robust Control*. Prentice Hall, Upper Saddle River, NJ, 1998.
175. K. Zhou, J.C. Doyle, and K. Glover. *Robust and Optimal Control*. Prentice Hall, Upper Saddle River, NJ, 1995.

Index

M-Δ configuration, 29
$\mathcal{H}_\infty$ loop-shaping design procedure, 59
$\mathcal{H}_\infty$ suboptimal problem, 39
∞-norm of a system, 11
μ-K iteration method, 77
μ-synthesis method, 75
2-degree-of-freedom control scheme, 38

absolute-error approximation methods, 80
accelerometer, 289
additive perturbation, 14
admissible point, 68
admissible set, 68
aerodynamic angle of roll, 291
aerodynamic centre of pressure, 291
aerodynamic coefficients, 293
aerodynamic damping moments, 294
aerodynamic moments, 293
ailerons, 289
algebraic Riccati equation, 40
angle of attack, 290
assumed-modes method, 336
asymptotic stability, 6

Balanced Realisation Algorithm, 81
balanced residualisation, 83
Balanced Stochastic Truncation method, 90
balanced system, 81
balanced truncation method, 81
bank angle, 291
Bezout identity, 8
body-fixed reference frame, 289
bottom product, 250
Bounded-Input-Bounded-Output stability, 6

central $\mathcal{H}_\infty$ suboptimal controller, 49
central controller, 43
Cholesky factors, 42
clamping hub, 336
closed-loop system, 4
complementary sensitivity function, 29
condensor, 252
continuous-time system, 5
control-system, 4
controllability gramian, 81
coprime factorisation, 8
coprime transfer functions, 8

D-K iteration, 75
diagonal scaling problem, 33
discrete Lyapunov equations, 86
discrete-time $\mathcal{H}_\infty$ case, 50
discrete-time Riccati equation, 51
discrete-time system, 5
disk sectors, 204
disk tracks, 204
distillate product, 250
distillation column, 250
disturbance, 28
disturbance attenuation, 28
drag force, 293
dynamic pressure, 293

elastic deflection, 336
embedded servo, 205

error signal, 28

fast part, 17
feedback system, 4
feedforward compensator, 60
feedforward path, 38, 60
fictitious output vector, 19
fins, 289
flexible-link manipulator, 336
flight-path angle, 291
flight-path reference frame, 289
Fractional Balanced Truncation method, 88
Fractional Singular Perturbation Approximation method, 88
frequency-weighted approximation methods, 92
Frequency-weighted Balanced Truncation, 94
Frequency-weighted Modulii Truncation Method, 96
Frequency-weighted Singular Perturbation Approximation, 95
full uncertainty blocks, 23

gain scheduling, 332
generalised plant, 36

Hankel approximation problem, 58
Hankel norm, 58, 83
Hankel singular value, 81
Hankel-norm approximation, 83
Hard Disk Drive, 203
Hard Disk Drive servo control system, 205

ill-conditioned problem, 39
ill-posed feedback system, 53
induced norm, 11
input, 4
input multiplicative perturbation, 14
interconnected system, 36
internal stability, 6
inverse additive perturbation, 14
inverse input multiplicative perturbation, 15
inverse output multiplicative perturbation, 15

left coprime factor perturbations, 15
lift force, 293
Linear Fractional Transformation
  lower, 21
  upper, 21
loop shaping design procedure, 59
low-order controller, 79
lower bound on μ, 33
LQG methods, 3
LV-configuration of the distillation column, 253
Lyapunov equations, 81

Mach number, 293
mass-damper-spring system, 101
Matrix Inversion Lemma, 169
measurement noise, 28
method of inequalities, 67
MIMO system, 4
minimal system, 5
mixed optimisation loop-shaping design method, 67
mixed sensitivity problem, 35
multivariable system, 5

natural frequencies, 339
noise rejection, 28
nominal model, 13
nominal parameter value, 18
nominal performance, 73
nominal stability, 73
noncollocated controller structure, 355
nonrepeatable runout, 205
norm of a signal, 9
normalised system, 43

observability gramian, 81
open-loop system, 4
order reduction, 80
orthonormal matrix, 84
output, 4
output multiplicative perturbation, 15

parametric uncertainty, 20
performance specifications, 28
pitch angle, 290
platters, 203
position bursts, 205
Position Error Signal, 205
postcompensator, 59

power signal, 10
precompensator, 59

rate gyro, 289
read/write heads, 204
reboiler, 252
reference area, 293
reference input, 28
relative-error approximation methods, 90
repeatable runout, 205
resonant modes, 207
right coprime factor perturbations, 15
robust control system, 25
robust performance, 73
robust stabilisation conditions, 27
robust stability, 73
robustly stable system, 26
roll angle, 290
rotational motion of the rocket, 293
runout, 205

scalar uncertainty blocks, 23
scaled model, 253
scaling matrix
  input, 253
  output, 254
seeking mode, 205
sensitivity function, 29
sideslip angle, 290
singular perturbation approximation, 83
singular value decomposition, 45
SISO system, 4
sliders, 204
slow part, 17
Small-Gain Theorem, 25
space eigenfunction, 337
spectral radius of a matrix, 31
stabilising controller, 26
stability, 6
stability margin, 31
statically stable rocket, 291
structured singular value, 30
structured uncertainty, 20
suboptimal discrete-time loop-shaping controller, 62
system norms, 10

time-invariant system, 5
track following mode, 205
trade-off between nominal performance and robustness of the closed-loop system, 202
transfer function matrix, 5
triple inverted pendulum, 164

unmodelled dynamics, 13, 17
unstructured uncertainty, 13
upper bound on μ, 33

vehicle-carried vertical reference frame, 289
Voice Coil Motor, 205

weighting functions, 29
winged rocket, 289

X-Riccati equation, 52

yaw angle, 290
Youla Parameterisation Theorem, 9

Z-Riccati equation, 52